Title
A THEORETICAL ANALYSIS OF THE AGING RESPONSE OF ORDER HARDENING ALLOYS

Author
Glazer, J.

Publication Date
1986-05-01

LBL-21849

A THEORETICAL ANALYSIS OF THE AGING RESPONSE OF ORDER HARDENING ALLOYS

J. Glazer
(M.S. Thesis)

May 1986

Lawrence Berkeley Laboratory
University of California
Berkeley, California 94720

Prepared for the U.S. Department of Energy
under Contract DE-AC03-76SF00098

Center for Advanced Materials

DISCLAIMER

A THEORETICAL ANALYSIS OF THE AGING RESPONSE OF ORDER HARDENING ALLOYS

Judith Glazer

M.S. Thesis

Lawrence Berkeley Laboratory
University of California
Berkeley, California 94720

May 1986

A THEORETICAL ANALYSIS OF THE AGING RESPONSE OF ORDER HARDENING ALLOYS

by

Judith Glazer

ABSTRACT

Most precipitation-hardened aluminum alloys are used in specified aging conditions. An understanding of the sources of strength and yielding behavior is fundamental to defining desirable microstructures and designing processing steps to achieve them. In this paper, a model of aging behavior of alloys hardened by coherent, ordered precipitates with relatively low misfit strains is developed and some of its consequences explored. The model is based on the Hanson and Morris solution for the critical resolved shear stress for dislocation glide through a random array of obstacles. The model is applied to the specific case of δ′ precipitates in binary aluminum-lithium alloys and found to be in good quantitative agreement with measured aging behavior. The effects of precipitate size, size distributions and shape on the critical resolved shear stress are explored via the model and predictions for more optimized microstructures presented.

ACKNOWLEDGEMENT

I would like to express my gratitude to my advisor and friend, Professor J.W. Morris, Jr., for innumerable discussions of the concepts embodied in this thesis. Without his input and continual encouragement this work would not have been possible.

Thanks are also due to the other members of my thesis committee, Profs. A.J. Ardell and R.O. Ritchie, for their careful reading and constructive criticism of this thesis.

I also thank my friends, both inside and outside my research group, for their moral support and their tolerance of my preoccupation during the writing of this document.

And, finally, I would like to thank my parents for their unwavering love and infinite patience.

This work was supported by the Director, Office of Energy Research, Office of Basic Energy Sciences, Materials Sciences Division of the U.S. Department of Energy under Contract No. DEAC03-76SF00098. I also received fellowship support from ATT Bell Laboratories.

A THEORETICAL ANALYSIS OF THE AGING RESPONSE OF ORDER HARDENING ALLOYS

TABLE OF CONTENTS

I. Introduction.

I.1 Summary.

Most precipitation-hardened aluminum alloys are used in specified aging conditions. An understanding of the sources of strength and yielding behavior is fundamental to defining desirable microstructures and designing processing steps to achieve them. In this paper, a model of aging behavior of alloys hardened by coherent, ordered precipitates with relatively low misfit strains is developed and some of its consequences explored. The model is applied to the specific case of δ′ precipitates in binary aluminum-lithium alloys and found to be in good quantitative agreement with measured aging behavior. The effects of precipitate size, size distributions and shape on the critical resolved shear stress are explored via the model and predictions for more optimized microstructures presented. The approach used to develop the model and the implications of the model are summarized below.

The yield strength of order-hardened alloys is generally modelled in terms of the behavior of single crystals. The property that defines yielding in single crystals is the critical resolved shear stress, the stress at which dislocations glide freely through the crystal.

It is simplest to define the important parameters of a theory of the critical resolved shear stress in the context of a model and its solution. The model selected here is common to many investigators. It considers the glide of a dislocation of constant line tension through a random array of point obstacles. The solution chosen was developed by Hanson and Morris (1975).

To place the Hanson and Morris model in proper context, the evolution of solutions to the random array model of the critical resolved shear stress is traced. A clear distinction can be made between models that describe the average behavior of a dislocation segment in the obstacle array and those that focus on the extrema of the dislocation's interaction with the array. The latter theories, termed strong line solutions, incorporate the concept that the critical resolved shear stress is controlled by the strongest line in the array, rather than the average configuration of the dislocation. New solutions and poten-

tial modifications of existing solutions may be assessed on the basis of this fundamental distinction.

In order to apply the strong line solution of Hanson and Morris quantitatively, a number of its assumptions must be reconsidered. To study the aging behavior of order-hardened alloys these include:

* the way in which the effects of obstacles of differing strengths sum;
* the variability of the line tension with dislocation character;
* the character of the dislocations that control glide;
* the coarsening behavior of precipitates;
* the relative energies associated with particle shear and looping; and,
* the formation of superdislocations and their effect on the deformation process.

The Hanson and Morris solution can be modified to incorporate these aspects of the behavior of real materials. It is then possible to use to model to do computer experiments that examine the effect of various possible microstructural changes on strengthening behavior. For example, the solution predicts that plate-like precipitates strengthen more efficiently than spherical precipitates and that a narrow precipitate size distribution strengthens more effectively than a wide one.

Finally, the model is used to make quantitative predictions about the aging behavior of binary aluminum-lithium alloys. Aluminum-lithium alloys are an ideal model system from two perspectives. First, they have received considerable attention recently as consequence of industrial interest in more complex aluminum-lithium based alloys. Secondly, the strengthening precipitate, δ', has an extremely low misfit strain. As a result, strengthening is dominated by order hardening, the mechanism the solution given here was designed to model.

I.2 Sources of hardening.

The strength of a crystalline material is determined by its resistance to shear. In a perfect crystal, which does not contain dislocations, the theoretical shear strength is determined by the intrinsic lattice resistance to the shear of one atomic plane past another. This stress is extremely high in comparison to the strengths generally observed in engineering materials and has only been approached in single crystal whiskers of high purity. However, dislocations usually are present in crystalline materials, and when they are, it is dislocation glide that controls the shear strength of the crystal. If the crystal is otherwise perfectly homogeneous and dislocations are so few in number that their interaction is negligible, the shear strength corresponds to the force required to overcome the lattice resistance to dislocation motion. In general, this strength is relatively low compared to that measured in practice. The increase in shear strength comes from the fact that crystals generally contain various types of defects, including dislocations, that interact with the gliding dislocation. It is this interaction that causes the phenomenon termed hardening.

A crystalline material is hardened by any inhomogeneity that interacts with dislocations. A dislocation is an elastic and a crystallographic defect. Accordingly, it interacts with any other elastic or crystallographic defect. The defects that harden crystals may be classified according to type:

* point defects -- broadly, defined this category includes all types of solute hardening including that by vacancies or electronic defects.

* line defects -- other dislocations. This type of interaction is also responsible for work hardening.

* surface defects -- grain boundaries and interfaces.

* volume defects -- long and short range ordering, second-phase inclusions and dispersoids, and precipitates.

These hardening mechanisms may either superimpose or interact.

The obstacles to glide can be classified into two admittedly nebulous categories according to whether they are local or diffuse in their nature. Localized, or discrete, obstacles are those whose ranges of interaction do not overlap. Misfit-free precipitates fit into this category since the boundaries of the precipitate can be precisely defined and the precipitates cannot overlap one another. If the range of interaction of the obstacles is not bounded and the elastic interaction between the obstacles is not negligible then the obstacles are termed diffuse. Short range ordering provides obstacles of this type. The ambiguity in these definitions is best illustrated by the case of solute atoms. The strain field of a solute atom extends significantly beyond its physical size, so if the concentration of solute atoms is high, the strain fields overlap and the solute atoms must be considered as diffuse obstacles. However, if the concentration of solute atoms is low enough, the strain field caused by the solutes is negligible in most of the crystal. In this case, the solute atoms may be validly treated as localized obstacles.

Ardell makes a useful differentiation between the diffuse and localized obstacle models in his recent review (1985). He suggests that the statistics of diffuse obstacles (sometimes referred to as Mott statistics) govern those situations in which the dislocation's motion is controlled by its release from obstacles it interacts with at zero stress, whereas local obstacle statistics (Friedel statistics) govern those cases in which the flow stress is controlled by obstacles which the dislocation interacts with and must bypass at finite stress.

Dislocation glide can only be impelled by the shear stress in the glide plane of the dislocation, i.e. the resolved shear stress. The resolved shear stress at which macroscopic deformation takes place is termed the critical resolved shear stress. It is this quantity that correlates to the yield strength of a polycrystalline material.

I.3. Precipitation hardening.

This work will focus on the critical resolved shear stress of alloys hardened by coherent precipitates. For the purposes of this paper, the term "precipitates" is used to refer to coherent precipi-

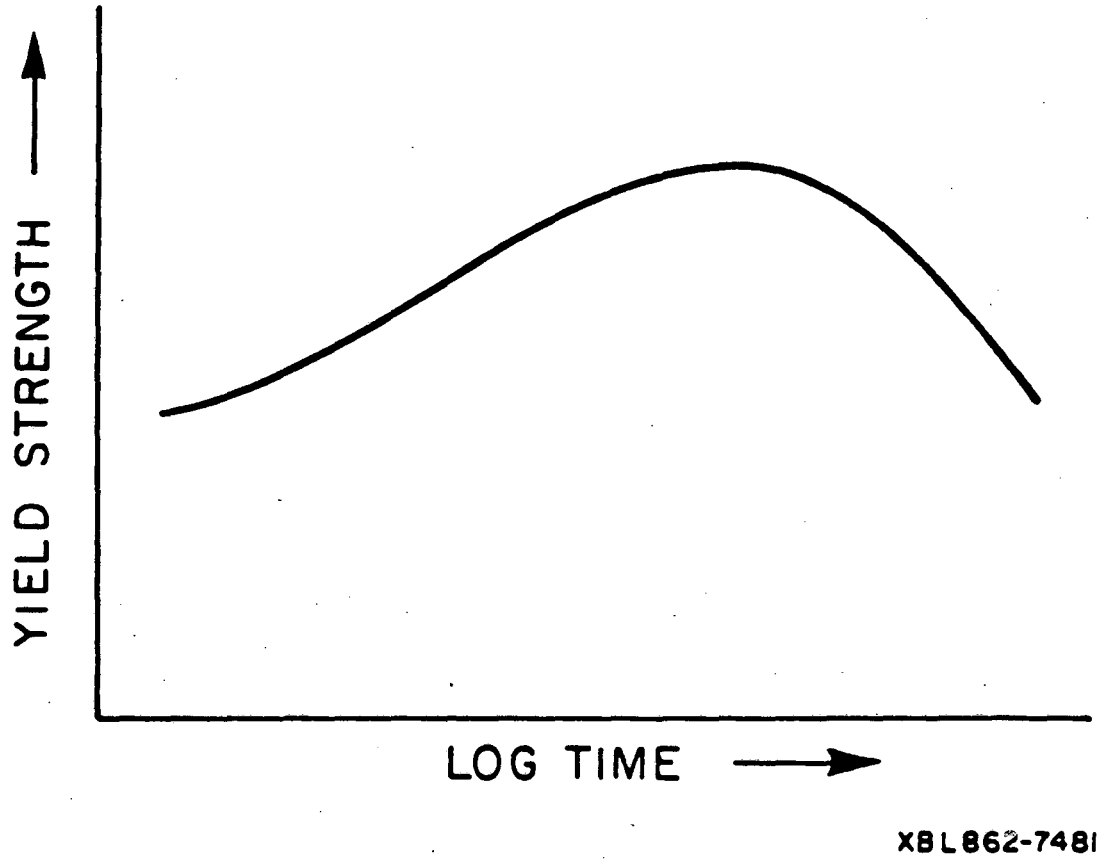

Figure I.1 Schematic plot of yield strength versus aging time for a typical precipitation-hardened alloy.

tates. Precipitates generally behave as localized defects. Since they are coherent with the matrix, they may be sheared by a matrix dislocation under some circumstances. The models applicable to this problem are applicable to hardening by other types of localized obstacles such as incoherent precipitates and dispersoids and dislocations intersecting the glide plane as well.

Models of precipitation hardening were developed to explain the experimentally observed hardening behavior illustrated in figure I.1 exhibited by certain materials when they are aged (often at elevated temperatures) after homogenization. The discovery that this phenomenon corresponds to the appearance and coarsening of precipitates led to a major theoretical effort that culminated in the development of theories that could at least approximate a quantitative explanation for both the rise and fall in strength.

Theories of the flow stress can be divided into two categories: those in which deformation is controlled by the liberation of dislocations that then glide easily (multiplication controlled), and those in which the deformation is controlled by the propagation of available dislocations (Gil Sevillano, van Houtte and Aernoudt, 1981). If the dislocation sources are considered to be dislocations pinned by the strongest obstacles in the microstructure, for instance in subgrain boundaries, then these two mechanisms are not fundamentally different. The microstructure of most precipitation-hardened materials early in the deformation process does not contain a subgrain or cellular substructure or a high density of dislocations. In addition, if the strength is controlled by dislocation sources in the microstructure, then age hardening should not be observed. Consequently, it is reasonable to expect that the critical resolved shear stress in precipitation-hardened materials is controlled by the propagation of dislocations through the array of precipitates.

The strength imparted to the material by the precipitate is determined by the interaction of the obstacle with the dislocation, which is in turn determined by the energy input required for the dislocation to shear or bypass the precipitate. A number of types of interaction have been suggested that may provide the source of the precipitate's resistance to shear. They are:

- modulus -- If the modulus of the precipitate and the matrix are different, the line tension of the dislocation is different inside and outside the precipitate. An obstacle strain field generally represents a modulus defect.

- coherency -- The interaction of the dislocation stress field with the stress field around a misfitting precipitate resists the motion of the dislocation.

- chemical -- The total surface energy of the precipitate is increased due to the creation of a new interface between the precipitate and the matrix in the glide plane of the dislocation.

- stacking fault -- If the matrix dislocation has dissociated into partial dislocations and the stacking fault energies of the precipitate and the matrix are significantly different the passage of the dislocation is impeded.

- order -- The passage of a matrix dislocation creates an antiphase boundary in an ordered precipitate. This boundary has an energy associated with it that must be supplied by the dislocation.

Of these mechanisms, order and coherency hardening are by far the strongest. However, in most real systems several of these mechanisms are operative. For instance, the increase in precipitate-matrix interface responsible for chemical strengthening always occurs when a precipitate is sheared, and the elastic constants of the precipitate and the matrix are almost never identical, so modulus hardening must also always occur. However, if other, more potent, strengthening effects also exist, these energies may be irrelevant to the strengthening provided by the precipitate. When several mechanisms provide significant strengthening, their effects are interactive so that experimental analysis of the strengthening due to each mechanism is complicated.

In general, the interaction of the dislocation with the precipitate may be characterized by a force-distance curve, even when more than one mechanism is operative. The obstacle strength is the determined by the maximum interaction force. The maximum forces due to the mechanisms listed above are spatially displaced from one another, so

that the maximum interaction force for the precipitate is not the sum of the maximum interaction forces for each mechanism. An additional complication is that theoretical calculation of the force-distance curve requires the input of thermodynamic quantities such as the stacking fault energy, various surface energies, the antiphase boundary energy, etc. depending on the operative mechanisms. It is not easy to determine precise values of these energies, and the scatter is often large. As a consequence it is difficult to check the results of strengthening theories experimentally.

The interaction of strengthening effects means that it is difficult to definitively determine which strengthening mechanism or mechanisms is dominant. Most of the experimental studies have been done on a few systems in which a single hardening mechanism is believed to largely explain the observed strength and deformation behavior. Ardell (1985) lists a number of examples in his review, for instance, binary Al-Zn (chemical), Al-Ag (stacking fault), Fe-Cu, Cu-Co precipitates and Al-Zn-Mg GP zones (modulus), Cu-Co, Cu_3Au-Co (coherency) and Al_3Li and Ni_3Al (order). Even in these cases, at least one other mechanism probably makes a measurable contribution to the strength.

II. The Critical Resolved Shear Stress of a Random Array of Point Obstacles.

II.1 The Problem.

The goal of much of the theoretical work in this area has been to solve the problem posed earlier of explaining the rise and fall of strength caused by precipitate coarsening. To approach this problem theoretically it is necessary to phrase it in terms of an idealized model whose consequences can be explored by mathematical or computer simulation approaches.

The first model that contained enough of the essential elements of the physical situation to predict age-hardening was proposed by Friedel (1956) and Fleischer and Hibbard (1963). This model, with only slight modifications, is still in use today.

The durability of this model perhaps lies in its simplicity. It may be stated as four premises.

(1) The material is modelled in terms of its glide plane, a hypothetical plane between two atomic planes, along which the dislocation is allowed to move.

This premise contains the implicit assumption that the dislocation may not leave its glide plane, i.e. cross-slip is neglected.

(2) The precipitates (or other obstacles) are idealized as point obstacles whose mathematical properties are adjusted so that they have the same properties as the physical precipitates. The obstacles resist the motion of the dislocation.

The point obstacle representation is a reasonable idealization if the obstacles are localized.

(3) The distribution of these point obstacles within the glide plane is assumed to be random.

The distribution of precipitates or other obstacles to glide in a cry-

stal is almost never truly random; however, the array is more random than it is regular.

(4) The dislocation is treated as a flexible, extensible string of constant line tension.

It has been known for years that the line tension of the dislocation varies with its character; however, the mechanics of the problem are considerably simplified by assuming that it is constant.

II.2 The Solution

Many workers have investigated the consequences of this model. The difficulties have revolved around the problem of formulating a suitable mathematical description of the model which does not involve major approximations that have qualitative consequences. The analytical efforts were guided by a number of computer simulation experiments, most notably by Foreman and Makin (1966 and 1967) and Morris and coworkers (Morris and Klahn (1974), Hanson (1975), Hanson, Altintas and Morris (1976), Altintas (1978) and Altintas and Morris (1986a)). This section describes the results of the most mathematically accurate formulations of the model. In the interests of clarity, discussion of the evolution of thought in this area will be deferred to Section III.

II.2.1 The "Physical" Picture

If the glide plane is acted upon by a resolved shear stress, a force is exerted on the dislocation. Under the action of this force, the dislocation moves forward until it is prevented from doing so by the obstacles in the array. The dislocation is restrained by the obstacles and bows out in elliptical arcs between them. If the force exerted by the dislocation on an obstacle is great enough, the dislocation may mechanically bypass it either by cutting it or by looping around it. The critical resolved shear stress is the stress at which the dislocation moves freely through the array.

II.2.2 The Strong Line Solution

The results described here are the product of the computer simulation experiments described above and the analytical work of Morris and Klahn (1973) and Hanson and Morris (1975a, 1975b). These studies led to important qualitative changes in our understanding of the critical resolved shear stress.

II.2.2.1 Qualitative Results.

To make the model mathematically tractable, several approximations are introduced. Only athermal glide is considered, that is, thermal activation of the dislocation is not permitted. The difference between edge and screw dislocations is neglected by setting Poisson's ratio υ to zero. The effects of elastic anisotropy and elastic self-interactions are also neglected.

First, the problem may be simplified by treating the dislocation in terms of its configuration, the unique set of pinning points with which it interacts. Since yielding requires the entire dislocation to move through the array, this approach is superior to the alternative of treating the interactions of the dislocation at each point along its line individually. The assumption of isotropic elasticity in conjunction with the assumption that Poisson's ratio is zero means that the dislocation will bow out in circular arcs between the obstacles that define the configuration.

This simplification made possible the most important result of this work, the strong line concept. The strong line is defined as the configuration which offers the greatest resistance to dislocation glide in the array. The computer experiments and the analytical approaches to the problem both led to the conclusion that the critical resolved shear stress is fixed by the strong line in the array and not by some average value of the resistance to dislocation motion. Furthermore, it is clear that the critical resolved shear stress will be controlled by the weakest point on the strong line. The strong line configuration for a given array is unaffected by the initial stress, the initial dislocation configuration and, for the case of athermal glide, the

order in which the dislocation bypasses the obstacles.

The computer experiments also indicated that the randomness of the array lowers the critical resolved shear stress with respect to an ordered array of obstacles. This result was considered surprising at the time, but is a logical consequence of the strong line concept. The randomness of the array has the consequence that some regions of the array will be considerably weaker than a regular square array and some much stronger. Since the critical resolved shear stress is controlled by the weakest point on the strong line, the weak areas are much more important than the strong ones and result in lower strength.

The effect of a distribution of obstacle strengths was investigated by computer simulation and analytically. The strengths were found to be quadratically rather than linearly additive, i.e. they sum according to the relation

$$(\tau_c)^2 = \Sigma_\alpha \, x^\alpha (\tau_c^\alpha)^2 \qquad \text{(II.1)}$$

where x_α is the fraction of obstacles of type α, τ_c^α is the critical resolved shear stress of the array if all obstacles are of type α, and τ_c is the critical resolved shear stress for the array.

II.2.2.2 Analytical solutions

The assumptions and basic equations used below are generalizations of those in Morris and Klahn (1973) and Hanson and Morris (1975a, 1975b) and are summarized here only briefly.

The glide plane of the dislocation is taken to be a square containing a random (Poisson) distribution of point obstacles whose density is given by the mean area, a, per obstacle or equivalently by the characteristic length $l_s = a^{1/2}$. The obstacle properties are randomly selected from a population of e distinct types with fractions x_e. These point obstacles may represent intersections with the glide plane of precipitates, gliding dislocations, forest dislocations, or dislocation loops. The properties of the point obstacles are adjusted so that the interaction of the dislocation with the obstacle is mathematically equivalent to its interaction with the physical obstacle (Morris and

Syn, 1974).

The dislocation is modeled as a flexible extensible string of constant line tension, T, with a Burgers vector of magnitude b in the glide plane. The resolved shear stress impelling glide may be written in dimensionless form:

$$\tau^* = \tau l_s b/2T. \tag{II.2}$$

The configuration of the dislocation is described by a unique set of pinning points. As shown in figure II.1, if the dislocation under the applied stress τ encounters a configuration (i) of obstacles, it will take the form of a circular arc of dimensionless radius R^* between adjacent obstacles, where R^* may be dimensionalized with l_s. The value of R^* is given by the relation

$$R^* = 1/(2\tau^*) \tag{II.3}$$

which is derived in Appendix A. If the distance between any two obstacles along configuration (i) exceeds $2R^*$, then the configuration is transparent to the dislocation and will be mechanically bypassed. If configuration (i) is not transparent then its mechanical stability is governed by the geometry of the configuration and the distribution of obstacle types along it.

The dimensionless force on the kth obstacle in configuration (i) is given by

$$\beta_i^k = F_i^k/2T = \cos(\Psi_i^k/2) \tag{II.4}$$

where F is the force the dislocation exerts on the obstacle, Ψ is the asymptotic angle included by the dislocation at the obstacle and $0 \leq \beta \leq 1$. The geometry of the situation is shown in figure II.2. If the maximum force that an obstacle (k,i) of type α can withstand is β_α, then the dislocation is locally stable at (k,i) if β_i^k is less than β_α, that is if

$$\beta_i^{*k} = \beta_i^k/\beta_\alpha < 1. \tag{II.5}$$

The condition of stability for the configuration (i) is that

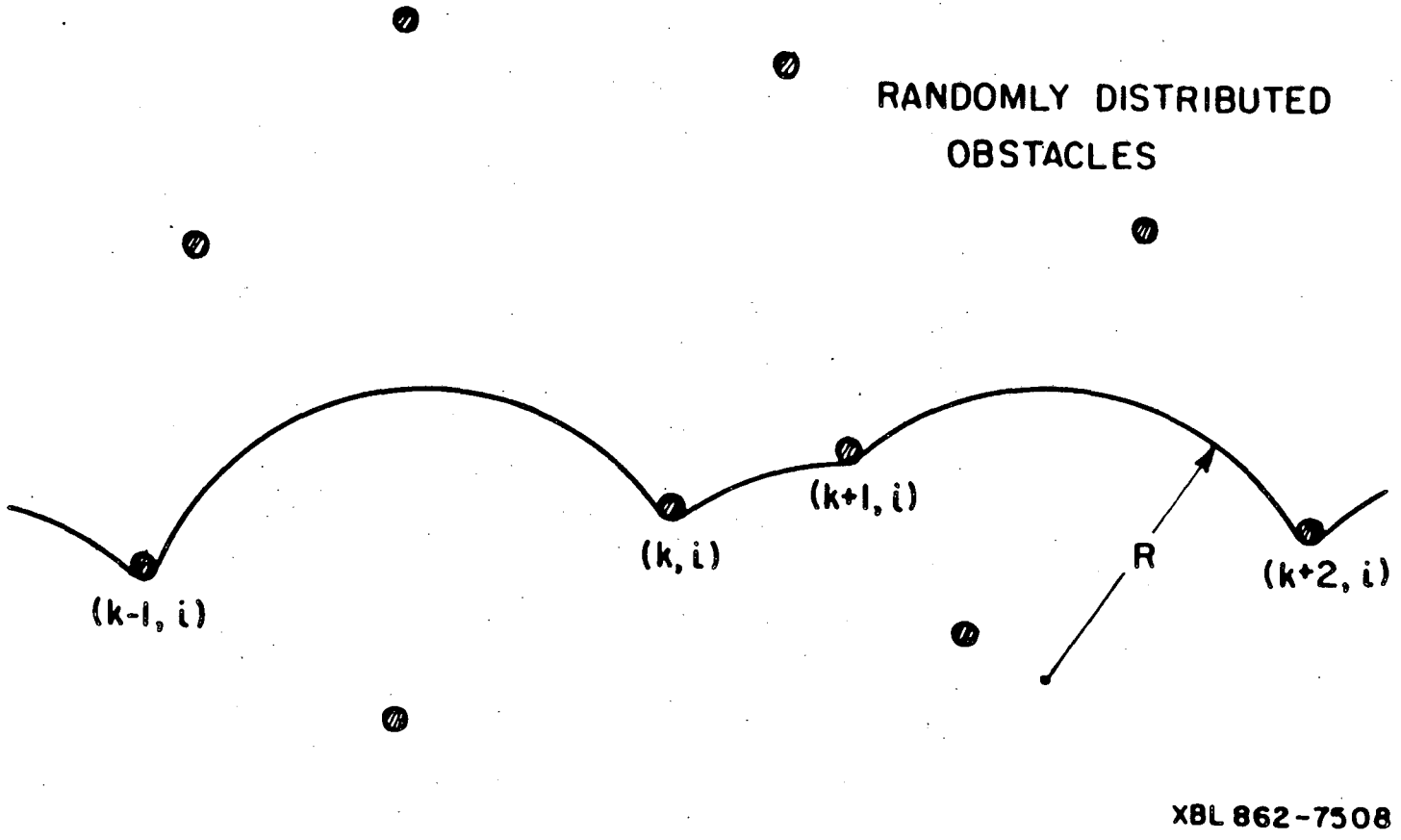

Figure II.1 Sample dislocation configuration in a random array of point obstacles.

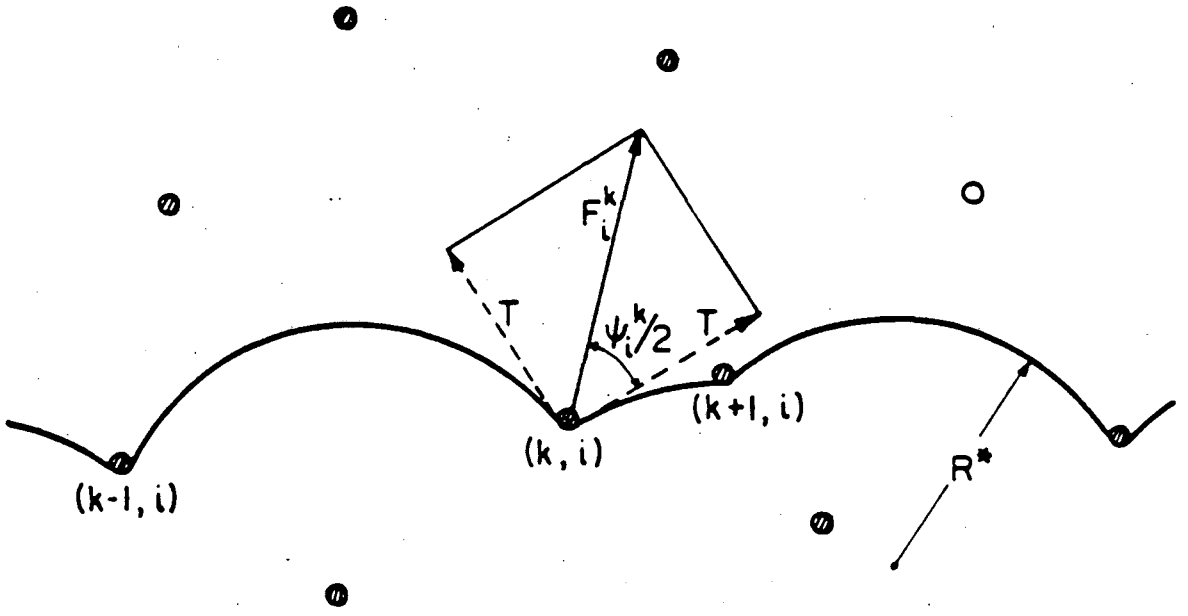

XBL862-7483

Figure II.2 Relationship between the force exerted on the obstacle, the dislocation line tension and the included angle of dislocation bow out.

$$\beta_i^* < 1 \qquad \text{(II.6)}$$

where β_i^* is the maximum of the β_i^{*k}.

The applied stress τ^* uniquely fixes the nontransparent configuration in the array and the forces β_i^k exerted on the obstacles. If τ^* is low enough that there is at least one stable configuration in the array, then the dislocation will be mechanically pinned and unable to glide unless thermally activated. The critical resolved shear stress for athermal glide, τ_c^*, is hence the minimum value of τ^* for which all configurations of the dislocation are mechanically unstable and represents an upper limit on the critical resolved shear stress at finite temperature. At finite temperatures, the critical resolved shear stress is lower than this limit because the dislocation may be thermally activated past obstacles it could not otherwise bypass.

Hanson and Morris (1975a, 1975b) consider the statistics of the dislocation configurations described above to derive the critical resolved shear stress as a function of the obstacle strengths. The approach is sketched here.

Hanson and Morris were the first to generate stable configurations of the dislocation by a circle rolling process illustrated in the figure. Each obstacle which extends the line in a stable fashion is the parent of a new branch. The geometry of circle-rolling is illustrated in figure II.3. A stable configuration requires that there is an obstacle k+1 in the area swept out by the rotating the circle of radius R^* counterclockwise about an obstacle k through the angle

$$\theta_\alpha = \pi - \Psi_\alpha = 2\sin^{-1}\beta_\alpha \qquad \text{(II.7)}$$

where β_α is the strength of the k^{th} obstacle. The angle of rotation is limited by the breaking angle of the last obstacle in the configuration. When all the obstacles are the same strength, the breaking angle θ_c defines the critical resolved shear stress τ_c^*. The circle-rolling process restricts the search so that when the applied stress τ_o^* is greater than τ_c^*, then there is no stable configuration.

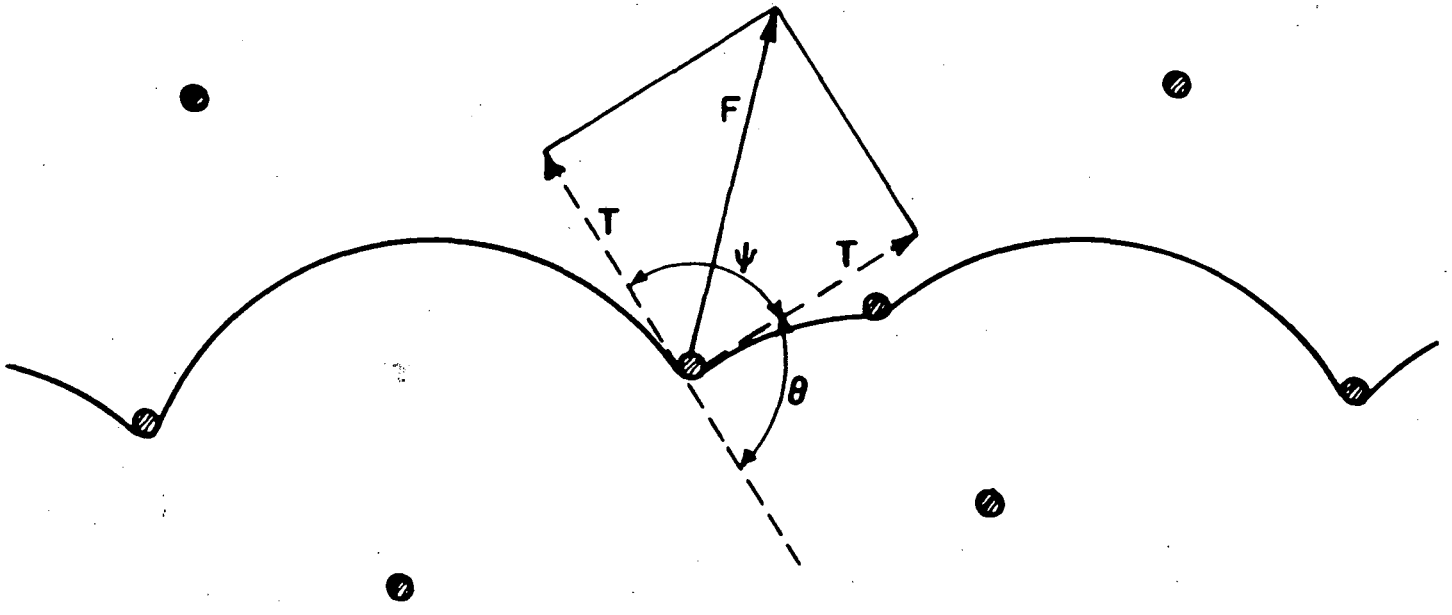

XBL862-7509

Figure II.3 Relationship between the angle Ψ included by the arms of the bowing dislocation and its complement θ.

The value of τ_c^* can be determined analytically using the statistics of branching theories under two constraints. The first constraint

$$\langle n \rangle \geq 1 \tag{II.8}$$

requires that the line does not become extinct (i.e. that the expected number of stable line descendants is greater than one). The second requirement is that the configuration must go across the array. This condition is phrased in terms of the angle ϕ defined in figure II.4, which provides a measure of the straightness of the dislocation. A necessary, but not sufficient, condition for the configuration to go across the array is

$$\langle \phi \rangle = 0. \tag{II.9}$$

The constraints on $\langle n \rangle$ and $\langle \phi \rangle$ can be phrased in terms of the search area of the dislocation, a_o. The search area is defined in terms of the angles θ and ϕ as shown in figure II.5. To maximize the critical resolved shear stress, a lower cutoff on the angle ϕ, ϕ_o, is introduced. It can be shown that if all the obstacles have the same strength, the critical resolved shear stress is given by

$$\tau^* = (1/2)a_o^{1/2}. \tag{II.10}$$

Since τ^* is uniquely determined by the search geometry via the circle radius R^*, the value of τ^* can be maximized within these constraints by a variational analysis of the geometry. The mathematics of this process are given in Hanson and Morris 1975a. The resulting critical resolved shear stress as a function of obstacle strength is shown in figure II.6. For values of $\beta \leq 0.7$, the result may be approximated

$$\tau_o^* = 0.8871\beta_o^{3/2}. \tag{II.11}$$

This result may be inverted to give β_o for a fixed value of τ_o^*. The inverted form is often used in computer simulation. The analysis also gives a distribution of segment lengths along the strong line configuration.

The effect of a distribution of obstacle strengths is also addressed by Hanson and Morris (1975b). The critical resolved shear stress is

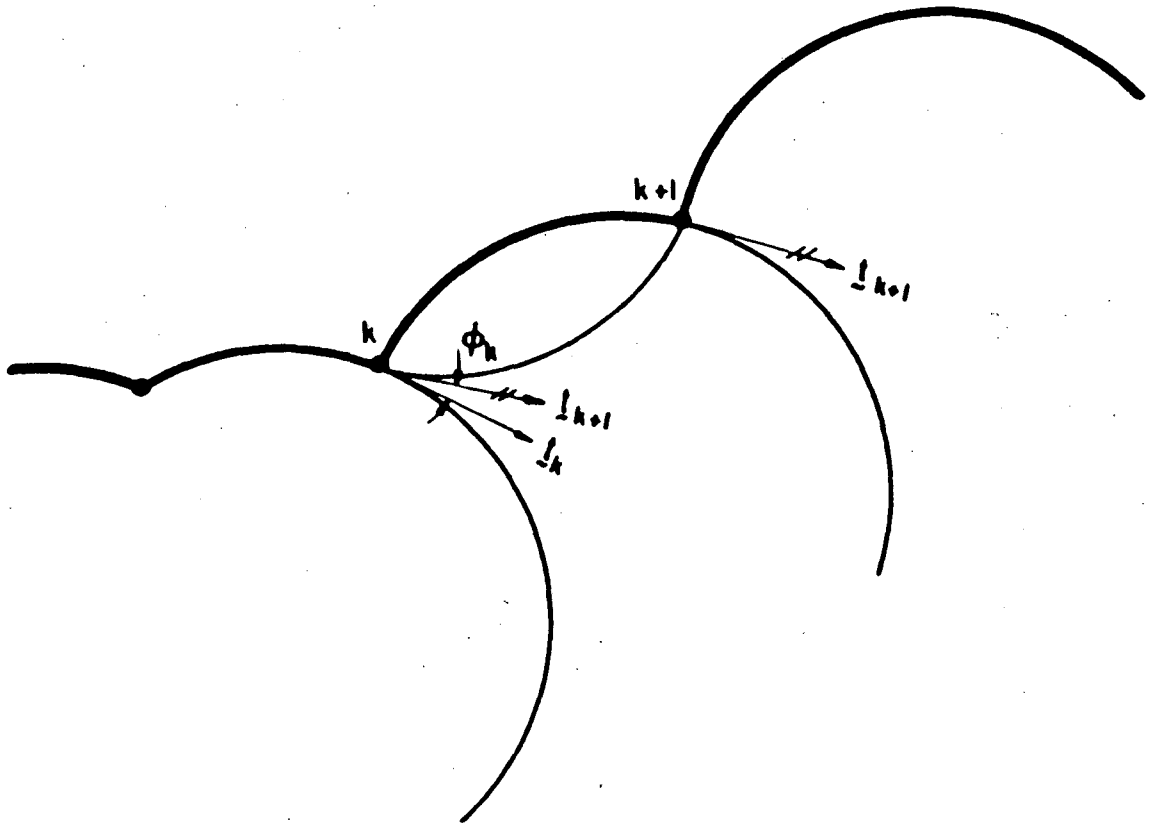

XBL748-6939

Figure II.4 Illustration of the meaning of the angle ϕ that defines the straightness condition for the dislocation. The $\underline{t}$ are the tangents to the dislocation line at the obstacle.

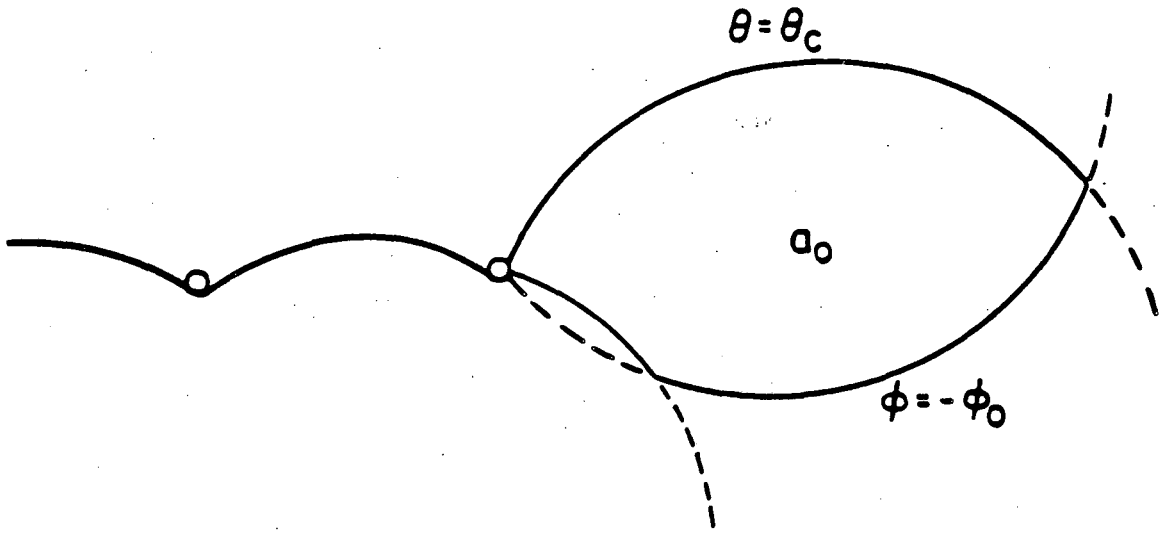

XBL 862-7507

Figure II.5 The search area of the dislocation a_o defined in terms of the angles ϕ and θ.

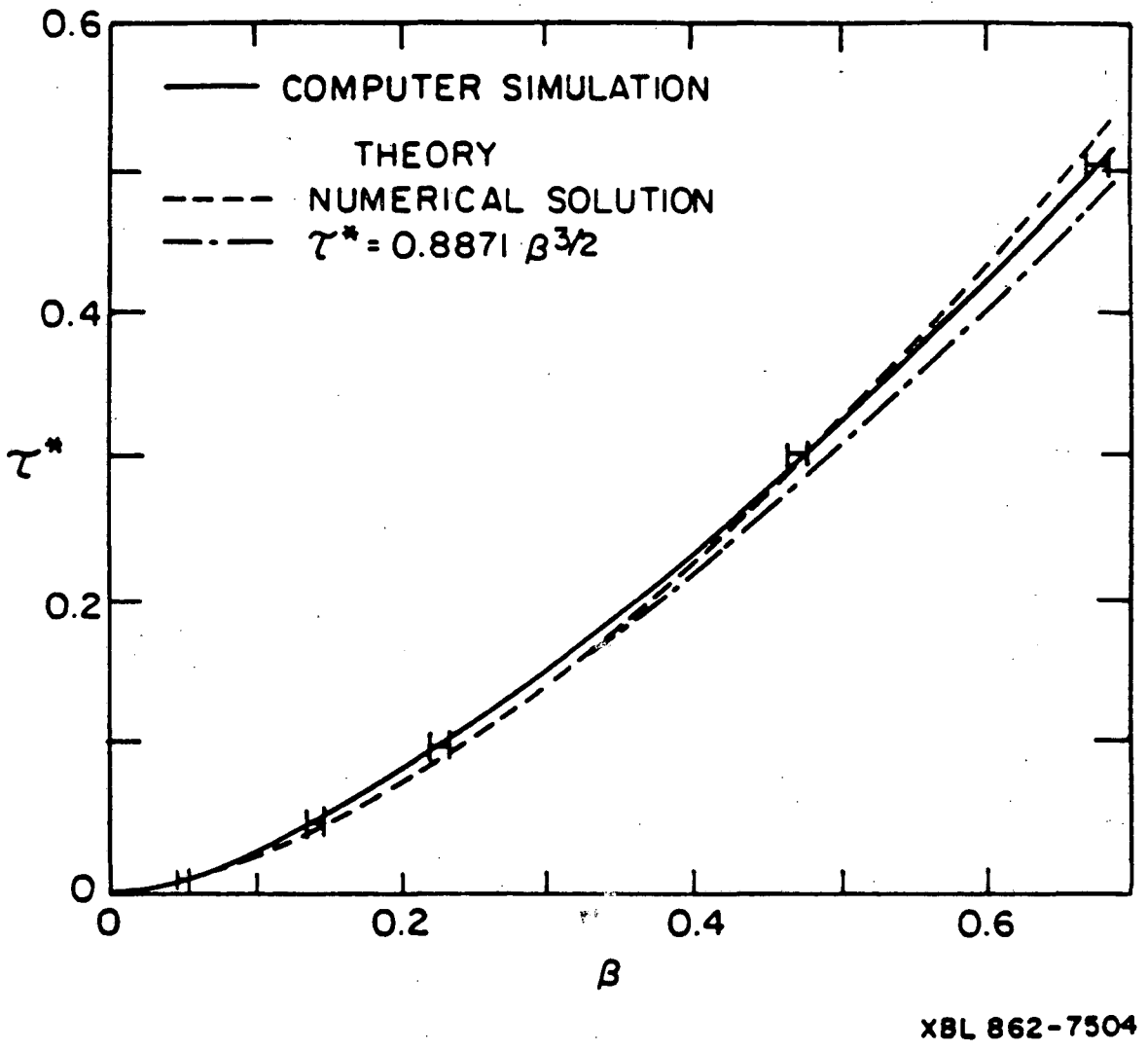

Figure II.6 Comparison of computer simulation results for the Hanson and Morris model to results from the analytical solution (after Altintas, 1978).

found by adding up separately the probability that extending the line from an obstacle α will add an obstacle of type β. On this basis the branches that are considered are given by the sum over all obstacle types

$$\Sigma_\beta \; f^{\alpha\beta} x^\beta \tag{II.12}$$

where $f^{\alpha\beta}$ is the fraction of obstacles in the search area used to extend the line and x^β is the fraction of obstacles of type β. This line of reasoning eventually leads to an expression for τ^* in terms of the search area to achieve a stable line composed of only one type of obstacle

$$\tau_o^* = 1/2[\Sigma_\alpha \; x^\alpha a_o^\alpha]^{1/2}. \tag{II.13}$$

where a_o is the search area of the dislocation line. Comparison with the parallel equation for the identical obstacle case (equation II.10) shows that each term in the sum contains the search area of the dislocation if all the obstacles were of that size. It follows that the critical resolved shear stress for a mixture of distinct obstacles is given by the quadratic sum (equation II.1). The distribution of obstacle strengths along the strong line may also be determined analytically.

III. Evolution of the theory of the critical resolved shear stress for a random array of point obstacles.

Section II.2 introduces most of the important concepts in the theory of the critical resolved shear stress in the context of a single solution to the model posed in Section II.1. To this point in the paper no justification has been provided for either the choice of the model or its solution. The description of the evolution of the theory contained in this section has three major aims. The first is to provide some background for the choice of the model and a justification for the selection of the solution of Section II over other solutions in the literature. The second is to place the model and its solution in their proper historical context through a critical review of the literature. The emphasis here will be on the development of the key concepts and heavily-debated issues that thread through much of the published work. Finally, this review will provide the basis for using the literature to assist in resolving the issues discussed in Section IV concerning the application of the theory to real problems. The ideas in the literature are often transferable to the strong line solution, although much of the discussion is in the framework of other solutions.

Accordingly, this section will begin with a general discussion of the elements of a theory of the critical resolved shear stress that must be contained either in the model or its solution. The various theories of precipitation hardening that have been proposed at one time or another will then be discussed systematically. The organization is not strictly chronological since the solutions have been classified according to whether or not they include the strong line concept.

III.1 Elements of a theory of the critical resolved shear stress

This discussion considers the assumptions that any solution of a model for the critical resolved shear stress must contain and the mathematical approximations that must be specified in order to solve the model.

a. Temperature

Athermal glide must be specified, or a statistical description of thermal activation processes must be included.

b. Glide plane

If the dislocation is constrained to move in the glide plane, the possibility of cross-slip is eliminated.

c. Dislocation parameters

The line tension T of the dislocation as it bows may be taken as constant or allowed to vary with the character of the dislocation (and therefore the bow-out radius of the dislocation).

d. Obstacle parameters

d.1 Spatial distribution. The spatial distribution of the obstacles to glide must either be a random or ordered array since these are the only types of arrays whose statistics are well defined. The density of the array may be characterized in either case by $l_s = n_s^{-1/2}$, where n_s is the number of obstacles per unit area and l_s is the mean square obstacle spacing.

d.2 Strength. The force-distance interaction curve of the localized physical obstacles such as precipitates or other dislocations must be specified. In general this requires representing the physical obstacle by an idealized obstacle whose mathematical interaction with the dislocation is identical to that of the physical obstacle. It may also be necessary to account for the finite size of the obstacle. The strength of the obstacle is defined by the maximum in the force-distance curve. Its physical expression is the critical bow-out radius of the dislocation before it bypasses the dislocation. The obstacle strength β may be defined as before for the geometry of figure II.2

$$\beta = F/2T = \cos(\Psi/2). \qquad \text{(III.1)}$$

e. Matrix parameters

The matrix may be taken to be elastically isotropic or anisotropic. Lattice resistance to motion of the dislocation must be specified

or taken to be zero.

f. Statistics of the obstacle-dislocation interaction

The various models in the literature differ most dramatically here. The dislocation may be treated by considering its overall configuration or by considering each link separately. The mathematical solution to the model must define the dislocation search path through the obstacle array.

g. Definition of critical resolved shear stress.

The critical resolved shear stress is the lowest stress at which the dislocation glides freely through the array. A consequence of the mathematical solution to the model is a condition for the critical resolved shear stress stated in terms of the obstacle strength and distribution. This criterion is generally some type of average over the force to required to bypass the obstacle in the array or some kind of estimate of the strongest configuration of obstacles in the array. It is convenient to define a dimensionless critical resolved shear stress

$$\tau^* = \tau l_s b/2T. \qquad \text{(III.2)}$$

The evolution of the various current models of the critical resolved shear stress is discussed in the following sections. In spite of the increasing sophistication of the statistics used to determine the value of the critical resolved shear stress as a function of obstacle density, distribution and strength, all of these solutions, which include increasingly better approximations to the actual model, lead to relations for the critical resolved shear stress of the form

$$\tau^* = Q\beta^{3/2} \qquad \text{(III.3)}$$

where Q is between 0.8 and 1.2 for an infinite array.

It is worth noting that real arrays are not infinite. There have been extensive efforts to derive critical resolved shear stress results for infinite arrays and equally extensive efforts to approximate infinite array solutions by computer simulation. The purpose of the efforts is to provide a point of comparison between the analytical and

computer simulation results. It is not clear that the value of Q for infinite arrays is a particularly good choice for analyzing experimental data for polycrystalline materials with small or even moderate grain size. However, it may not be worth trying to chose a correct value of Q for each case since there are other large errors in any comparison with experimental data. What a good theoretical value of Q for an infinite array does do is vindicate the assumptions used in its calculation.

III.2 Early theories of precipitation hardening.

Cottrell (1953) has summarized the development of the first precipitate strengthening theories, developed principally by Mott and Nabarro. These theories were designed to explain the observed phenomenon of strengthening followed by softening as the precipitate distribution coarsened. Mott and Nabarro (1940, 1948) postulated that the precipitates could be modelled by an internal stress field that resists the motion of the dislocation. This assumption reduces the problem of determining the critical resolved shear stress to one of determining an appropriate average of the internal stress field in the crystal.

The problem of finding the correct average of the internal stress field was a formidable one at the time. An average of the arithmetic magnitude of the stress leads to a yield strength proportional to the concentration of particles but independent of their spacing. This relationship does not lead to age hardening and softening during precipitate coarsening. On the other hand, the algebraic average of the stresses on a rigid, straight dislocation is zero, which leads to the conclusion that the precipitates have no hardening effect at all. The key to the problem is that the dislocation is not rigid, but flexible, so that different sections of the line move independently. This flexibility has the consequence that the random forces acting on the dislocation line do not cancel one another out. The scaling of the strength with the obstacle spacing comes from the fact that the length of the independently moving segments of the dislocation is determined by the separation of the obstacles. Each segment takes on a radius of curvature dependent on the applied stress and the obstacle spacing. If the dislocation is modelled in this fashion, the observed behavior can be qualitatively explained.

III.3 Average configuration theories.

The solutions to the random array model of the critical resolved shear stress may be divided into two broad categories: those that find the critical resolved shear stress in terms of the average configuration of the dislocation and those that determine it in terms of the strong line configuration. The average configuration solutions preceded the strong line solutions in part because they are mathematically simpler and in part because computer simulation data was not available until the late 1960's.

The average line solutions are lineally descended from the early papers by Mott and Nabarro. The realization that the dislocation must be flexible rather than rigid led to a somewhat misplaced emphasis on the spacing of obstacles along the dislocation line and the way in which this spacing is altered by the flexibility of the dislocation and the applied stress. As described in the discussion of the strong line solution in Section II, the focus on the behavior of individual segments of the dislocation obscures the fact that the critical resolved shear stress is determined by the strongest overall configuration of the dislocation and not by isolated interactions. Nonetheless, many of the solutions mentioned below are formulated by considering the dislocation segment interaction with the obstacles in various limits that lead to straightforward mathematical solutions.

III.3.1 The Friedel solution

The simplest model was proposed by Friedel (1956) to explain thermally activated creep but was later applied by Fleischer and Hibbard (1963) and Brown and Ham (1971) to athermal glide. The model assumes a random array of point obstacles. The strength of the obstacles is defined by the bow-out radius of the dislocation at the time when it bypasses the obstacle. However, the theory is restricted to the case when the obstacles are weak and all have the same strength. The dislocation is assumed to have a constant line tension.

The critical resolved shear stress is defined to be the stress at which "steady state unzipping" can occur. This process is illustrated

in figure III.1. Each time the dislocation bypasses an obstacle and sweeps forward it encounters exactly one obstacle. This condition specifies τ_c since at a stress ε greater than τ_c the dislocation will not encounter an obstacle and will move unencumbered through the array. This criterion is clearly based on the **average** dislocation-obstacle configuration within the array. The statistics of the process are contained entirely within the steady state unzipping condition

$$S_f n_s = 1 \qquad \text{(III.4)}$$

where S_f is the area swept out by the dislocation as it moves forward to a new configuration and n_s is the number of obstacles per unit area. The steady-state unzipping criterion is a rather gross approximation to the random array model described in Section II. It is not put forward as an accurate solution to the model; its virtue is that it leads to a simple mathematical solution.

This theory leads to relation III.3 with Q = 1 (derived in Appendix A) i.e. $\tau^* = \beta^{3/2}$. The value of the obstacle strength β in terms of the array depends on the effective spacing of obstacles that applies. The derivation leading to the expression for the critical resolved shear stress includes the implicit assumption that the obstacles on the dislocation line are collinear. This assumption essentially negates the effect of the randomness of the array!

Given that computer simulation results of Foreman and Makin (1966 and 1967), Altintas (1978) and Altintas and Morris (1986a) discussed later suggest that Q = 0.96 one might question the need for a more sophisticated, albeit physically more realistic, theory. However, the computer simulations also showed that the solution did not even qualitatively describe the motion of the dislocation through the array. Furthermore, attempts to extend the Friedel solution to random arrays of obstacles of different strengths have been unsuccessful (Brown and Ham, 1971).

III.3.2 Modern adaptations of the Friedel solution.

Much of the work that tries to fit the theory of the critical resolved shear stress to experimental data is based on average configu-

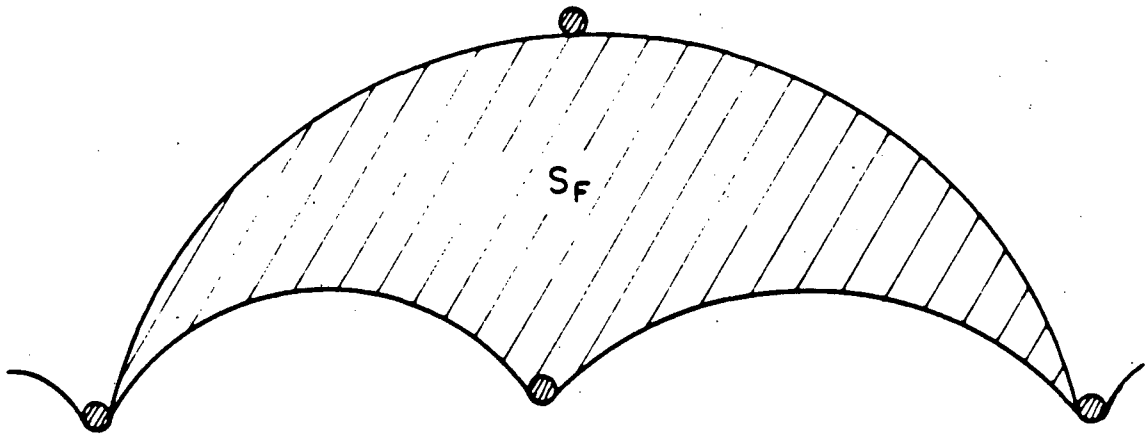

XBL 862-7506

Figure III.1 The area S_f swept by the dislocation when it bypasses the central obstacle as it is defined in the Friedel model.

ration solutions to the random array model. The computer simulation results of Foreman and Makin, discussed briefly in Section II and again later in this section, have been incorporated into this work in spite of the fact that the simulation results clearly showed that the critical resolved shear stress was determined by the strong line and not the average configuration (see, for example, Brown and Ham, 1971). Generally, the results of Friedel were adapted by changing the constant Q in equation III.3 from 1.0 to 0.8 and adding an additive constant in the particle shearing region, and sometimes by adding a second regime in which Orowan looping predominates in which the critical resolved shear stress is proportional to β. In an effort to make the theory applicable to real systems, a number of investigators have modified the solution to include other effects on the critical resolved shear stress (see Section IV). These adaptations generally attempt to describe these effects in terms of the average configuration.

III.3.3 The Kocks solution.

Kocks (1966, 1967) was the first to attempt to simulate the motion of the dislocation through the array. Because he did a geometrical rather than a computer simulation, his solution contains many unsubstantiated assumptions. Nonetheless, his solutions were the first attempt at a mathematical solution that might be more realistic than the Friedel solution described above.

Kocks's development uses a combination of probability theory and geometrical arguments. His probabilistic argument is more sophisticated than Friedel's in that he does not restrict the distribution of obstacles in any way. The major conceptual advance is that Kocks treats the motion of the dislocation past an obstacle as coupled to the motion of the dislocation at adjacent points in the array. The next step in the logical development is to treat the dislocation as fully coupled, that is in terms of its overall configuration, rather than in terms of its segments. The configuration is one of the important concepts that distinguishes the strong line theories discussed in Section III.4. Because Kocks does not use the dislocation configuration, his theory is again formulated in terms of the average dislocation line. His fundamental equation incorporates segment coupling by relating the increase in the area swept by the dislocation to the increase in the probability

that an obstacle pair is penetrable. The full development of these assumptions leads to a theory of the critical resolved shear stress for both infinitely strong (Kocks, 1966) and penetrable (Kocks, 1967) obstacles.

III.4 Strong line statistical solutions

The second class of solutions to the random array problem was suggested by the results of computer simulations by Foreman and Makin (1966, 1967), Morris and Klahn (1974), Hanson (1975) and Hanson, Altintas and Morris (1976). The computer simulation results led to a search for an analytical solution that incorporated the concept that the passage of a dislocation by an obstacle is dependent on the interaction of the dislocation with other nearby obstacles. The realization that the motion of the dislocation past an individual obstacle is coupled to its motion everywhere along the line eventually led to the strong line concept embodied in the analytical solution of Hanson and Morris (1975a, 1975b). This concept is also incorporated in later work, for example in the computer simulations of Schwarz and Labusch (1978).

III.4.1 Computer simulations

III.4.1.1 Foreman and Makin

Foreman and Makin's work (1966 and 1967) represents the first use of a computer to simulate the motion of a dislocation through a large array of obstacles. Their greatest contribution may have been the realization that the random array model for the critical shear stress described in Section II lends itself to computer simulation if the assumptions are properly chosen.

Foreman and Makin made the following simplifying assumptions:

(1) Thermal activation is not permitted. This assumption corresponds physically to either very low temperatures or very high strain rates.

(2) The difference between edge and screw dislocations, elastic anisotropy, and elastic self-interactions are all negligible.

(3) The line tension of the dislocation is constant. This statement has the mechanical consequence that the dislocation bows outward from the obstacles restraining it in a circular arc. The line tension is fixed at the value

$$T = Gb^2/2 \qquad \text{(III.5)}$$

where G is the shear strength of the material.

(4) The strength of a point obstacle is characterized by its breaking angle Ψ. The force to bypass the obstacle is given by

$$F = 2T\cos(\Psi/2) \qquad \text{(III.6)}$$

or $$\beta = F/2T = \cos(\Psi/2).$$

where the angles are defined as they were in figure II.2. This assertion, combined with the assumption that the line tension is constant, converts the determination of the critical resolved shear stress of a particular array by computer simulation to a purely geometric problem.

The basic algorithm involves bowing the dislocation outward using a circle-rolling procedure until it reaches a stable configuration, then increasing the applied stress slightly and bowing the dislocation outward while allowing it to bypass obstacles as necessary until it reaches a new stable configuration. The stress at which no stable configuration could be found is the critical resolved shear stress for the array.

An important contribution of Foreman and Makin to later work is the concept that the critical resolved shear stress for an array is determined by a unique dislocation configuration within the array, later referred to as the strong line. Foreman and Makin realized and verified by computer experiment that this configuration is unaffected by the initial stress, the initial dislocation configuration, and the order of release of the dislocation from unstable points after an increase in stress.

Foreman and Makin also characterized qualitatively the motion of a dislocation through a random array of identical obstacles. For very strong obstacles, long fingers of the dislocation move forward along paths of easy movement eventually encircling groups of obstacles. However, this regime is $0.7 < \beta < 1.0$ which is probably rarely never

reached in practice (Bacon, Kocks and Scattergood, 1973). This point is discussed in more detail in Section IV.2. For obstacles of medium strength (β approx 0.7) the dislocation is not straight, but it cannot easily encircle difficult groups of obstacles. For weak obstacles the dislocation remains quasi-straight at all times. Clearly, the dislocation may never be mathematically straight, because if it were, it could only intersect two point obstacles. The critical resolved shear stress of the array would then be zero.

Foreman and Makin found empirically that the critical resolved shear stress was a function of obstacle strength and spacing. They fit their results to the Friedel-type relation

$$\tau = (Gb/l_s)[\cos(\Psi/2)]^{3/2}. \qquad \text{(III.7)}$$

where l_s is the mean square obstacle spacing.

To get a better fit to their simulation data for obstacles of low and intermediate strengths, they replace l_s with the Friedel effective obstacle spacing

$$l_f = (\mu b/N\tau)^{1/3}. \qquad \text{(III.8)}$$

The agreement is excellent until β is nearly 0.7. At higher values of β the fit is not as good. Equation III.7 is probably the better choice since it can be shown that the circle rolling procedure must lead to an equation of the form

$$\tau^* = Q\beta^{3/2}. \qquad \text{(III.3)}$$

Using the Friedel spacing, which depends on τ, wrongly alters the proportionality. Reasonably good agreement is obtained by retaining the mean square obstacle spacing l_s and inserting the Hanson and Morris value of Q, 0.8871.

Foreman and Makin also point out that the randomness of the array lowers the critical resolved shear stress versus a regular square array, which was not commonly realized at the time.

Foreman and Makin investigated the effect on the critical resolved

shear stress of a range of obstacle strengths. This problem is central since in a real material there will always be a distribution of obstacle strengths. They determined by computer experiment that the quadratic sum rule for two kinds of obstacles (mentioned in Section II.2.2.2 and discussed at more length in Section IV.1) worked reasonably well for values of β less than about 0.7.

III.4.1.2 Morris and coworkers

A large amount of additional computer simulation work was done by Morris and coworkers at Berkeley on this problem. The development of an extremely rapid algorithm made it possible for them to simulate many more cases than Foreman and Makin were able to examine, in addition to confirming their results. The formulation of the computer model made it possible to examine a wide variety of situations within a single framework. These included simulations of thermal activation (Morris and Klahn, 1973), multiple barrier types (Hanson, 1975; Hanson, Altintas and Morris, 1976; Altintas, 1978; and Altintas and Morris, 1986b), multiple dislocations (Hanson and Morris, 1978) and inhomogeneities in plastic glide (Altintas, Hanson and Morris, 1976a and 1976b).

III.4.2 Analytical strong line solutions

Two analytical strong line solutions for the critical resolved shear stress of a random array of point obstacles exist. The first was derived by Hanson and Morris (1975a, 1975b). The Hanson and Morris solution, with a few changes, has been used by Melander and Persson (1978a, 1978b, 1978c) to predict experimentally determined aging curves. The second solution, a modification of the Hanson and Morris approach, was proposed by Labusch (1977) a few years later.

It is perhaps appropriate here to reiterate a point made at the beginning of this section. The value of Q obtained by analytical solution for an infinite array represents an important, if imperfect, point of contact between the analytical and computer simulation solutions. In addition, the solution may be characterized by other properties of the strong line. Much space in the literature has been devoted to discussions over the superiority of one analytical solution over ano-

ther on the basis of how these parameters compare to the computer simulation results. Unfortunately, this type of comparison is inherently limited, since it ignores the important issue of whether or not the solution contains the essential qualitative elements of a good description of the critical resolved shear stress in favor of quantitative measures.

However, for what it is worth, the historical benchmark for the analytical solutions is the value of Q obtained by Altintas (1978) for very large arrays; Q = 0.96.

III.4.2.1 The Hanson and Morris solution

Hanson and Morris derived the first analytical solution that incorporated the assumptions and circle-rolling procedures of the computer simulation work. The derivation is included in Section II and will not be repeated here.

The key contributions of the solution (also discussed in Section II) are worth mentioning again. The most important conceptual advance is that the unit process in dislocation motion is not the progress of a single segment of the dislocation, but the bypassing of a configuration. Given the concept of the configuration, it is possible to see that the critical resolved shear stress is determined by the strongest configuration the dislocation must bypass, a result foreshadowed by the computer simulation work described above. However, it is not at all obvious that there should be a strongest line in an infinite array, and therefore a critical resolved shear stress. The Hanson and Morris solution contains the first analytic proof that such a line exists. By deriving the solution using the statistics of a process known from computer simulation to generate stable dislocation lines, the circle-rolling process, Hanson and Morris ensured that their solution would approximate the model reasonably well. This solution was the first analytical solution to the critical resolved shear stress of a random array of point obstacles to do so. Finally, Hanson and Morris (1975b), were the first to derive a procedure for summing the effects of obstacles of different strengths.

As illustrated in figure II.6, the value of Q that results from the approximate mathematical solution to the final equations in the

Hanson and Morris analysis (0.8871) leads to lower values of the critical resolved shear stress than either the computer simulation results or the numerical solution of the equations.

III.4.2.2 The Labusch modification

Labusch (1977) has revised the Hanson and Morris solution to reflect the statistics of a somewhat different strategy of selecting the strongest configuration in the array. His rationale for doing so is that the Hanson and Morris value of Q, 0.8871, is significantly below the result of 0.96 from computer simulation for large arrays. Labusch's final answer, 0.95, is closer to the simulation results (see figure III.2). Although the spread between these results is only a few percent, the difference is relevant if it has implicit physical consequences. Since there is a greater spread between the other parameters used to characterize the solution, it seems likely that there are important differences between the models. Despite the apparently good agreement of the Labusch solution with the computer simulation data, it is not obvious that it is the superior theory. The following discussion considers the differences between the two solutions.

Hanson and Morris find the strength of the strong line by fixing the expectation values of various parameters of the array on the strong line. The theory is a prescription for finding a strong line whose strength is within ε of the strength of the strongest line in the array. For an infinite array, there are infinitely many distinguishable lines which meet this criterion; the solution does not necessarily identify all of them. Consequently, the solution should accurately predict the expectation values of parameters on the strong line, but not the actual distribution of those parameters.

The most important parameters of the strong line are the distribution along it of obstacle strengths $\rho(\beta)$, of segment lengths $\rho(1^*)$ and of directional change $\rho(\emptyset)$. These distributions may be obtained both by conputer simulation and by analytic solution. The solutions obtained by computer simulation (Altintas and Morris, 1986b) are compared with the results of Hanson and Morris and Labusch in figures III.3, III.4 and III.5.

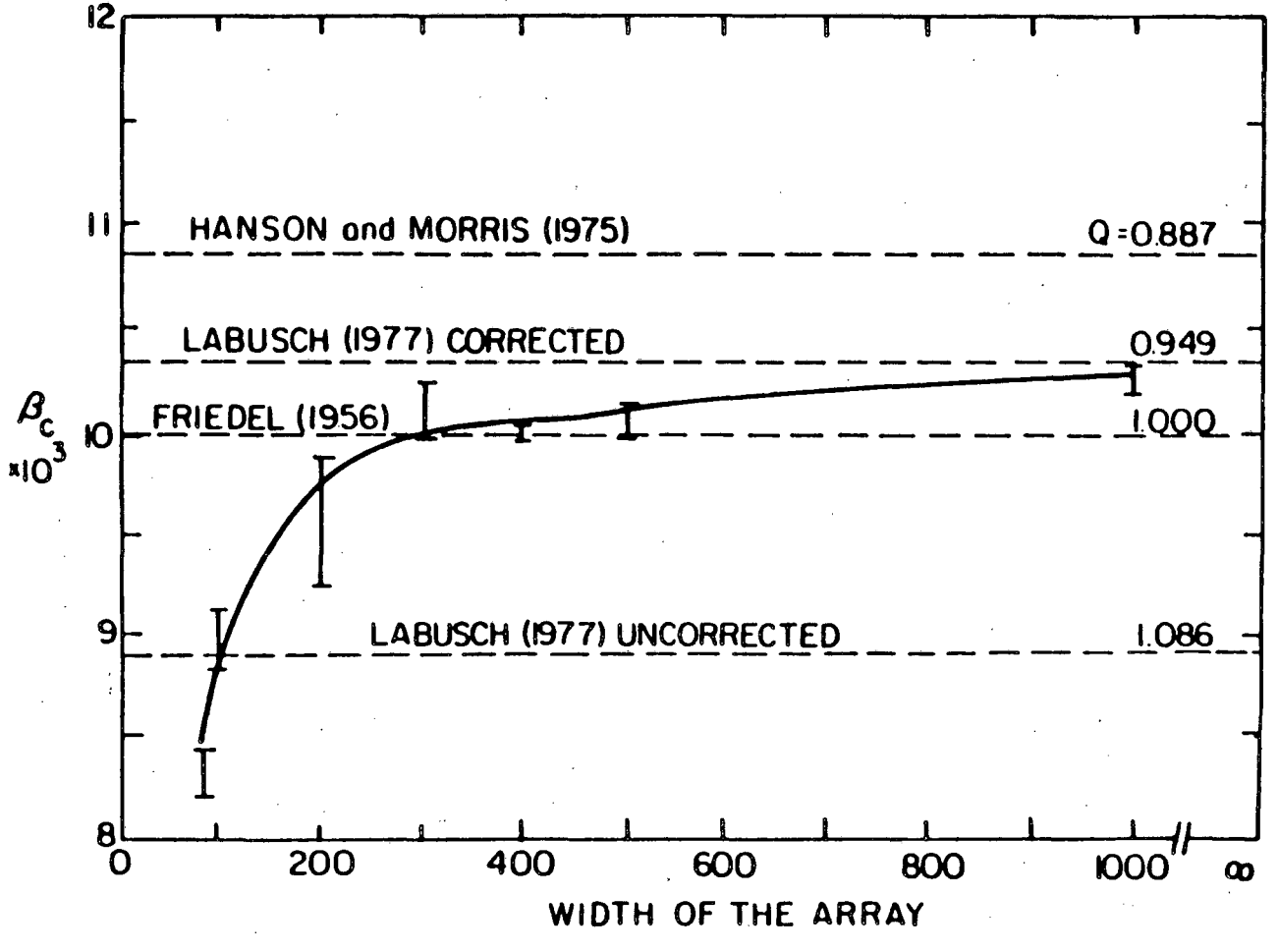

XBL 863-7531

Figure III.2 Comparison between theoretical solutions for the critical resolved shear stress and computer simulation results as a function of array width.

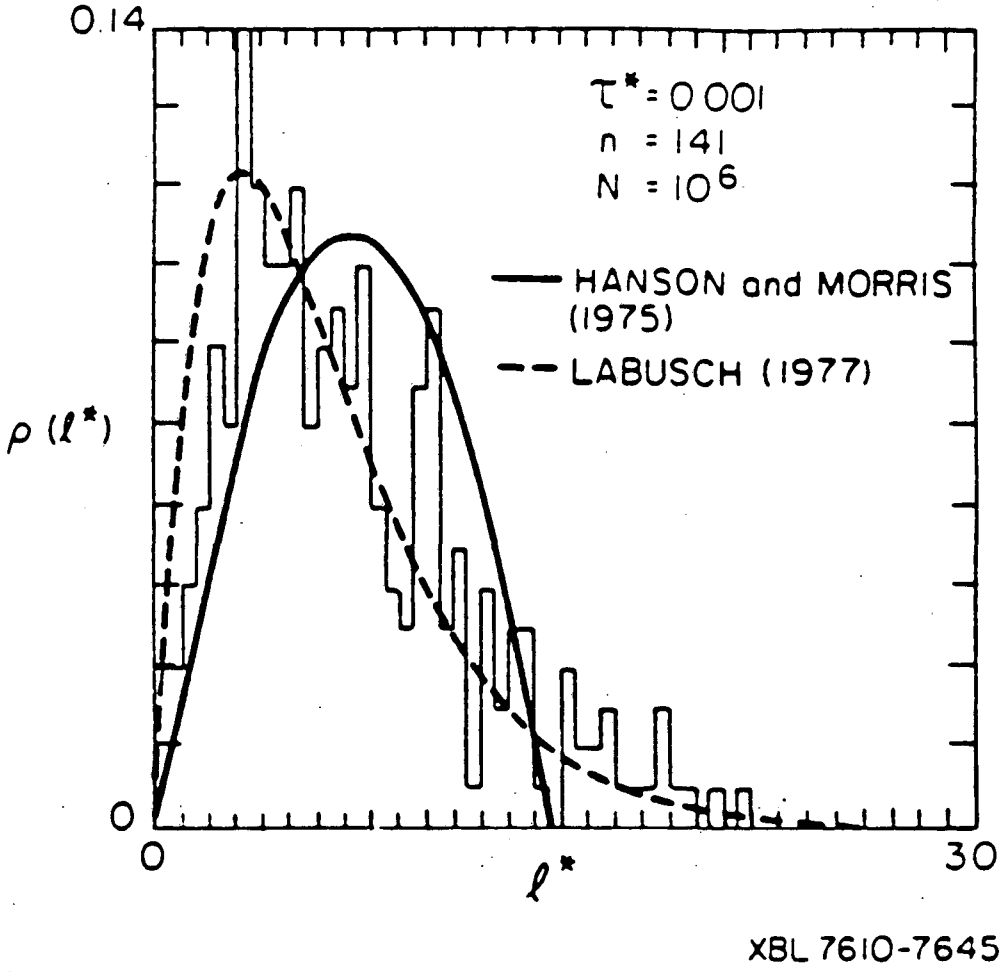

Figure III.3 Comparison between computer simulation results for the strong line solution and theoretical solutions for the distribution of segment lengths along the strong line (from Altintas, 1978).

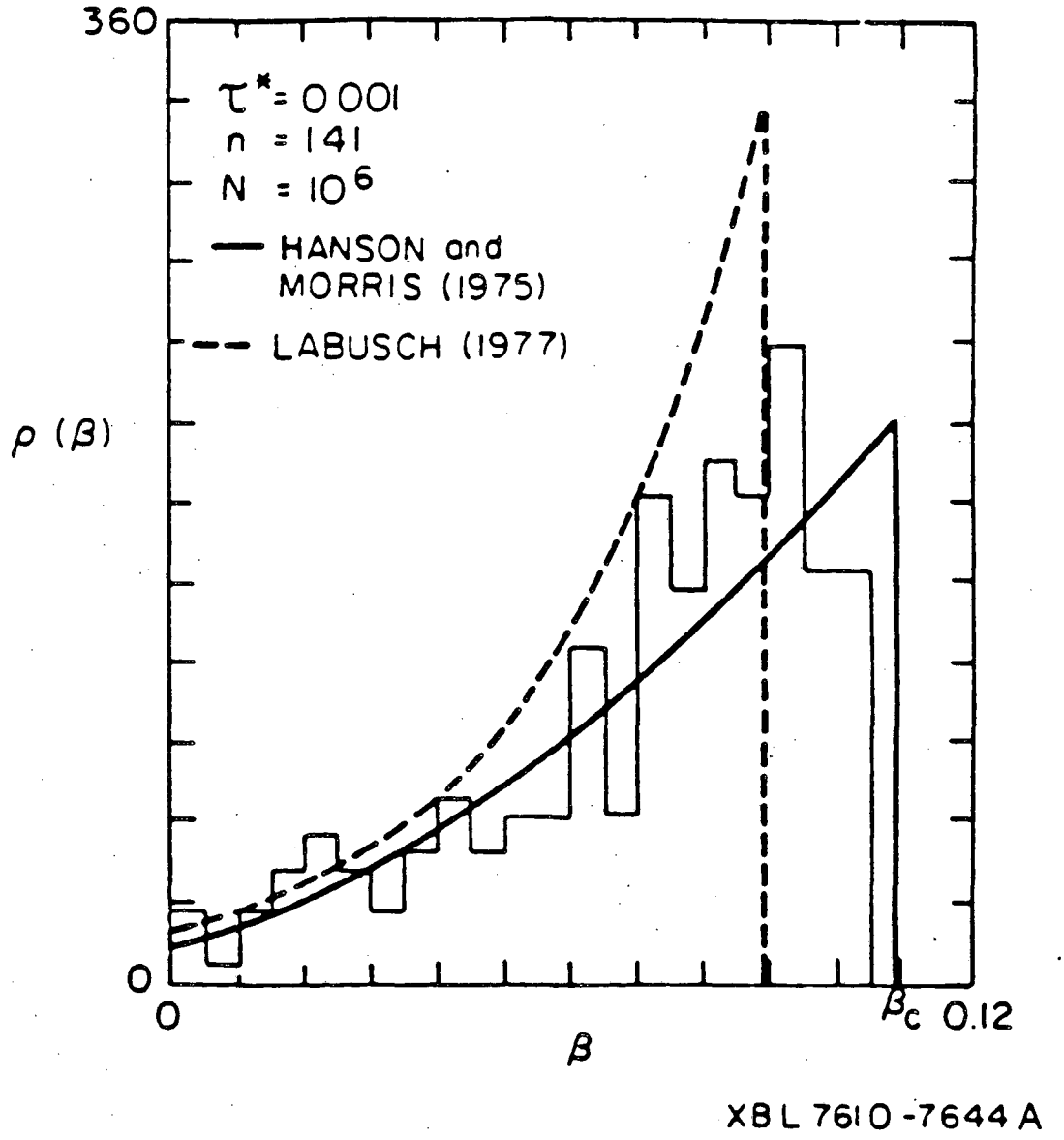

Figure III.4 Comparison between computer simulation results for the strong line solution and theoretical solutions for the distribution of obstacle strengths along the strong line (from Altintas, 1978).

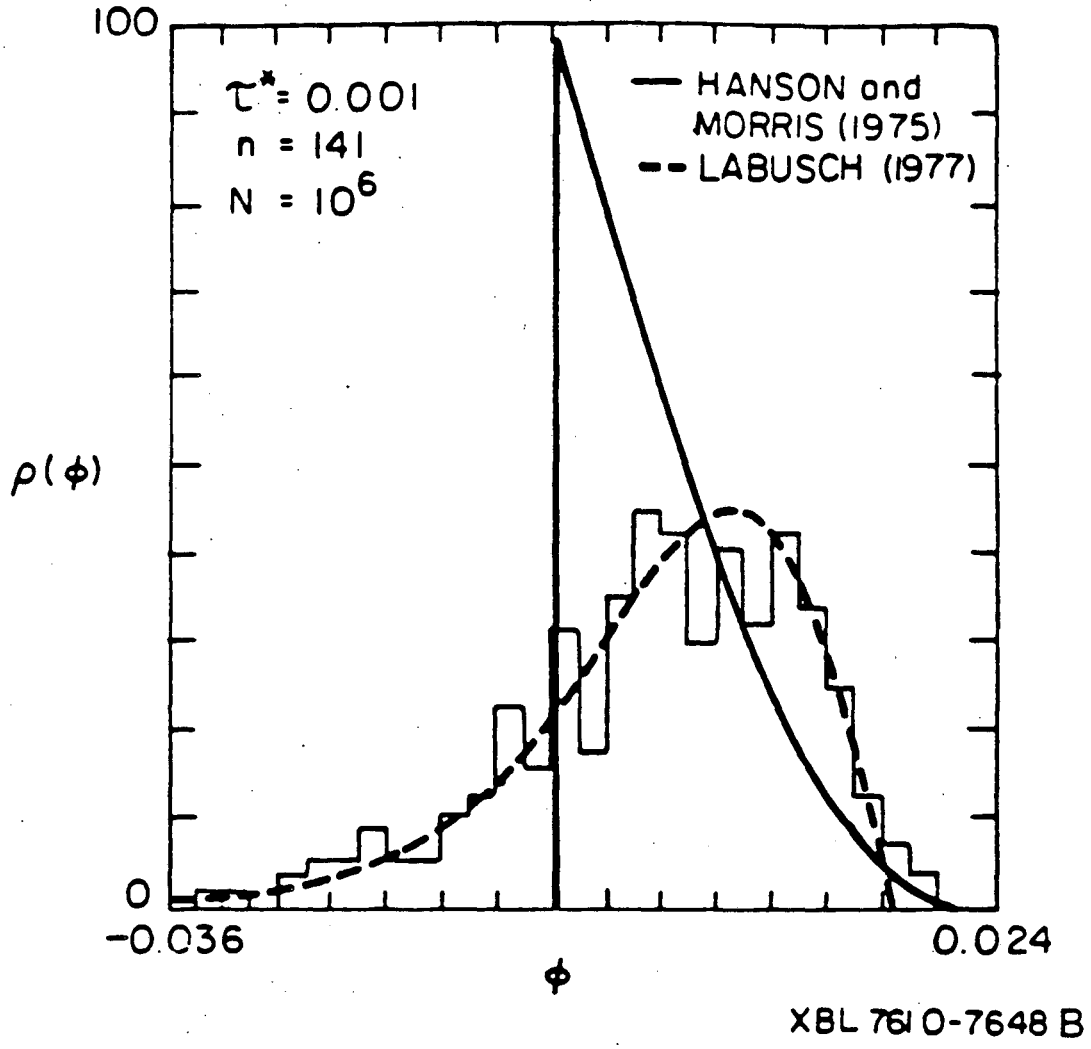

Figure III.5 Comparison between computer simulation results for the strong line solution and theoretical solutions for the distribution of angular changes in direction along the strong line (from Altintas, 1978).

Comparison of the analytic solutions to computer simulation results indicates that the Hanson and Morris solution does a good job of predicting $\langle 1^* \rangle$ and $\rho(\beta)$ but not of $\rho(1^*)$ or $\rho(\emptyset)$. The value of $\langle \emptyset \rangle$ is fixed in the solution. The failure of the theory to predict $\rho(\emptyset)$ is not surprising since a lower cutoff on $\emptyset$ is also employed in the solution. The distribution $\rho(1^*)$ has an upper cutoff not found in computer simulation. Since 1^* and $\emptyset$ are related, the upper cutoff is probably tied to the cutoff on $\emptyset$. The rather good match for the distribution of forces along the strong line $\rho(\beta)$ seems rather surprising; however, it may be a direct consequence of the fact that the theory is formulated to ensure that the strength of the line is arbitrarily close to the strong line. This condition may imply a reasonably accurate distribution of forces.

Labusch's approach is to begin by counting all possible stable lines at a given stress level. In theory all the lines with strength within ε of the strong line are examined. This comprehensiveness may explain why the Labusch solution leads to distributions of 1^* and $\emptyset$ that are more similar to the computer simulation results than those derived by Hanson and Morris. These distributions are determined relatively early in the solution, before Labusch uses two questionable arguments that together bring his value of Q close to that found in computer simulation.

Labusch's first calculation gives Q = 1.1862, which is much larger than the computer simulation results for large arrays. He corrects this value downward by arguing that some of the lines he has counted are degenerate because they can be generated by more than one potential parent line. On this basis he adjusts his value of Q to 0.949, which is very close to the computer simulation results. It is odd that an argument about degeneracy should change the value of Q since the strength of the strong line should not be affected by the number of times it is counted. The flaw in the mathematics may be that in calculating W in terms of his partition function Z (Labusch, 1977, p. 4551), Labusch argues that the integral may be simply evaluated because it is zero almost everywhere. This simplification may be equivalent to looking only at the most probable string of parents of the strong line. If this is the case, any degeneracy in the solution is eliminated.

Labusch also finds an upper limit on the the value of Q that is

lower than his original value. His essential point seems to be that the strongest line may not be accessible to the dislocation as it moves through the array since the direction of dislocation motion is predetermined. However, it seems obvious by definition that the strong line must be reached as the dislocation moves through the array. It is possible that Labusch description of a stable line allows some totally impossible lines. Consequently, it is possible that this correction may apply to his original solution. However, Labusch also applies this correction to the Hanson and Morris solution. Since the Hanson and Morris solution includes a prescription for finding stable lines, these lines must be accessible, and the dislocation must reach the strong line; the correction cannot apply.

In conclusion, although the Labusch solution may be a good way of examining $\rho(l^*)$ when this distribution is relevant, it is not an improvement on the Hanson and Morris solution. The overestimate of Q in the original Labusch solution may indicate more serious flaws in the derivation; for example, Labusch does not prove that the line he describes exists. It is also not clear whether the Labusch solution leads to a simple rule for summing the effects of obstacles of various strengths like the quadratic sum approximation derived by Hanson and Morris. Barring a new approach to the statistics of the problem, the Hanson and Morris strong line solution would seem to the best strong line solution available, despite the fact that it leads to a value of Q slightly below that obtained by computer simulation.

III.4.3 Haasen and Labusch theory of precipitation hardening.

The most recent theory of precipitation hardening is an adaptation by Haasen and Labusch (1979) of work by Schwarz and Labusch (1978) on solution hardening. In his review, Ardell (1985) argues that the extension to precipitation hardening is not valid. He claims that the "successes" of the theory in the analysis of experimental data for order hardening are achieved only with unreasonable choices of adjustable parameters such as the line tension and the antiphase boundary energy. However, the approach cannot be entirely ignored since it has become a popular way to analyze experimental data for precipitation hardening (Haasen and Labusch, 1979; Nembach, 1981; Reppich, Schepp and Wehner, 1982; Thompson and Brooks, 1982; Grohlich, Haasen and Frommeyer, 1982). Accordingly, the theory will be summarized here.

The Schwarz and Labusch solution is based on an empirical fit to computer simulation results. The simulation is intended to address a variety of situations encountered in solid solution hardening. The solution considers both localized and diffuse obstacles and cases for which the inertial effects range from negligible to dominant. The only case that will be examined here is that of dislocation motion obstructed by point obstacles when inertial effects are negligible (i.e. overdamped motion). These conditions correspond to those assumed in the other theories discussed in this section.

Schwarz and Labusch seek a strong line solution for the critical resolved shear stress of a random array of obstacles. In common with the strong line solutions discussed above, the Schwarz and Labusch simulation assumes that the strength of the obstacles is determined by the maximum in the force-distance curve for the dislocation-obstacle interaction and that the dislocation has a constant line tension. The major addition in this simulation is the inclusion of η, a dimensionless parameter that describes the range of the dislocation-obstacle interaction. Schwarz and Labusch do not provide an analytical solution that takes this parameter into account. For the non-inertial case, the critical resolved shear stress as a function of η is determined empirically by fitting the computer simulation data. The result is

$$\tau^* = 0.94\beta^{3/2}(1 + \eta m) \qquad \text{(III.9)}$$

where m is a constant determined by a least squares analysis of the data. The value of m depends on the shape of the force-distance profile of the obstacle.

The limitation of the Schwarz and Labusch solution is that early in the derivation (1978, p. 5175) the calculations are restricted "to the case of weak obstacles ($F \ll T$) in which case the dislocation remains almost straight." This restriction is not severe for solid solution hardening, which the simulation is intended to address, but it is clearly inappropriate to consideration of precipitation hardening. This point appears to have escaped those who have applied the theory to precipitation hardening. The restriction on the results is much stronger than weak restriction contained in the Hanson and Morris solution that β be less than 0.7 (or equivalently $F < 1.4T$). As Ardell (1985) points out, the requirement that β be small allows the radius of curvature of the dislocation to be given simply by

$$R^{-1} = d^2y/dx^2 \qquad \text{(III.10)}$$

which is only a good approximation for the exact equation

$$R^{-1} = \frac{d^2y/dx^2}{[1 + (dy/dx)^2]^{3/2}} \qquad \text{(III.11)}$$

if the dislocation is nearly straight. As a result, Ardell suggests that a practical limit on the validity of the Schwarz and Labusch computer simulation results is $\beta < 0.3$.

The first paper to apply the Schwarz-Labusch theory of solid solution hardening to precipitation hardening is Haasen and Labusch (1979). The first equation in the paper for the additional flow stress due to precipitate particles at small volume fractions is attributed to Fleischer (1964) although it is nowhere to be found in that paper. A derivation similar to that given by Nabarro in his reviews of solid solution hardening (1972, 1977, 1985) is given in Appendix B. A derivation of the second equation (for large volume fractions of precipitates) can be found in Labusch (1970, 1972) or in the review papers by Nabarro and is also included in Appendix B.

Haasen and Labusch (1979) use equations 1 and 2 of their paper to describe the critical resolved shear stress associated with a continuum of values of η_o, a parameter proportional to η that describes the range of the dislocation-obstacle interaction. They use the formulas of Schwarz and Labusch to interpolate between the limiting cases of equations 1 and 2. Unfortunately, for $\beta>0.3$, the restrictions on the Schwarz and Labusch derivation make this approach invalid.

There are several other objections to the methods used by Haasen and Labusch and their successors. Haasen and Labusch convert the solution hardening results of Schwarz and Labusch to the case of precipitation hardening by replacing c, the number of solute atoms per unit area, with c', the areal density of particles in the slip plane (l_s^{-2}). They define the areal density in terms of particle size by

$$c' = v/r^2 \qquad \text{(III.12)}$$

where v is the volume fraction of particles, and r is chosen so that c' is the areal density. The value of r is related to the size of the particle, but is not necessarily the particle radius. For example, in an earlier paper Kocks, Labusch and Schwarz (1976) vary r to account for the diffuseness of the obstacle in addition to varying η_o. This procedure adds another adjustable parameter to the solution.

Haasen and Labusch further argue when the volume fraction of precipitates is relatively high, diffuse obstacle statistics should apply, since the dislocation will see many obstacles at once. This point is not all obvious, nor is it clearly confirmed by experimental data (Munjal and Ardell, 1975; Ardell, Munjal and Chellman, 1976). As Ardell (1985) points out, a point obstacle (or collection of point obstacles) with a diffuse range of interaction and a finite obstacle with a range of interaction essentially localized to the obstacle are not the same thing. In the case of a non-misfitting ordered precipitate, the range of interaction is entirely localized to the particle and the dislocation is influenced by this force only when it is within the precipitate.

A final point is that the critical resolved shear stress is controlled by the maximum force each obstacle can exert on the disloca-

tion. The question of whether much smaller attractive or repulsive forces such as those due to the stress field of a misfitting precipitate can significantly alter the motion of a dislocation which has already bypassed the particle by acting as a weaker pinning site at a new location remains unanswered. To answer this question requires reexamining the original definition of a point obstacle and whether it applies to this type of physical situation.

IV. Application of the CRSS model to real systems

The Hanson and Morris solution and the various other solutions described in Section III are limited by the idealizations contained in the model of the critical resolved shear stress described in Section II. Each solution includes additional assumptions needed to simplify the mathematics or computer simulation. The choice of assumptions is restricted by the desire to keep the solution as simple and general as possible. However, if these solutions are to be applied to real systems, they must be reassessed. First, the parameters of the imaginary model system must be related to properties of the physical system. Second, the assumptions and idealizations in the model and its solution must be considered with respect to specific systems.

In this section, a series of issues will be discussed which relate to the application of the model to real systems. Although most of these issues must be considered to apply any of the solutions described in Section III, the focus in this section and throughout the remainder of this paper is on the Hanson and Morris strong line solution outlined in Section II. The emphasis is on the problem of predicting the age hardening behavior of a material strengthened by coherent ordered precipitates. The applications topics are discussed in order of increasing specialization, beginning with those relevant to all types of obstacle-controlled hardening and finishing with those specific to alloys hardened by coherent ordered precipitates.

The following is a brief summary of the issues discussed in this section.

IV.1 Obstacle strength sums. The effect of obstacles of various strengths must be accounted for. For comparison with experimental single crystal data, the matrix contribution must be included. For polycrystals, grain boundary strengthening must also be considered.

IV.2 Line tension. The line tension of the dislocation varies with the degree of screw or edge character. The effect of finite obstacles on the dislocation bow-out and elastic self-interaction of the dislocation is considered.

IV.3 Dislocation character. Since macroscopic deformation requires the glide of both edge and screw dislocations, the critical resolved shear stress will be controlled by the type of dislocation that is most difficult to move through the obstacle array.

IV.4 Precipitate distribution. To predict the age hardening behavior of a precipitation-hardened material the precipitate size distribution and its coarsening behavior must be understood.

IV.5 Obstacle Strength. The strength of the obstacles to glide provided by the ordered precipitates must be quantified.

IV.6 Superdislocations. Deformation in materials hardened by ordered precipitates occurs by the motion of coupled dislocations that magnify the applied stress at the obstacle.

IV.1 Summing of strengthening mechanisms.

IV.1.1 The need for superposition laws.

Because dislocations interact with any and all crystallographic or elastic defects present in a material, it is clear that predicting the strength of any real material requires an understanding of how various types of strengthening mechanisms superimpose. The debate on the general problem has been somewhat confused by the fact that several distinct cases must be considered, all of which generally are discussed under the heading of superposition. The superposition problems may be divided into three distinct areas according to the type of strengthening mechanism: obstacle-controlled, friction-controlled, and interface-controlled. The goal in each case is to determine the increment in strength due to the particular microstructural feature in question.

IV.1.2 Superposition of obstacle-controlled strengthening mechanisms.

An obstacle-controlled strengthening mechanism is one whose source is a distinct, relatively localized microstructural feature that may be modelled as a point obstacle. The model for the critical resolved shear stress discussed in Section II and the Hanson and Morris strong line solution both consider the effect of such obstacles. There are actually three different kinds of superposition effects that must be considered. Some of these have been discussed previously; however, it seems appropriate to consider all three cases in a single discussion.

The first of these is the superposition of several strengthening mechanisms for a single physical obstacle. The summation is done in the course of computing the force-distance curve for the interaction of the dislocation with the physical obstacle. The problem here is much simplified by considering only athermal glide, since in that case the strength of the obstacle is determined only by the peak in the force-distance curve. (If thermal activation is considered, then the entire force-distance curve is relevant (Morris and Klahn, 1973).) A schematic plot of the summation of two interaction forces (for instance, the misfit and order interactions for the first dislocation to shear a misfitting, ordered precipitate) is shown in figure IV.1. For this

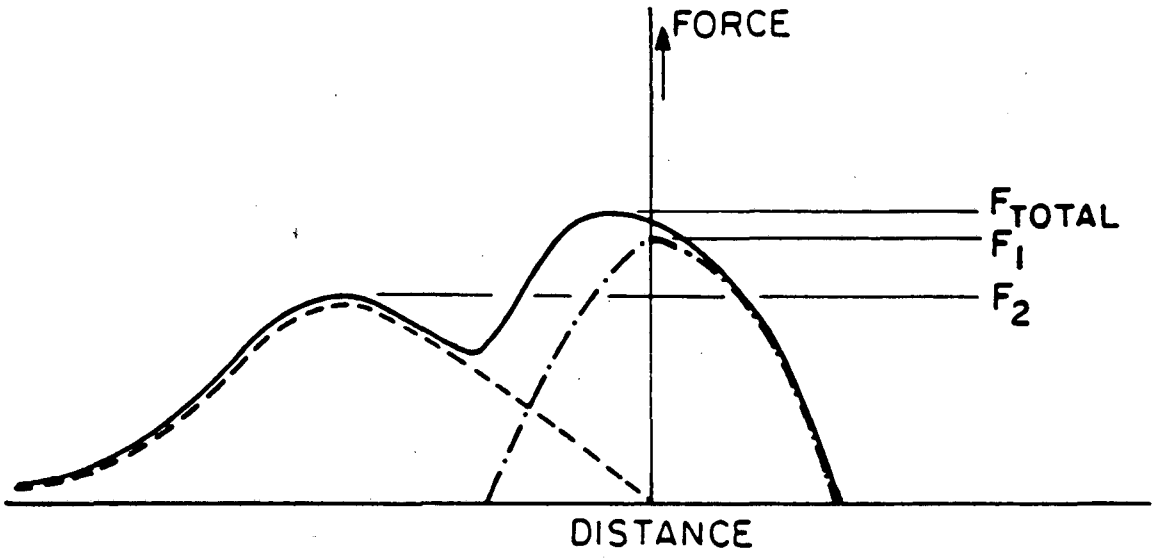

Figure IV.1 Superposition of spatially displaced strengthening mechanisms for a single obstacle.

particular precipitate cross-section, the force F_2 (e.g. from the misfit strain) contributes very little to the total strength of the precipitate because the peaks in the interactions are spatially displaced. One of the consequences of this displacement is that experiments designed to measure the effect of increasing misfit strain, for example, can be misleading. Because two mechanisms are operating that have spatially displaced peaks in the force-distance curve, a large change in the interaction force due to one mechanism may result in only a small change in the total strengthening from the precipitate. This point is often relevant for particles that strengthen by misfit and order hardening (Ardell, Chellman and Munjal, 1976; Lee and Ardell, 1979).

The other two types of obstacle-controlled superposition cases pertain to the effect of obstacles of the same type, but different strengths and the effect of obstacles of different types. On the assumption that all classes of obstacles are randomly dispersed, these may be handled together. In both cases the obstacles to glide are represented as point obstacles whose chief characteristic is their breaking strength, fixed by the peak in the force-distance curve. The new element of the problem is that the obstacles along the dislocation line are no longer identical.

No less than five possible techniques for handling the superposition of distinct obstacles have been seriously proposed at one time or another (Ardell, 1985). The various formulae are listed in Table 1. Of these possibilities, several can be quickly eliminated. The law of mixtures does not seem to fit any of the experimental data particularly well. Labusch's formulation (Labusch, 1970) was proposed for the summing of diffuse obstacles, not at issue here. Most of the attention has focussed on the linear and quadratic sum rules. The Buttner and Nembach (1983) and Nembach and Neite (1985) suggestion is intermediate to the linear and quadratic sums, and leaves q as an adjustable parameter that lies between one (1) and two (2). The authors show good agreement with experimental data using this formula, but the since the theory always has a multiplicative constant as well, agreement may be a foregone conclusion. There is other evidence that for mixtures of very strong and very weak obstacles a summing rule of this type may be necessary (Huang and Ardell, 1986) to explain the experimental data. However, the remainder of this discussion will focus on the linear and quadratic sum

Table 1. Proposed obstacle-controlled strengthening superposition mechanisms

mechanism	equation	references
linear	$\tau^* = \tau_1^* x_1^{1/2} + \tau_2^* x_2^{1/2}$	-
quadratic	$(\tau^*)^2 = (\tau_1^*)^2 x_1 + (\tau_2^*)^2 x_2$	Hanson and Morris (1975b) Koppenaal and Kuhlmann-Wilsdorf (1964)
adjustable	$(\tau^*)^q = (\tau_1^*)^q x_1^{q/2} + (\tau_2^*)^q x_2^{q/2}$	Buttner and Nembach (1983) Nembach and Neite (1985)
law of mixtures	$\tau^* = \tau_1^* x_1 + \tau_2^* x_2$	Brown and Ham (1971)
diffuse	$(\tau^*)^{3/2} = (\tau_1^*)^{3/2} x_1^{3/2} + (\tau_2^*)^{3/2} x_2^{3/2}$	Labusch (1970)

rules both of which have at least some theoretical foundation and seem to agree with experimental results in certain regimes.

For random arrays of point obstacles, both theoretical analyses and computer simulation point toward the quadratic sum. Hanson and Morris (1975b) provide a theoretical argument for the quadratic summing rule in their derivation of the statistics of the critical resolved shear stress for a mixture of distinct point obstacles. The proof, in the limit of small β, is outlined in Section II. This solution is the only one in which a superposition rule has been derived as a consequence of a mathematical solution of the random array point obstacle model. An additional argument in favor of the quadratic sum is that as $d\tau/dx_s$ goes to zero (where x_s is the fraction of strong obstacles) the linear sum becomes infinite, whereas the quadratic sum remains finite (Altintas, 1978; Ardell, 1985). Any summing rule with an exponent q less than two will also have an infinite derivative as the number of strong obstacles goes to zero.

Both Foreman and Makin (1967) and Altintas (1978) have attempted to delineate the regimes in which the linear and quadratic sums apply by computer simulation. The linear sum is expected to apply (by its proponents) for mixtures of very weak obstacles and for mixtures of weak obstacles containing a few strong obstacles. Foreman and Makin considered three mixtures of varying composition ($\beta_1 = 0.42$, $\beta_2 = 0.77$; $\beta_1 = 0.42$, $\beta_2 = 0.997$; $\beta_1 = 0.77$, $\beta_2 = 0.997$). However, as will be discussed at some length in Section IV.2, dislocation self-interactions generally cause Orowan looping to occur at values of β closer to 0.7 (see Section IV.2). The latter two cases, for which the quadratic sum does not seem to apply, are unphysical. The data are in good agreement with the quadratic sum rule for the first case, where both of the β are of reasonable size.

Altintas considered a much more extensive set of cases. Unfortunately, after reproducing Foreman and Makin's results for $\beta < 0.7$, all of the other cases he includes are for fairly weak obstacles ($\beta < 0.1$). In particular, he considers the case $\beta_s = 0.1$ and $\beta_w = 0.01$ for fractions of strong obstacles from 0.1 to 0.001. These cases should provide the best simulation of the argument for the linear sum described below, since the numerous small obstacles provide an almost continous frictional stress. The quadratic sum is a good fit to all the computer

simulation data; however, the simulations also show that the difference between the linear and quadratic sums for $x_s \ll x_w$ and $\beta_s \gg \beta_w$ is extremely small (see figure IV.2 for an example). Since there is no compelling theoretical reason to suggest the use of the linear sum, these results would seem be a sufficient basis to justify the use of the quadratic sum for all obstacle-controlled cases.

There is a limited amount of experimental evidence that provides empirical support for the quadratic sum rule. Nembach and Martin (1980) compared the predictions of a linear and a quadratic summing rule for the superposition of solution and particle strengthening in (Cu-Au)-Co single crystals. They found that the predictions of the quadratic sum rule are much closer to the experimentally observed strength than those of the linear sum. However, the reliability of these results is limited by the accuracy of the theory of coherency hardening on which they are based. On the other hand, Ebeling and Ashby (1966), who also examined the superposition of solid solution and particle hardening, but in the (Cu-Au)-Si system found that the linear sum represented the data well.

If the array of obstacles is **regular** with respect to the distribution of each distinct type of obstacle, then a linear summing rule may apply. Kocks, Argon and Ashby (1975, p161) provide a justification of the linear sum rule for regular arrays that applies in cases in which one type of obstacles is so weak that it provides essentially a frictional stress. Their argument works if the the average curvature of the dislocation is essentially unchanged by the presence of the weak obstacles. The situation is illustrated in figure IV.3. The geometry in the figure is representative of the situation only if the array is regular (so that what Kocks et al. call the line glide resistance is equivalent to the plane glide resistance or critical resolved shear stress). Although Kocks et al. extrapolate their results to the random array case, the extension is not valid for point obstacles. The argument runs as follows.

From the geometry of figure IV.3, we have

$$\tau - F_1/bL_1 = [2T\cos(\Psi/2)]/bL_2 \qquad \text{(IV.1)}$$

where L_1 is the spacing between the weak obstacles, L_2 is the spacing

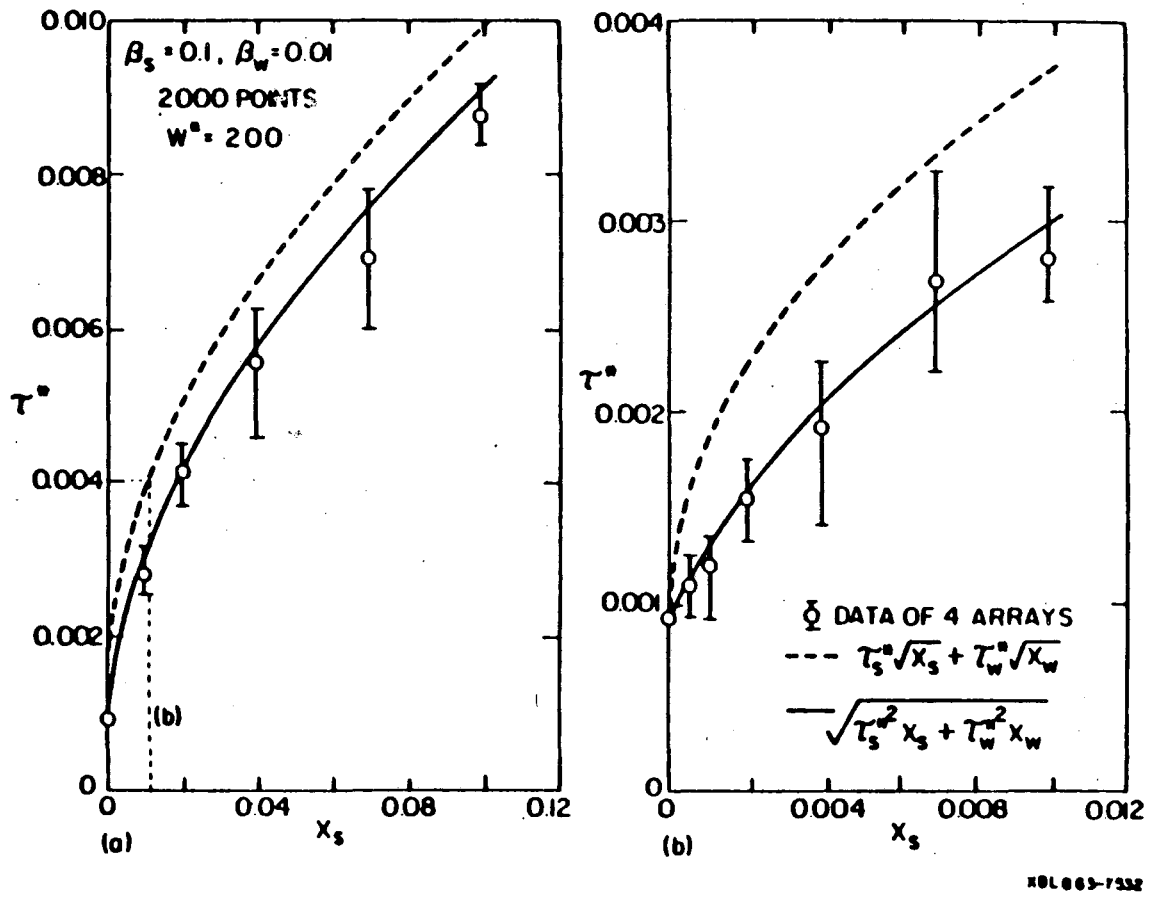

Figure IV.2 Comparison of computer simulation results for the strong line solution for mixtures of obstacles strength with predictions of quadratic and linear summing laws (from Altintas, 1978).

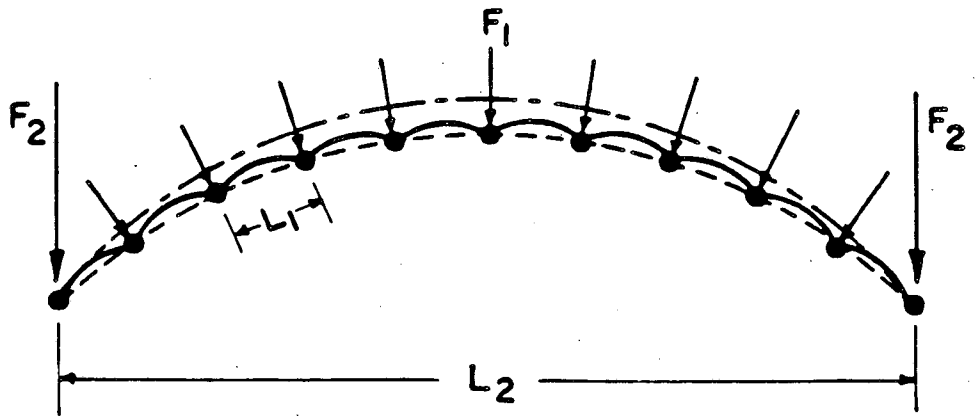

XBL 863-7537

Figure IV.3 Geometry used by Kocks, Argon and Ashby (1975) to derive a linear summing law for very weak obstacles (strength F_1) in the presence of a few strong obstacles (strength F_2).

between the strong obstacles and F_1/bL_1 may be considered as the effective constant back stress due to small obstacles. (Note that for a regular array $\tau^* = \beta$ rather than $\beta^{3/2}$ (Kocks, et al, 1975, p. 43)) If the average curvature is the same as the curvature if only strong obstacles are present, then

$$2T\cos(\Psi/2) = F_2 \qquad \text{(IV.2)}$$

where F_2 is the strength of the strong obstacles. Combining equations IV.1 and IV.2 gives

$$\tau - F_1/bL_1 = F_2/bL_2 \qquad \text{(IV.3)}$$

or

$$\tau = \tau_1 + \tau_2 \qquad \text{(IV.4)}$$

which is a linear superposition rule for a regular array of obstacles.

IV.1.3 Superposition of friction-controlled strengthening

The only type of frictional strengthening that will be discussed here is the effect of the matrix on the motion of the dislocation. Although neither Hanson and Morris, Foreman and Makin, Altintas or Kocks, Argon and Ashby provide a sound basis for a linear superposition rule for randomly arrayed obstacles, the linear sum rule does seem to be the appropriate way to include frictional contributions to the strength, which are not obstacle controlled.

If the matrix is relatively pure, the motion of the dislocation is not obstacle-controlled. Consequently, the argument described above for the regular array by Kocks, Argon and Ashby applies strictly to the strengthening effect of the matrix if the back stress is considered to come from the matrix rather than small obstacles.

IV.1.4 Superposition of interface-controlled strengthening

The only case of interface-controlled strengthening of interest here is the grain size strengthening effect. Grain size strengthening is classified here as a special case because despite its obvious com-

mercial importance, the origin of the strengthening effect is not well understood at this time. An understanding of the appropriate summing technique is significant from a theoretical viewpoint because the additive effect of grain size strengthening is generally assumed implicitly when predictions of the critical resolved shear stress are compared to yield strength results for polycrystalline materials.

The empirical Hall-Petch relation may be stated

$$\sigma_y = \sigma_c + k_{HP} d^{-1/2} \qquad \text{(IV.5)}$$

where σ_y is the stress at which slip which has started in the most suitably oriented grains propagates to other grains, σ_c and k_{HP} is a constant, and d is the average grain diameter (Friedel, 1964; pp266-268). It is generally assumed that it is legitimate to write

$$\Delta\sigma_y = M\Delta\tau_c$$

where M is the Taylor factor and τ_c is the critical resolved shear stress for the single crystal. This relationship requires that the single crystal strength be included in the σ_c term. It is also known that k_{HP} varies with precipitate size (e.g. Hansen and Bronsted, 1980).

There are three radically different types of models that can be used to provide a theoretical basis for the Hall-Petch relation. It is probably unlikely that any of them is applicable in all materials. At this writing it is not yet clear which of these models is correct. The oldest model is based on the idea that dislocations will pileup at the grain boundary, concentrating the applied stress. The second model assumes that the dislocation density in the interior of the grain will vary with the grain size. The suggestions are discussed in a recent review by Hansen (1985). The third model is based on the strong line solution for the critical resolved shear stress and suggests that the Hall-Petch relation is the result of array size effects. All three models are discussed below.

IV.1.4.1 Stress concentration model

The oldest derivations of the Hall-Petch relation are contained in the original papers by Hall (1951) and Petch (1953). The chief assump-

tion is that the grain boundary acts as an important barrier to dislocation motion. The derivation runs as follows.

If the grain boundary limits the passage of gliding dislocations or the activation of quiescent ones, then the dislocations will pile up at the grain boundary. If we make the further assumption that the stress applied to the dislocation pileup at the grain boundary is actually $\sigma_y - \sigma_c$ where σ_y is the yield stress of the material and σ_c is an internal back stress caused by the obstacle-controlled resistance to dislocation motion in the grain interior, then the relationship between the applied stress and the grain size can be determined. Since the generation or unpinning of the dislocation must be the result of a shear stress, it makes sense to rewrite this condition in terms of the shear stresses in the grain as

$$\tau_{gb} = \tau_y - \tau_c \tag{IV.6}$$

where τ_{gb} is the stress at the grain boundary.

The number of dislocations in the pileup, n, is a function of the applied stress and is given by

$$n = \pi L \tau_{gb} g/Gb \tag{IV.7}$$

where L is the length of the pileup and g is a constant on the order of unity. When the internal stress caused by the pileup reaches the value τ_d required to nucleate or unpin dislocations in the adjacent grain

$$\tau_d = n\tau_{gb} \tag{IV.8a}$$

$$= \pi L(\tau_{gb})^2 g/Gb. \tag{IV.8b}$$

A proof for equation IV.8a is given in Appendix C. If L is on the order of half the grain diameter, d, then equation IV.8 leads to

$$\tau_{gb} = [2\tau_d Gb/\pi g]^{1/2} d^{-1/2} \tag{IV.9}$$

or

$$\tau_y = \tau_c + k_{HP} d^{-1/2}. \tag{IV.10}$$

Cottrell (1964) provides a rationalization for the Hall-Petch

relationship based on equation IV.6 above. Cottrell makes an analogy to the stress concentration ahead of a shear crack, and defines the stress in the next grain as

$$\tau(r) = (\tau_y - \tau_c)(d/r)^{1/2} \qquad \text{(IV.11)}$$

where r is the distance from the grain boundary. If yielding occurs when the stress reaches some constant and finite value τ_d, then IV.11 can be rewritten

$$\tau_y = \tau_c + \tau_d r^{1/2} d^{-1/2}. \qquad \text{(IV.12)}$$

Multiplying through by the Taylor factor M, leads to the usual form of the Hall-Petch relation given in equation IV.5 if $M\tau_c$ is identified with τ_c and k_{HP} with $M\tau_d r^{1/2}$. This equation does not provide a rationalization for the strong dependence of k_{HP} on temper.

IV.1.4.2 Dislocation density model

The dislocation density model was first proposed by Li (1963), who noted that dislocation pileups were rarely observed in pure metals. The model assumes that the grain boundaries are the principal source of dislocations in the grain interior. Since the ratio of grain boundary area to grain volume is much higher for small grains than large ones, Li proposed that the dislocation density in small grains would tend to be much higher than for larger grains. If this model is correct, then grain size strengthening is actually obstacle-controlled, since the strengthening effect would arise from the presence of the dislocations.

In general, the critical resolved shear stress is proportional to the square root of the number density of the point obstacles to glide. This suggests that if the matrix were pure, except for an array of dislocations of density ρ, the critical resolved shear stress would be given by

$$\tau = \tau_{matrix} + k\rho^{1/2}. \qquad \text{(IV.13)}$$

If the grain size and the dislocation density are inversely proportional, then the critical resolved shear stress is

$$\tau = \tau_{matrix} + kd^{-1/2} \qquad \text{(IV.14)}$$

which has the form of the Hall-Petch relation. However, since the grain size contribution in this formulation is obstacle-controlled, if the matrix contains other types of obstacles, then the effect of these obstacles should be quadratically summed with the effect of the dislocation distribution. This type of sum does not lead to the simple form of the Hall-Petch relation given in equation IV.5, but it may be consistent with the variation of k_{HP} with temper. It is not entirely clear if the experimental data do or do not support this prediction.

IV.1.4.3 Strong line distribution model.

It is an interesting, but little known, fact that even if grain boundaries merely define the crystallography and do not represent major barriers to dislocation propagation, a Hall-Petch type relation is still be predicted. In general, deformation must be dominated by either the stress to propagate yielding from one grain to the next or the stress to move the dislocation through the array. The previous two sections lead to a Hall-Petch relation for yielding dominated by grain-to-grain propagation of slip. This section will show that a Hall-Petch relation still arises, even if the glide through the grain interior dominates yielding.

It has been known for some time from computer simulations that the critical resolved shear stress is strongly dependent on the array size and shape. There have been questions for some time about how results from arrays of increasing size converge toward solutions for infinite arrays (Labusch, 1977; Altintas, 1978). This issue is physical as well as academic since the arrays in real crystals and grains are not infinite. The value of Q determined for infinite arrays is an underestimate of the values of Q that apply in grains of finite size.

Altintas (1978, p65) considered the effect of array size on the critical resolved shear stress. He was able to predict the variation in the value of Q as a function of array size by assuming that the chance that certain obstacles would lie on the strong line of an infinite array decreased as the array size decreased. The smaller sampling

of all possible obstacle configurations along a given dislocation line in the small array makes it likely that the weakest point on the strong line will be stronger than it would be in an infinite array. As a consequence, a small array is stronger than a larger one, since it has a larger value of Q associated with it.

Figure IV.4 illustrates the technique used by Altintas to predict the strength of arrays of finite size. The probability that the strongest line will contain an obstacle of strength less than some particular value of β may be determined statistically from the probability of finding obstacles of particular strengths along the strong line. Thus the strength of the finite array is predetermined in a statistical sense by the distribution of obstacle strengths along the strong line for an infinite array.

In the light of these comments, one can look at the data for the critical resolved shear stress as a function of array size in a new way. Figures IV.5 and IV.6 are replotted from figures 13 and 25, respectively, in Altintas (1978). As can be seen in the figures, the simulated critical resolved shear stress is proportional to $(w^*)^{-1/2}$, where w^* is the dimensionless array size, w/l_s. As will be shown below, these computer simulation results predict an additive effect of grain size on strength.

The additivity of grain size and intragranular hardening may be shown simply by comparing the empirical Hall-Petch relation to the equation describing the variation in the critical resolved shear stress with array size. The empirical Hall-Petch relation is

$$\tau_y = \tau_c + k_{HP} d^{-1/2} \qquad \text{(IV.10)}$$

or

$$\tau_y^* = \tau_c^* + k_{HP}(l_s b/2T) d^{-1/2}.$$

The results of computer simulation for finite arrays (and the theoretical analysis) lead to an equation for τ^*

$$\tau^* = \tau_{inf}^* + K_\beta w^{-1/2} l_s^{-1/2} \qquad \text{(IV.15)}$$

where τ_{inf}^* is the critical resolved shear stress of an infinite array,

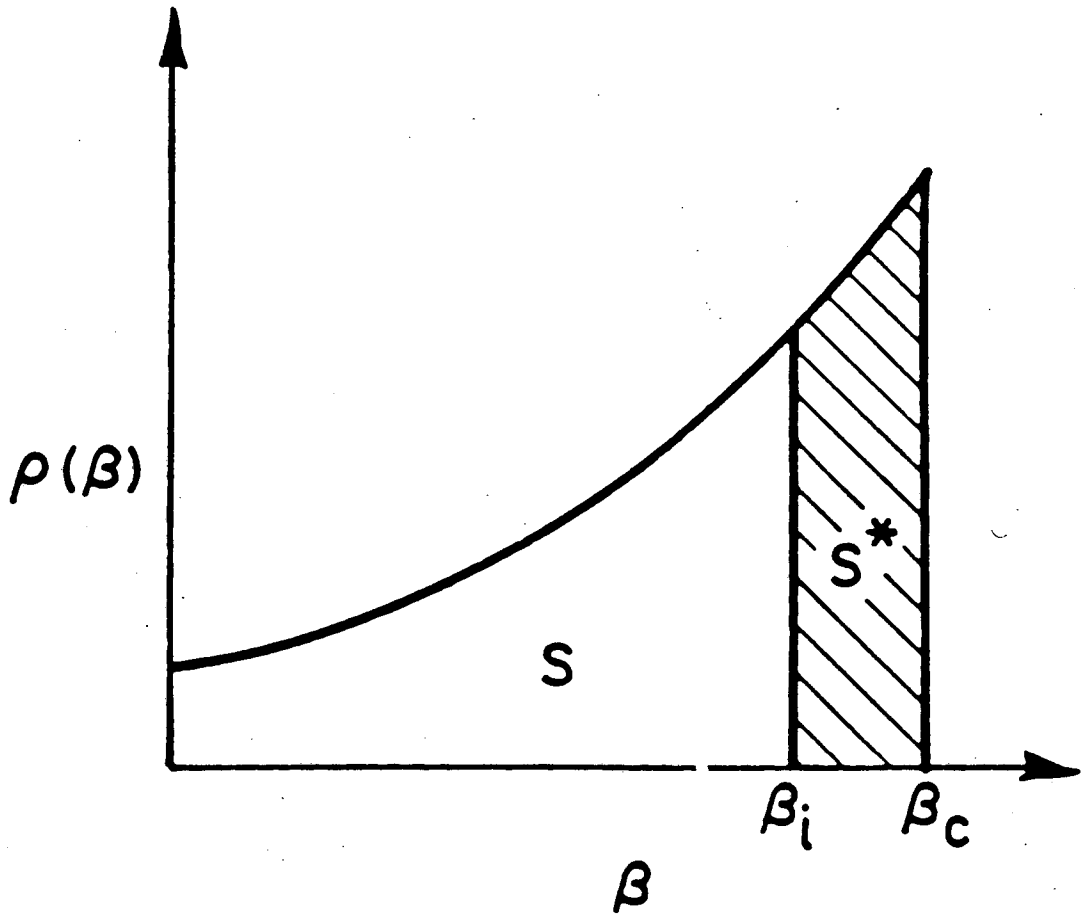

Figure IV.4 Schematic of the technique used to analyze the effect of array size on the strength of the strongest line in the array. The probability that an obstacle with strength $\beta_i < \beta < \beta_c$ will lie on the line is denoted by S^*.

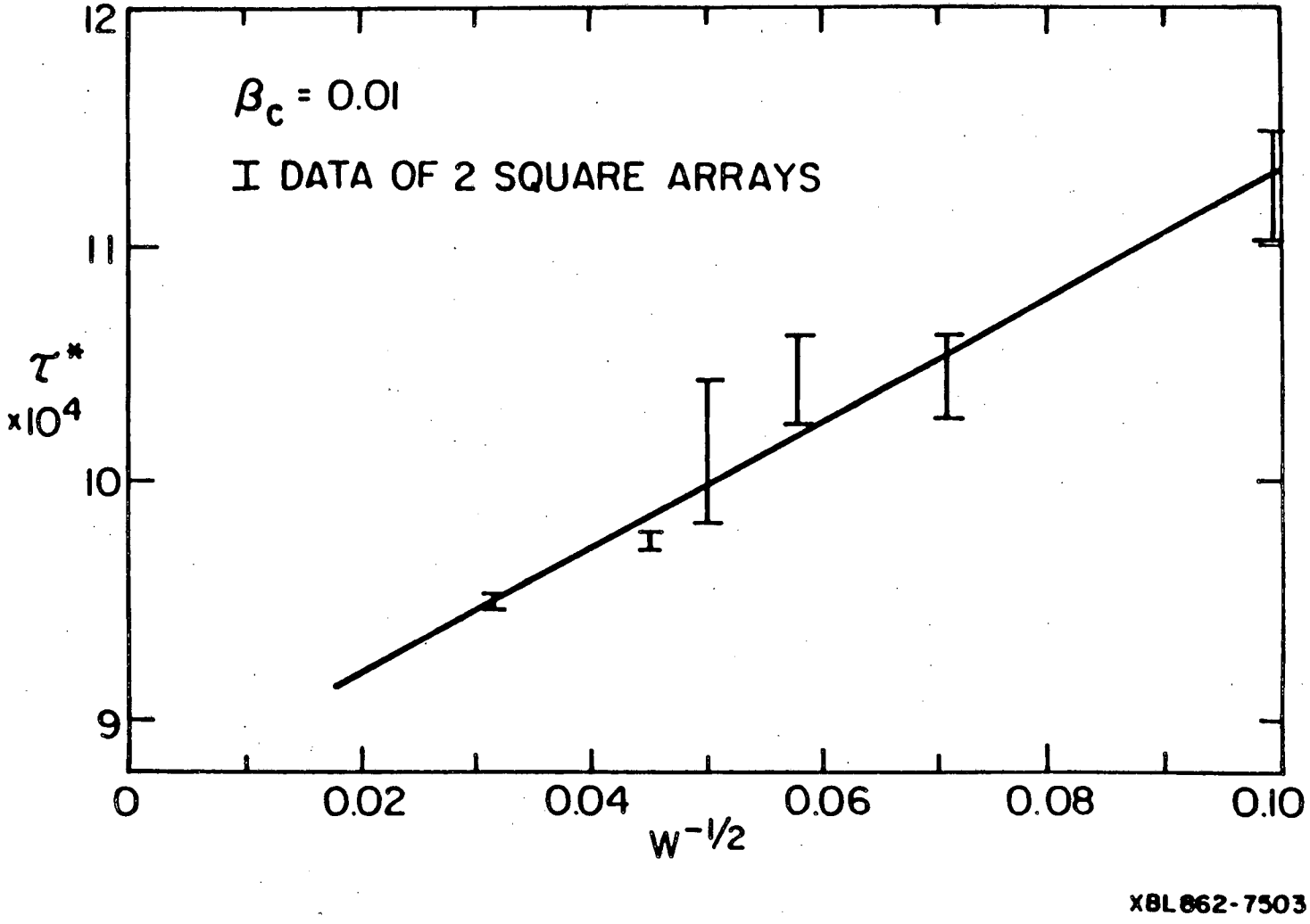

Figure IV.5 Illustration of the linearity of strength with the square root of the array width (data from Altintas, 1978).

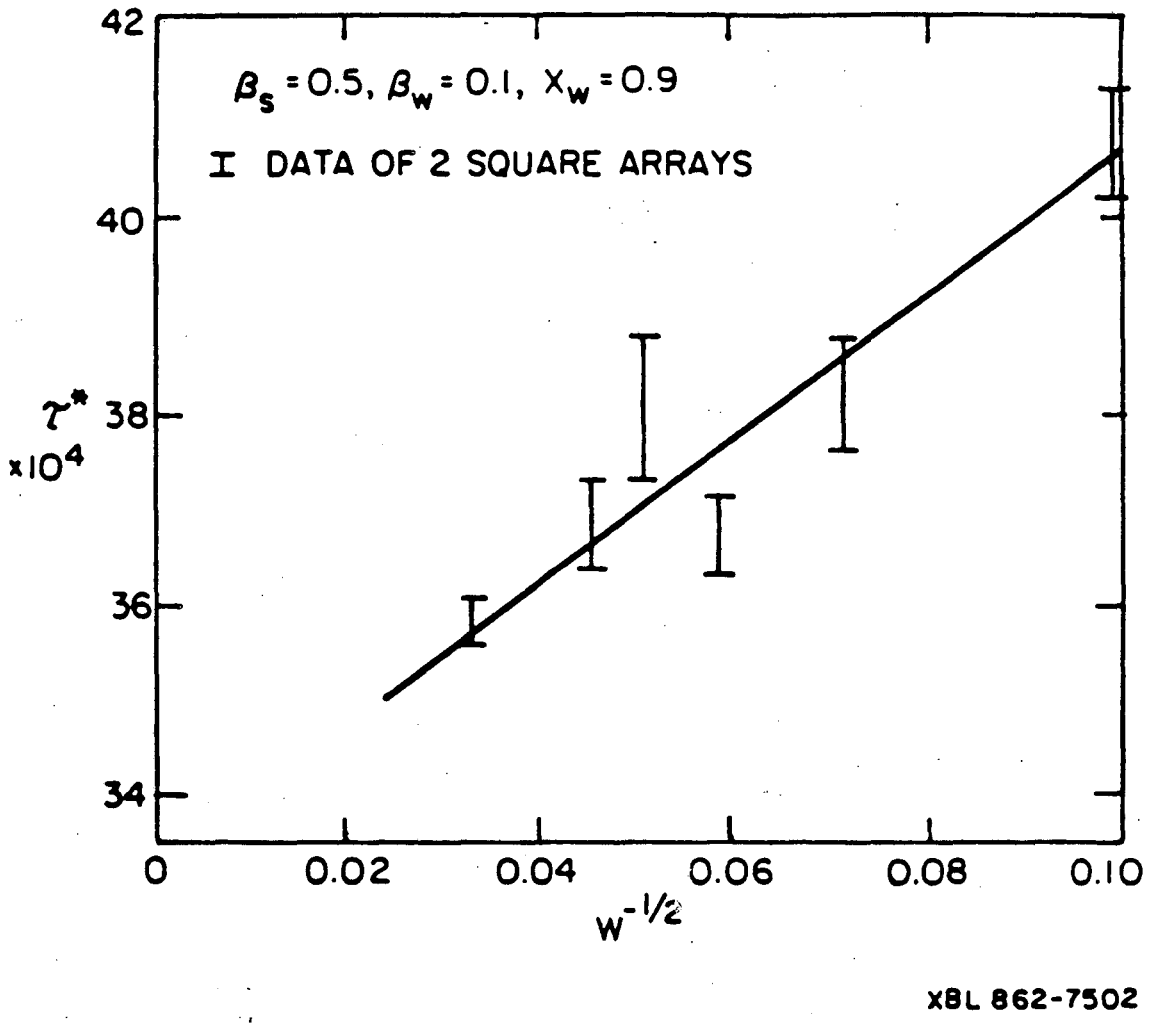

Figure IV.6 Illustration of the linearity of strength with the square root of the array width for a mixture of obstacle strengths (data from Altintas, 1978).

and K_β is a function of the distribution of obstacle strengths on the strong line. Equating these two relations gives

$$\tau^*_{inf} = \tau^*_c = Q\beta^{3/2} \qquad \text{(IV.16a)}$$

and

$$k_{HP} = 2K_\beta T/bl_s^{1/2}. \qquad \text{(IV.16b)}$$

Substituting into the Hall-Petch relation, we have

$$\tau = \tau_{inf} + [2K_\beta T/bl_s^{1/2}]d^{-1/2}. \qquad \text{(IV.17)}$$

Labusch (1977) has also considered the relationship between the critical resolved shear stress of a finite array and an infinite array in the context of his version of the Hanson and Morris statistical theory. He derives the formula

$$\tau_c = \tau_{c-inf}[1 + \{1/(2\sqrt{2}W\sqrt{\beta})\}\{\ln H^2/W\sqrt{2}\sqrt{\beta}\}] \qquad \text{(IV.18)}$$

where H and W are the height and width of the array respectively. As shown in figure IV.7 (after Altintas, 1986a), this formula leads to similar results to those of Altintas described above.

Equation IV.17 is a Hall-Petch type relation for situations in which strength is dominated by obstacle-controlled yielding in the grain interior rather than bypassing the grain boundary. This equation has a number of consequences, some of which will be discussed below. If the equation in fact describes an experimentally significant case, then these predictions should explain at least some of the existing experimental data. The following discussion is intended to provide a focus for future research, not a definitive analysis.

(1) Age-hardening at constant grain size.

As the particles coarsen, the value of l_s increases, causing the value of τ_{inf} to increase. The variation of the grain size term as l_s increases is uncertain since the variation of K_β with particle strength has not been analyzed. However, if the dependence is weak, it would be an excellent approximation at constant grain size to consider the grain size term as a constant matrix contribution that is independent of the hardening particles and linearly additive. This relationship is usual-

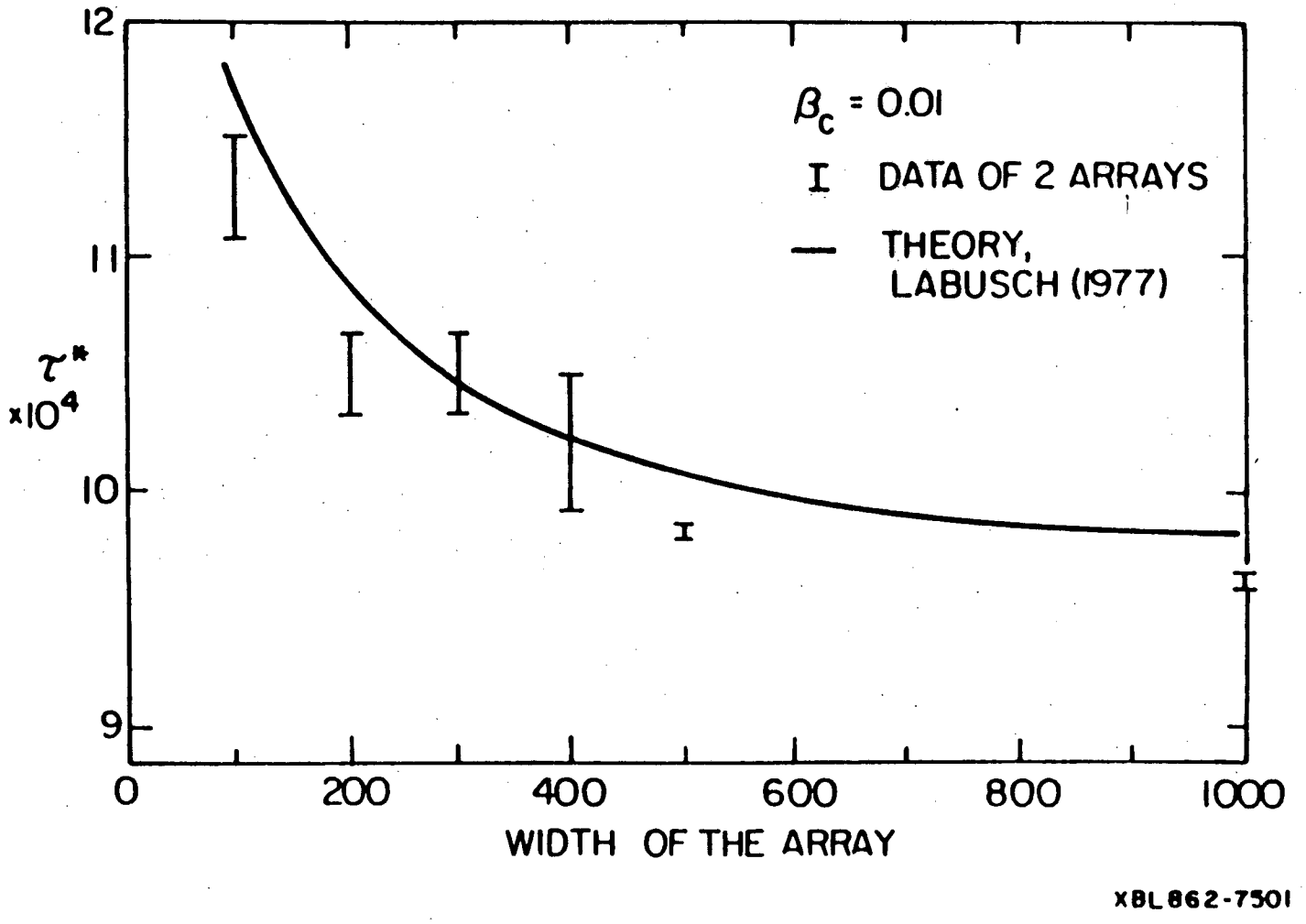

Figure IV.7 Comparison of strong line solution computer simulation data to prediction by Labusch (1977) of the array size effect.

ly assumed without justification.

(2) Effect of grain size for constant particle strength distribution.

If the distribution of particle strengths is constant, then τ_{inf}, K_β, T and l_s are all constant as well. Then the grain size term reduces to a constant multiplier of $d^{-1/2}$ and equation IV.18 reduces to the Hall-Petch relation, equation IV.10.

(3) Variation of k_{HP} with l_s.

Noting that the line tension is proportional to $\ln(l_s)$, the Hall-Petch coefficient varies with l_s as

$$k_{HP} \sim \ln(l_s)/l_s^{1/2}.$$

Hansen and Brondsted (1980) have measured the variation of k_{HP} with l_s in Cu hardened by Al_2O_3 particles. They determined that k_{HP} was proportional to $1/l_s$ rather than the proportionality above. However, the experimental error is large enough that the data do not allow an unambiguous differentiation between the two relationships. Precise measurements are difficult since K_β is a strong function of the precipitate size distribution as well as the average precipitate radius.

(4) Use of mean grain size.

All experimental verifications of the Hall-Petch relation use the mean grain size. From the discussion above, it seems that the extrema of the distribution of grain sizes rather than the mean grain size should control the grain boundary effect. However, self-similarity during grain coarsening has been predicted theoretically (Mahin, Hanson and Morris, 1980). For a particular material, processed to achieve various grain sizes, the mean grain size probably describes the entire distribution of grain sizes. The effect of the distribution is to modify the value of the Hall-Petch coefficient. The magnitude of this variation has not been estimated.

IV.2 Geometric corrections to the model

The purpose of this section is to consider the consequences of some of the assumptions made in either the point obstacle model or the strong line solution to simplify the geometry. The effects of three deviations of real materials from the basic assumptions will be discussed in detail: variable line tension, finite sized obstacles, and self-interaction of the dislocation. Isotropic elasticity is still assumed, although the introduction of anisotropy also has important geometric consequences. Each of the effects mentioned above will be considered separately. Following this treatment is a discussion of a model proposed by Bacon, Kocks and Scattergood (1973) that attempts to model all three of these factors. Finally a method of adapting their results to the strong line solution is suggested.

IV.2.1 Dislocation line tension

The basic model for prediction of the critical resolved shear stress of an array described in Section II makes the idealization that the dislocation line tension is constant. For $\upsilon = 0$ and isotropic elasticity, this assumption simplifies the geometry considerably because it ensures that the dislocation will bow out between obstacles in a circular arc. However, it is generally recognized that the line tension is not constant in real materials. The variation of the line tension with the angle ξ between the dislocation line and the Burgers vector may be approximated by the De Wit-Koehler formula (De Wit and Koehler, 1959)

$$T = (Gb^2/4\pi)[(1 + \upsilon - 3\upsilon\sin^2\xi)/(1 - \upsilon)]\ln(\lambda/r_o) \qquad \text{(IV.19)}$$

where υ is Poisson's ratio and λ and r_o are the outer and inner cutoff radii, respectively, of the strain field of the dislocation.

Equation IV.19 has the consequence that the line tension varies along the line of a bowing dislocation. It also implies that edge dislocations ($\xi = \pi/2$) have a lower line tension than dislocations that are initially pure screw in character ($\xi = 0$). The chief difficulty with applying equation IV.19 is that the values assigned to the cut-off radii are somewhat arbitrary.

Neither an extensive computer simulation study nor an analytical model of the critical resolved shear stress for glide of a dislocation of variable line tension exists. Including variable line tension in a statistical model of the Hanson and Morris variety appears to be complicated since both the shape and size of the search area become configuration dependent. In view of this difficulty, several attempts have been made to incorporate the qualitative effects of variable line tension into existing theories that assume a constant line tension.

Melander (1978a) and Ardell (1985) both suggest assigning the value of the average line tension of the bowed dislocation to the constant line tension. Melander uses equation IV.19 by assigning values to the unspecified variables from the properties of the strong line. In particular, he equates λ to $\langle 1 \rangle$, the average segment length on the strong line, and $[1 - (\omega \cdot \langle \beta \rangle)^2]$ or $[\omega \cdot \langle \beta \rangle)^2]$ to $\sin^2 \xi$ for edge and screw dislocations, respectively. ω is an adjustable fitting parameter close to one (1) that describes how fast the dislocation acquires mixed character. The inclusion of $\langle \beta \rangle$, the average obstacle strength along the strong line, makes the solution for the critical resolved shear stress iterative.

Melander and Ardell both assume implicitly that the change in the shape of the bowed out dislocation has negligible consequences. The average line tension may be calculated using the average value of the obstacle strength, but should be improved if the average value of the strengths of the obstacles actually lying on the strong line are used instead, as Melander does. However, given the inaccuracies in the dislocation search area, it is not obvious that this iterative solution is significantly more accurate.

Foreman and Makin (1966) considered the effect of the altered bow-out shape of the dislocation in a random array of obstacles. They argue that since a random array is still random if it is sheared, whether the dislocation bows out in an ellipse or a circle is irrelevant. The statistics of the process are essentially unchanged. However, this argument no longer applies if dislocation self-interactions are considered (Bacon et al., 1973).

IV.2.2. Finite obstacle size

It is clear that the existence of finite-sized obstacles to glide in real materials will result in differences between the behavior of the solution to the point obstacle model and real materials. The differences between point obstacles and finite obstacles enter through various factors, chiefly the bowed-out shape of the dislocation and the self-interaction of the dislocation arms where they wrap around the obstacle.

The effect of dislocation self-interaction will be discussed in greater detail below; at this point it is sufficient to note that the finite size of the obstacle holds the arms of the bowing dislocation apart, thus reducing their interaction (Bacon, et al., 1973).

Melander (1977) attempted to account for the effect of finite obstacle size on the dislocation search algorithm used in the Hanson and Morris strong line solution (1975a and 1975b). Ardell (1985) also discusses this question in the context of an average line solution. His argument is less rigorous in the sense that it uses an average line theory, but should nonetheless be qualitatively correct. However, his results are opposite to those of Melander. The reason for this discrepancy is not clear.

IV.2.3 Dislocation self-interactions

The term dislocation self-interaction is used to describe the elastic interaction between different parts of the same dislocation that occurs if the dislocation is bowed or bent on a scale that brings segments of the dislocation into close proximity relative to the range of the elastic strain field associated with the dislocation. As shown schematically in figure IV.8, if the dislocation bends around an obstacle, components of the dislocation line vector perpendicular to the original straight dislocation cancel. Since the total line energy of the dislocation is reduced, this interaction is energetically favorable. Consequently, dislocation self-interactions act to pull the arms of the bowing dislocation together near the obstacles. The force due to the self-interaction of the dislocation thus adds to the force from the applied shear stress and assists the dislocation in looping or

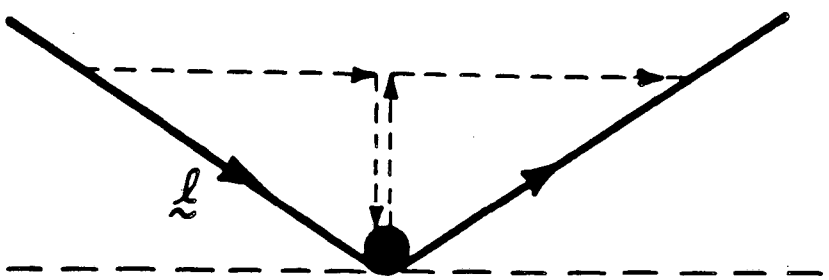

XBL 863-7538

Figure IV.8 Schematic illustration of cancellation of line tension components perpendicular to the dislocation line $\underset{\sim}{\ell}$ as the dislocation bends.

shearing the particle.

The effect is similar for shearing and Orowan looping of the precipitate, but it is perhaps simpler to consider the looping case. Orowan looping occurs when the stress is so high that a stable configuration of the bowing dislocation can no longer be found. In practice, the Orowan stress is reached when neighboring dislocation arms are approximately antiparallel (i.e the tangent angle to particle is $\Psi = 0$ and the neighboring arms of the dislocation have opposite line vectors 1.)

Self-interactions pull the arms together around the particle so that the force to bow-out the dislocation in an elliptical arc until the arms are antiparallel is much less than the force to bow-out the dislocation in a circular arc until the arms are antiparallel (β = 1.0). It follows that if the elliptically bowed dislocation is approximated by a circular arc, then looping occurs long before the arms of the circular arc dislocation are antiparallel (see figure IV.9). This result implies that Orowan looping occurs at value of β (calculated for circular bow-out) that may be considerably less than 1.0.

IV.2.4 The Bacon, Kocks and Scattergood model.

Bacon, Kocks and Scattergood (1973) consider the effect of dislocation self-interaction on the shape of a dislocation bowed between two obstacles and the effect of this shape distortion on the stress for Orowan looping. The equilibrium configuration of the dislocation is calculated by dropping the constant line tension approximation and assuming a lower cutoff radius r_o for the dislocation-dislocation interaction and then relaxing the dislocation into a stable configuration. Finite obstacles of various sizes are considered. (The problem is solvable only for finite obstacles.) The results indicate that array strength is increased by finite sized obstacles. Finally, they propose a modification for constant line tension point obstacle models that accounts for the dislocation self-interaction as a function of particle size and spacing.

Bacon et al. begin by considering only dislocations initially screw or edge in character since in all cases one or the other of these

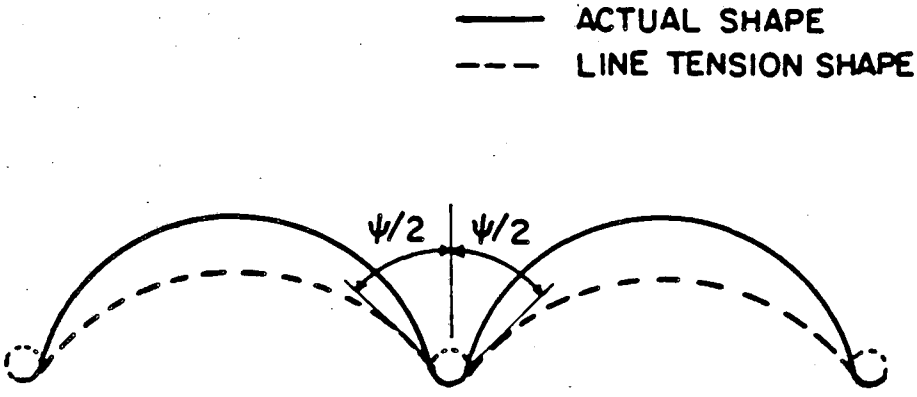

AFTER BACON, KOCKS and SCATTERGOOD, 1973

XBL 863-7539

Figure IV.9 Comparison of the actual shape of the dislocation at the Orowan stress when elastic self-interactions are considered to the shape in the constant line tension model at the same stress (after Bacon, Kocks and Scattergood, 1973).

will control yielding (see Section IV.3). In the discussion that follows isotropic elasticity is assumed, although this assumption was dropped in a later paper (Scattergood and Bacon, 1975).

The effect of the self-interaction can be modeled by treating the impenetrable obstacles as penetrable (or equivalently, point) obstacles in the constant line tension (circular bow-out) model. The effects of this correction on the constant line tension point obstacle treatment are two. Most importantly, Orowan looping occurs at $\beta < 1.0$. In addition, the area sampled by the dislocation as it bows out will be underestimated causing the strength of the array to be slightly underestimated. The dislocation shapes calculated by Bacon et al. (1973) are quite similar to the de Wit-Koehler shapes except in the region near the obstacle.

This penetrable obstacle model works best when the ratio D/L (particle diameter/particle spacing) is small (i.e. when the shape of the dislocation is not strongly perturbed by the actual particle which the dislocation must wrap around.) In this case, it is possible to define an effective strength F of the particle assuming that it behaves as a penetrable obstacle:

$$F = \cos(\Psi/2)\ (Gr_o^2/2\pi K)\ln L \qquad \text{(IV.20)}$$

where r_o is again the inner cutoff radius of the dislocation and K is 1 for an edge dislocation and $1 - \upsilon$ for a screw dislocation.

Equating the force on the dislocation $\tau b L r_o^2$ (r_o for units) to the effective strength of the obstacle we can solve for the critical cusp angle. Bacon et al. start with

$$\tau = (Gb/L)A[\ln \bar{D} + B] \qquad \text{(IV.21)}$$

where

$$\bar{D} = [D^{-1} + L^{-1}]^{-1} \qquad \text{(IV.22)}$$

because this equation is the simplest one with the right proportionalities. They find A and B by empirical data fitting to be $1/2\pi K$ and 0.7, respectively. Plugging in gives the critical cusp angle

$$\cos(\Psi/2) = (\ln \bar{D} + 0.7)/\ln L. \qquad \text{(IV.23)}$$

Bacon et al. use this solution for the critical cusp angle for Orowan looping to correct empirical solutions for random arrays of point obstacles for the effect of dislocation self-interactions and finite obstacle size. The empirical result of Kocks (1967) and Foreman and Makin (1966) for the motion of a dislocation through a random array of point obstacles is

$$\tau = (\cos \Psi/2)^{3/2}(Gb/L)[(\ln L)/2\pi K]. \qquad \text{(IV.24)}$$

For this case $\bar{D} \sim D$ and $0.7 \ll \ln D$ are reasonable assumptions (small but finite obstacles at moderate to large spacings, volume fraction not too big). Then the critical cusp angle is approximately $(\ln D/\ln L)$ and the corrected value of τ is

$$\tau = (\ln D/ \ln L)^{3/2}(Gb/L)[(\ln L)/2\pi K]. \qquad \text{(IV.25)}$$

The origins of the terms in this equation are as follows: Gb/L, the classical Orowan looping value; $\ln L/2\pi$, the interactions over one bowing loop; and $(\ln D/\ln L)^{3/2}$, the self-interactions in a random array.

Equating L, the particle spacing, to l_s/r_o, the dimensionless mean square obstacle spacing in these units, in equation IV.25 and comparing the resulting equation for the critical resolved shear stress to $\tau^* = Q\beta^{3/2}$ leads to a line tension of the form

$$T = (Gb^2/4\pi K)\ln(l_s/r_o). \qquad \text{(IV.26)}$$

The value of the inner cutoff radius of the dislocation, r_o, is usually taken to be between b and 4b, where b is the Burgers vector. The most physically reasonable choice is $r_o = b$. Ardell (1985) suggests that a good approximation for the line tension is $\lambda/r_o \sim 55$, which leads to average radii of about 10 nm at peak strength. The choices suggested here lead to larger values of the logarithmic term. Since the average radius at looping can be somewhat larger (see section VI.3.9.1), the values from this equation may not be unreasonable. Ardell (1985) lists computed values of the line tension for various materials. For pure screw dislocations a constant line tension value of $Gb^2/2$ seems to be the best approximation for the obstacle strength and spacing dependent

form.

IV.2.5 Application of the self-interaction to the strong line solution

To apply the model of Bacon et al. (1973) in the context of the strong line solution of the point-obstacle model, several issues must be resolved. Some of these are discussed briefly below.

1. $\beta_c^{max} = 0.7$

It is not clear exactly where the idea that β_c^{max} is rarely bigger than 0.7 in practice comes from, although 0.7 is the value recommended by the authors to Hanson and Morris. Bacon et al. do comment that $\Psi/2 > 40^o$ which implies $\beta=0.77$ for the range $D<L/10$ and $L>1000$ (which is a very dilute solution). These are the same constraints that lead to the simplification to (ln D/ln L) in equation IV.25 above. However, the general solution for the critical cusp angle is

$$\cos(\Psi/2) = (\ln \bar{D} + 0.7)/\ln L. \qquad \text{(IV.27)}$$

From this equation β may be greater than 0.7. The value of β increases as the the ratio D/L increases. Physically, the separation of the arms of the dislocation increases as the obstacle size increases. The strength of the interaction between the arms is correspondingly lowered. In the context of the strong line solution, decreasing the self-interaction has the effect of increasing the values of β and β^{max} appropriate to the particle.

Bacon et al. also show that when the obstacles are non-collinear the flow stress will be lowered. In fact, if the angles are sharp enough, the force from the self-interaction can cause obstacles to be bypassed at zero stress.

There is a somewhat cryptic plot of the Orowan stress as a function of various assumptions about Orowan looping in the Bacon et al. paper that indicates that for Q = 0.8871, β_c may be about 0.7 to make Orowan looping continuous with the point obstacle solution of Hanson and Morris (1975a), but the origin of the plot is unclear.

The actual value of β_c is important only to the numerical accuracy of the calculation. What is important is whether its value changes significantly over the range of precipitate radii of interest. An additional question is the validity of extending this line tension approximation for impenetrable particles to fairly weak, penetrable obstacles that the dislocation will eventually shear.

2. Variation of β^{max} with obstacle size and spacing

Use of equation IV.27 to find β^{max} requires β to be a function of particle size and spacing. The only feasible way to do the calculation is to use the average particle size and spacing, in spite of the fact that this assumption is somewhat contradictory in the context of a strong line solution for the critical resolved shear stress.

3. Experimental values of β_c.

The looping radius and the value of β_c in the constant line tension approximation can only both be determined from experimental data if the strength of the array and the strengthening theory are assumed. It is simplest to assume the value of β_c is fixed at 0.7.

4. Line tension.

Note that the line tension that results from the Bacon, et al. analysis (equation IV.26) differs from that calculated by De Wit and Koehler (equation IV.19).

IV.3 Dislocation Character

It is generally agreed that macroscopic yielding requires the motion of screw, edge, and mixed dislocations. The force required to move each type of dislocation is not equivalent, since the interaction of the dislocation with the matrix and the various obstacles it contains depends on the character of the dislocation. Yielding is controlled by whichever of type of dislocation is most difficult to propagate through the crystal -- dislocations that are initially either pure screw or pure edge. This dislocation type will be the one visible in transmission electron microscopic studies of deformed crystals since dislocations that move at lower stress will tend to glide out of the crystal.

From equation IV.19, in an isotropic material the line tension of an initially screw dislocation is greater than the line tension of an edge dislocation by a factor of $(1+\upsilon)/(1-2\upsilon)$. This difference in line tension is responsible for the difference in the required stress for edge and screw dislocation glide. Although this line of reasoning seems straightforward, the predictions of the analysis below do not always correspond well to experiment.

There are two classes of dislocation-obstacle interactions of interest: those in which the resistance to dislocation glide is determined by the force required to shear the obstacle, and those in which the resistance is controlled by the value of β (i.e. cases in which the force to bypass the obstacle is proportional to the line tension) (Kocks, Argon, and Ashby, 1975; pp. 62-63). In both cases, whether the critical resolved shear stress is bigger for screw or edge dislocations is determined by (a) whether the maximum resistance to dislocation glide depends on dislocation character and (b) the relative magnitude of the line tension for each dislocation type.

IV.3.1 Force-controlled glide.

The fully dimensional form of the critical resolved shear stress is

$$\tau = QF^{3/2}/[l_s b(2T)^{1/2}]. \qquad \text{(IV.28)}$$

The line tension of a screw dislocation is greater than the line tension of an edge dislocation. If the force of interaction between the dislocation and the obstacle is equal for edge and screw dislocations or if the interaction force is greater for edge dislocations then the critical resolved shear stress is controlled by the edge dislocations. If the force of interaction is greater for screw dislocations then whether yield is edge or screw controlled depends on the magnitude of that difference.

On this basis, order hardening, for which the interaction force is equivalent for screw and edge dislocations, is expected to be edge-controlled. In the case of coherency hardening, the edge dislocation has a stronger interaction with the precipitate since there is a volume distortion associated with an edge dislocation, but not with a screw dislocation. Consequently, yielding in a coherency-hardened material should also be edge-controlled.

Edge-controlled yielding has been observed in alloys hardened by Ni_3Al, which provides both misfit and order strengthening (Ardell, Munjal and Chellman, 1976). Screw-controlled deformation in underaged material has been observed in the aluminum-lithium system (Miura, Matsui, Furukawa and Nemoto, 1985). Humphreys (1985) suggests that if cross-slip occurs, yielding in alloys hardened by misfitting, coherent precipitates will be screw-controlled. However, if cross-slip is an important factor, the pinning of the dislocation by a jog is an important obstacle to glide that should be simulated by including additional strong obstacles in the model. This point deserves further investigation.

IV.3.2 β-controlled glide.

If the force of interaction between the dislocation and the obstacle is proportional to the line tension, then the equation for the critical resolved shear stress in terms of independent variables is

$$\tau = 2Q\beta^{3/2}T/l_s b. \qquad \text{(IV.29)}$$

If β for the interaction is equal for edge and screw dislocations, the

critical resolved shear stress is greater for glide of screw dislocations. This result also holds if the interaction is stronger for screw dislocations. If the interaction is stronger for edge dislocations then the magnitude of the difference determines which dislocation type controls yielding.

Orowan looping is an example of a hardening mechanism for which the force of interaction is proportional to the line tension. Since the resistance is independent of dislocation character, yielding in materials principally hardened by non-shearable precipitates should be screw controlled (Melander, 1978). Melander and Persson (1978a) make this argument for modulus hardening on the basis of the relation suggested by Russell and Brown (1972)

$$\beta \cong (1-\{T_{matrix}/T_{particle}\}^2). \qquad \text{(IV.30)}$$

The line tension ratio is approximately independent of dislocation character. Transmission electron microscopy indicates that screw dislocations are present in the deformed material when it is hardened primarily by GP zones, which Melander and Persson argue strengthen primarily by modulus hardening.

IV.3.3 Implications.

In alloys hardened by ordered precipitates that are shearable at small sizes, there is a transition in deformation mode near peak strength when the precipitates become large enough that dislocation looping is preferred over shear. This transition implies that in materials in which the yielding is edge-controlled in the underaged condition will exhibit screw-controlled yielding in the overaged condition and some mixture in the vicinity of peak strength. This suggestion has not been experimentally verified. In particular, observations of screw-controlled deformation in underaged aluminum-lithium alloys suggest that the entire analysis may be flawed.

IV.4 Precipitate coarsening

IV.4.1 Experimental parameters.

A model of the critical resolved shear stress should predict the aging curve of a precipitation hardened material as the precipitates coarsen and account for the experimentally observed hardening and softening. A general model of the effect of precipitate coarsening on yield strength would ideally incorporate the volume fraction of precipitate present, a description of the shape of the precipitate size distribution and the evolution of the precipitate size distribution and volume fraction as a function of time, temperature and/or average precipitate radius. Unfortunately, a material-independent general expression of this sort does not exist. In lieu of an exact expression, the simplest assumption is that the precipitate size distribution coarsens at constant volume fraction in a self-similar fashion, so that the shape of the distribution as a function of $r/\langle r \rangle$ does not evolve with time. The viability of this assumption is discussed below.

IV.4.2 Models of precipitate coarsening.

A number of theoretical models of diffusion-controlled coarsening exist (Lifshitz and Slyozov, 1961; Wagner, 1961; Ardell, 1972; Brailsford and Wynblatt, 1979; Davies, Nash and Stevens, 1980; Voorhees and Glicksman, 1984a, 1984b). All of these approaches give rise to the Lifshitz-Slyozov-Wagner (LSW) coarsening relation

$$r^3 - r_o^3 = kt. \qquad \text{(IV.31)}$$

However, the models differ with regard to the predicted shape of the asymptotic precipitate size distribution. The Lifshitz-Slyozov model predicts a strict cutoff at $r/\langle r \rangle = 1.5$ in the limit of zero volume fraction. Because larger radii are observed experimentally, other investigators attempted to eliminate the upper limit by accounting properly for the finite volume fraction of precipitates (Ardell, Brailsford and Wynblatt) and the possibility of encounters (Davies, et al.). The Davies, Nash, and Stevens model leads to a more symmetric distribution than the others that may better reflect reality. However, none of these models is in perfect agreement with the limited amount of

precise experimental data.

IV.4.3 Evolution of the shape of the precipitate size distribution.

Precipitate size distributions of various shapes can be created by appropriate thermal treatments. This point is illustrated by the sample distributions for binary aluminum-lithium alloys shown in figure IV.10 (data from Gu, Liedl, Sanders and Welpmann, 1985a and Baumann, 1984; see also Jensrud and Ryum, 1984). At least some of these are almost certainly non-equilibrium distributions; their coarsening behavior is not known. (The Voorhees and Glicksman model (1984a) can be used to consider the evolution of a distribution, but the computation is difficult.) None of the theoretical predictions for the shape of the precipitate size distributions fit the experimentally measured distributions exactly. The Davies model is probably most satisfactory because it leads to the most symmetrical distribution.

Gu et al. have done an extensive study of the behavior of the precipitate size distribution during coarsening in binary aluminum-lithium alloys (Gu, Liedl, Kulwicki and Sanders, 1985b; Gu, Liedl, Mahalingam and Sanders, 1986). These alloys provide an excellent model system for coarsening studies because the precipitates are spherical in shape (an assumption of all coarsening theories that is not always fulfilled) and almost exclusively of one type (δ'). The precipitate size distributions were found to coarsen self-similarly over the range of compositions examined. Gu, et al. (1986) found that it was possible to specify the precipitate size distribution as a function of lithium content by the two parameters of a Weibull distribution. The distributions were essentially independent of aging temperature and time. They have a symmetrical shape better approximated by a normal curve than by the skewed curves suggested by all the theories except Davies et al.; however, Gu et al (1985b) could not find evidence for the encounters assumed by that model.

The work of Gu, et al. suggests that it may eventually be possible to describe experimental precipitate size distributions by a small number of easily determined parameters. It also suggests that for a given distribution, the assumption of self-similar coarsening is probably a rather good one. This assumption has the advantage of not

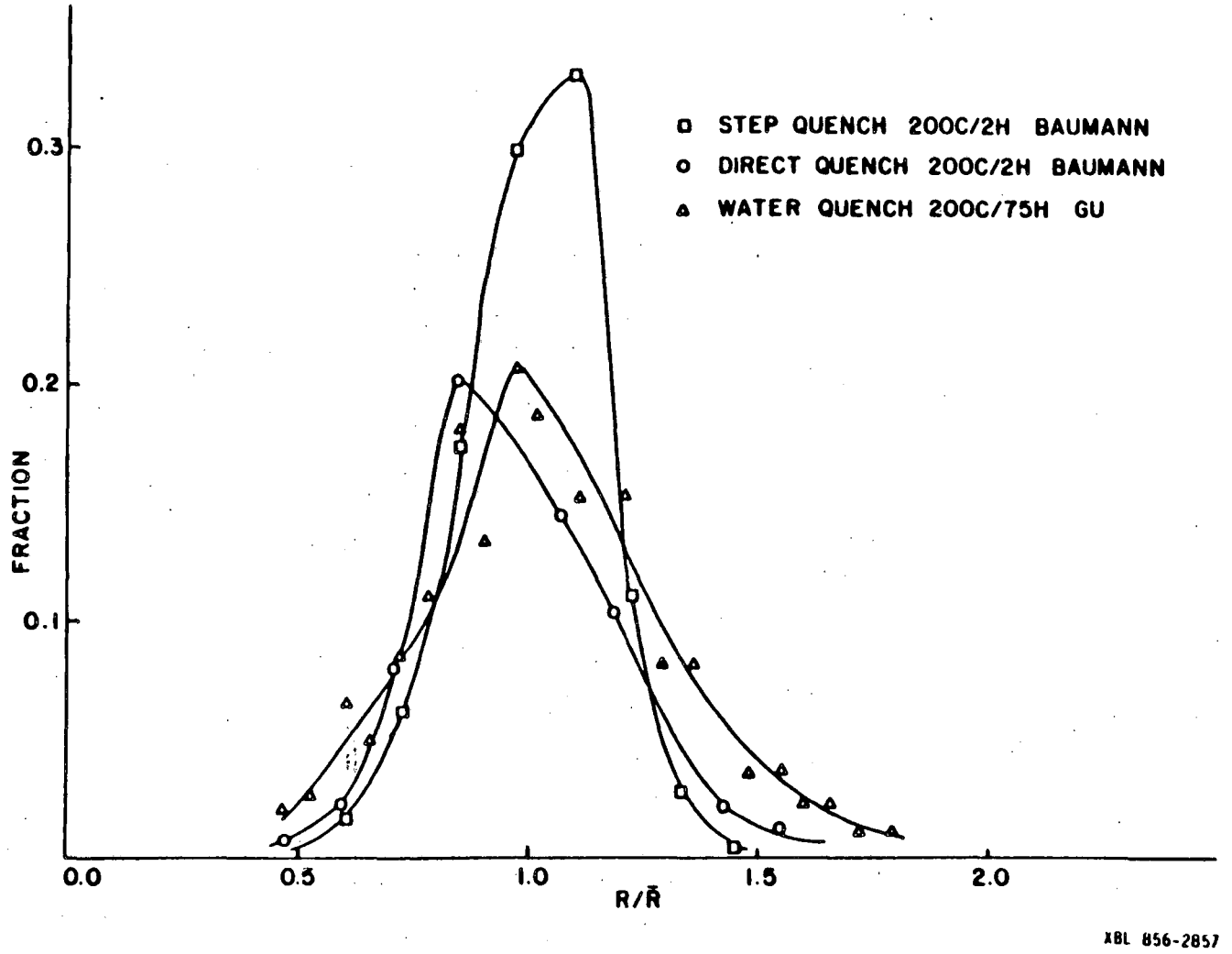

Figure IV.10 Experimentally measured precipitate size distributions for binary aluminum-lithium alloys (data from Baumann, 1984 and Gu et al, 1985a).

adding an additional parameter to the model. If the initial precipitate size distribution is far from the asymptotic shape and coarsens toward it, then there may be an error associated with this assumption. However, even in this case, the approximation should improve as the alloy approaches peak strength, the region of greatest engineering interest.

IV.4.4 Volume fraction effects during coarsening

The change in volume fraction during precipitate coarsening can be estimated on thermodynamic grounds (Porter and Easterling, 1981). The impetus for the change is the fact that the presence of the precipitate-matrix interface alters the equilibrium between the matrix and precipitate phases. The requirement of mechanical equilibrium across the curved interface leads to a pressure difference

$$\Delta P = 2\gamma_{\alpha\beta}/r \qquad \text{(IV.32)}$$

where $\gamma_{\alpha\beta}$ is the surface energy of the interface. The pressure difference decreases the magnitude of the free energy change for the reaction by the amount

$$\Delta G_{\gamma} = V\Delta P. \qquad \text{(IV.33)}$$

As the precipitate radius increases during coarsening, the free energy change due to the interface decreases in magnitude, resulting in further precipitation of the second phase and decreased solubility of the solute species.

The concentration of solute in the matrix may be expressed as a function of particle radius:

$$X_r = X_o \exp(2\gamma_{\alpha\beta}\Omega/k_B T) \qquad \text{(IV.34)}$$

where X_r and X_o are the concentrations corresponding to precipitates of average radius r and infinity (i.e. at equilibrium), respectively, $\gamma_{\alpha\beta}$ is the interfacial free energy, Ω is the atomic volume in the precipitate and k_B is Boltzmann's constant. Brailsford and Wynblatt (1979) use this equation in their coarsening theory to predict a change in

precipitate volume fraction given approximately by

$$\phi(r) = \phi(r_i) + [1-\phi(r_i)](2\gamma_{\alpha\beta}\Omega X_o/k_BT)(1/\langle r_i\rangle - 1/\langle r\rangle) \quad \text{(IV.35)}$$

where $\phi(r)$ is the volume fraction when the average particle radius is $\langle r\rangle$, and r_i and $\phi(r_i)$ are the initial precipitate radius and initial volume fraction, respectively.

Figure IV.11 shows the cumulative change in precipitate volume fraction during coarsening for the specific example of Al_3Li (δ') in aluminum. As can be seen from the figure, the increase is most pronounced when the volume fraction of precipitates is low and most of the increase occurs while the precipitates are less than 20b in diameter. Peak strength generally occurs at radii greater than 40b. At that size, the rate of change of the volume fraction with precipitate radius is extremely low. Not surprisingly, the larger the surface energy of the precipitate-matrix interface, the greater the effect. Since the critical resolved shear stress is proportional to the square root of the volume fraction of precipitates, the maximum effect on the critical resolved shear stress is a factor of $\{\phi(\text{inf})/\phi(0)\}^{1/2}$. For aluminum-lithium the increase is unlikely to ever be greater than 2%. Only when the precipitates have a high interfacial energy or when the volume fraction is extremely low is the effect significant enough to require its inclusion in the computation of aging curves.

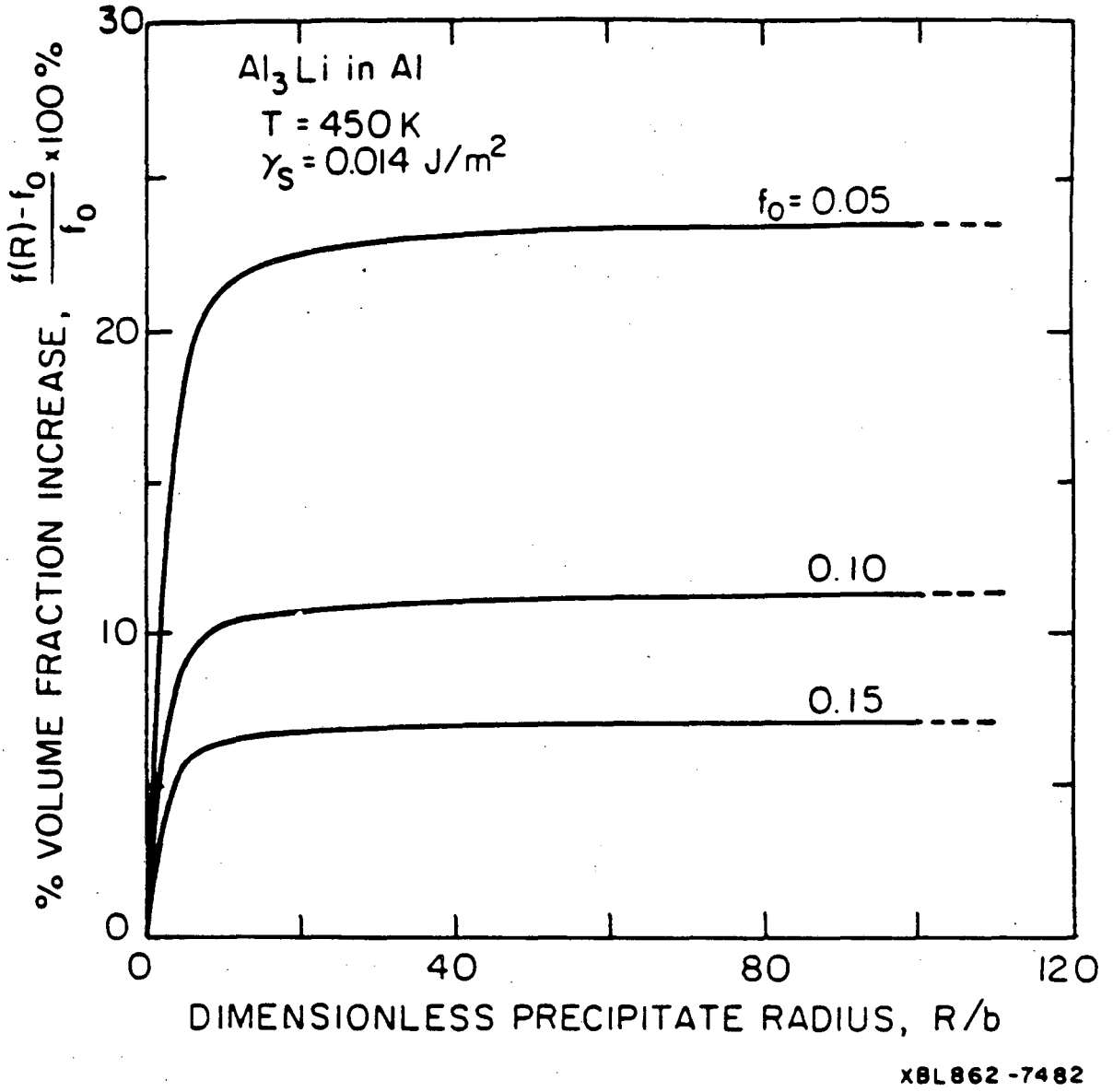

Figure IV.11 Effect of interfacial surface energy on the equilibrium volume fraction of precipitate during precipitate coarsening as a function of initial volume fraction.

IV.5 Obstacle strength in order-hardened alloys

In theory, the determination of the strength of an obstacle to dislocation glide is straightforward; it is given by the peak force in the force-distance curve that describes the dislocation-obstacle interaction. In practice, obstacle strength must be quantified by computing the maximum interaction force in some fashion. Since the details of the interaction are not always known, this procedure is not always trivial. The following discussion will consider ways of quantifying the interaction force for the particular case of alloys hardened by coherent, ordered precipitates with relatively low misfit strains.

In alloys that are primarily order-hardened, the principal determinant of strength is the antiphase boundary energy γ of the precipitated phase. Considerable effort has been expended to determine its value by a variety of techniques in various model systems. First principles calculations of the strengthening due to ordering generally depend on knowledge of the antiphase boundary energy as do predictions of superdislocation spacings and activation energies for cross-slip, etc.

Correct superposition of several strengthening mechanisms for the same obstacle (discussed in IV.1.2) is important for determinations of obstacle strength. Since the objective here is to quantify the strength of the precipitate, even if the strengthening is dominated by order hardening, other contributions must be considered. There are three distinct methods commonly used to find the antiphase boundary energy: (1) theoretical calculation of disordering energy, (2) measurement of minimum Orowan loop size, and (3) measurement of superdislocation pair spacing. The theoretical calculation is the simplest technique, but it gives a value for the antiphase boundary energy that is independent of the misfit strain, which must then be accounted for separately. In the other two methods, it is possible to include the effect of a small misfit strain in the order strengthening term. The three methods are discussed below. Unfortunately, each has its disadvantages and the value of this critical experimental parameter is always somewhat uncertain.

IV.5.1 Theoretical calculations of the antiphase boundary energy.

Calculation of the energy associated with an order-disorder transformation at a given temperature is a problem that has been much studied by materials scientists and solid state physicists who wish to calculate phase diagrams. The simplest model, termed the Ising model, considers the energy change on ordering due to first nearest neighbor interactions only

$$\sigma = \Delta F = V_{ab} - 1/2(V_{aa} + V_{bb}) \qquad \text{(IV.36)}$$

where a and b represent two types of atoms. Using a model of this type, Flinn (1960) derives the energy of an antiphase boundary of the type $a_o/2\langle 110\rangle$ in the $L1_2$ crystal. For this case he gets

$$\gamma = 2hV/N^{1/2}a^2 \qquad \text{(IV.37)}$$

where $h \geq k$, a is the lattice parameter of the disordered phase, and $N = h^2+k^2+l^2$. The above formula assumes that the long range order of the phase is perfect. If it is not, the energy must be multiplied by S^2, where S is the long-range order parameter, in order to give the correct answer.

The real sticking point is the value of the ordering potential V. A Bragg-Williams type approximation gives a value of the form

$$V = k_B T_c/2F_aF_bZ \qquad \text{(IV.38)}$$

where T_c is the critical order-disorder temperature (determined from the phase diagram), k_B is Boltzmann's constant, F_a and F_b are the atomic fractions of a and b atoms, and Z is the number of first nearest neighbors (Muto and Takagi, 1955).

For the $L1_2$ structure, quasichemical calculations that describe atomic interactions in more detail give (Marcinkowski, 1963)

$$V = k_B T_c/0.82 \qquad \text{(IV.39)}$$

which gives considerably larger answers. Quasichemical calculations are probably more accurate, so equation IV.39 is the preferred form for

the ordering potential. Combining with equation IV.37 gives

$$\gamma = 2.42\ hk_BT_c/N^{1/2}a^2 \qquad \text{(IV.40)}$$

for the $L1_2$ crystal structure.

The calculations above are intended to determine the antiphase boundary energy in bulk material, not precipitates. The simplest adaptation to the precipitate case (admittedly without theoretical basis) is to use the T_c for the bulk phase. If the T_c is not known the highest temperature at which the precipitate is stable is often substituted. This substitution gives a lower limit (sometimes very low) on the antiphase boundary energy.

Unfortunately, many of the papers in which these calculations are done for Al_3Li and Ni_3Al quote these formulas incorrectly. The confusion propagates forward into later papers that use these papers as sources. Copley and Kear (1967), Furukawa, Miura and Nemoto (1985) and Jensrud (1985) all have erroneous equations. Sample calculations for binary aluminum-lithium alloys are included in section VI.9.3.2.1.

IV.5.2 Minimum precipitate size for Orowan looping.

The minimum precipitate size for Orowan looping is an easily measurable experimental quantity that has a relatively precise value. As such it is a good descriptor of strength. If the exact criterion for Orowan looping in a particular system were known, then γ and the looping radius would be redundant information since they would depend on one another directly in a known way. Orowan looping begins when the precipitate size reaches the point of equality in the force balance between the stress for Orowan looping and the stress for particle shear. In the simplest case, when the particle strength comes entirely from the formation of the antiphase boundary (i.e. when misfit is negligible), the looping condition is

$$2T = 2r_{loop}\gamma. \qquad \text{(IV.41)}$$

In order to make numerical comparisons with the results of others possible, it is assumed in this equation that Orowan looping occurs

when β is equal to one (1) rather than the value of 0.7 suggested by Bacon et al. (1973). Substituting the de Wit-Koehler form of the line tension given in equation IV.19 gives an expression for the antiphase boundary energy in terms of the minimum looping radius

$$\gamma = (Gb^2/4\pi r_{loop})\{(1 + \upsilon - 3\upsilon\sin^2\xi)/(1 - \upsilon)\}(\ln (1_s/b)). \qquad (IV.42)$$

For screw dislocations, this equation reduces to

$$\gamma = (Gb^2/4\pi r_{loop})\{(1 + \upsilon)/(1 - \upsilon)\}(\ln (1_s/b)). \qquad (IV.43)$$

Note that the antiphase boundary energy calculated from this equation is larger than the one that would be obtained from the results of Bacon et al. (1973) by a factor of $(1 + \upsilon)/(0.7)$ or approximately a factor of two (2). These factors have been omitted so that literature results for the antiphase boundary energy as determined by various techniques can be compared.

Similar calculations exist in the literature for other definitions of the Orowan stress. Kelly and Nicholson (1963) use $\tau = Gb/L$, Raynor and Silcock (1970) use

$$\gamma = Gb^2/8\pi r_{loop}[(2 - \upsilon)/(1 - \upsilon)]\ln (8r_{loop}/b) \qquad (IV.44)$$

and Chaturvedi, Lloyd and Chung (1976) use a more sophisticated version that includes two additional terms to account for the effect of coherency strains and the applied stress on the energy to form an Orowan loop.

IV.5.3 Dislocation pair spacing calculations.

Dislocations that shear ordered precipitates are weakly coupled since later dislocations restore the order of the precipitate removed by the first dislocation. For the $L1_2$ structure, the superlattice dislocation has twice the Burgers vector of matrix dislocation, so the dislocations travel in pairs.

The spacing of the second dislocation from the first and its effect on the strength of the material depend on its interaction with

the precipitates. If the sheared obstacles are either attractive or transparent to the second dislocation, then the pair spacing is a meaningful descriptor and may be simply calculated. If the sheared precipitates repel the second dislocation (for instance in the case of a misfitting ordered particle), then the second dislocation assumes a local strong line configuration and the dislocation spacing varies significantly along the dislocation line. In this case the dislocation pair spacing is some type of average of the various spacings observed.

Despite the problem of finding a suitable average dislocation pair spacing, the pair spacing is often calculated in terms of the antiphase boundary energy of the precipitate from the repulsive force between two dislocations. This repulsive force is

$$R' = Gb^2/(2\pi K\delta)(1 - \upsilon\cos^2\xi) \qquad \text{(IV.45)}$$

where ξ is the angle between the Burgers vector and the dislocation line and δ is the dislocation spacing (Raynor and Silcock, 1970). If the trailing dislocation is reasonably straight, the force due to the applied stress that is opposed by the precipitates is

$$F = 1/2(\gamma^{3/2}{}_r{}^{1/2}{}_f{}^{1/2}/T^{1/2} + \gamma f) \qquad \text{(IV.46)}$$

where the γf term comes from the attractive force from the antiphase boundary area between the two dislocations. (This equation again neglects dislocation self-interactions.) Equating IV.45 and IV.46 and solving for the dislocation pair spacing (since solving for γ is complicated although possible) we have

$$\delta = (Gb^2/\pi)(1-\upsilon\cos^2\xi/1-\upsilon)/(\gamma^{3/2}{}_r{}^{1/2}{}_f{}^{1/2}/T^{1/2} + \gamma f). \qquad \text{(IV.47)}$$

Ardell et al. (1976) also calculate the dislocation pair spacing for the case when the second dislocation does not lie within the precipitates. Using a model which considers the area swept out by the dislocation when it is released by the precipitate, they get the equation

$$\delta = Gb^2/\pi u(1-\upsilon)\gamma \qquad \text{(IV.48)}$$

where

$$u = \{(4B + B^{2/3})^{1/2} - B\}/2(1-B/6) \qquad \text{(IV.49)}$$

and

$$B = 3\pi^2\gamma f\langle r\rangle/32T. \qquad \text{(IV.50)}$$

This equation is considerably simplified if either f or $\langle r\rangle$ is small since u reduces to $B^{1/2}$ when $B\ll 1$. The simplified equation is almost the same as equation IV.49, but omits the factor of $(1-\upsilon\cos^2\xi)$. If the dislocation is straight, u should be replaced by (u + f). Ardell et al. get reasonable agreement with the spacings observed experimentally in Ni_3Al if they measure $\langle r\rangle$ and f, and assume T and γ.

IV.5.4 Discussion of methods for determining strength of ordered precipitates.

It should be clear from the above discussion that in an alloy hardened by ordered precipitates with low misfit strains the dislocation pair spacing, the minimum radius for Orowan looping, and the antiphase boundary energy are closely related quantities. If our theories of dislocation-dislocation and dislocation-precipitate interactions were exact and our measurements of experimental parameters and material properties accurate, these quantities would be entirely redundant; any two could be calculated if the third were known. The theory could then be written using these properties interchangeably as convenient. Then it would only be necessary to determine one of these properties for a particular material in order to use the theory to predict strengthening behavior. However, each of the equations above that relates these parameters contains approximations. It is obviously relevant to assess which method contains the most realistic approximations on a case by case basis.

Some experimental input is required no matter what method is used. This input may be the dislocation pair spacing, the minimum observable loop size, the strength at some point on the aging curve (Melander and Persson, 1978a) or the γ that makes the theory fit the experimental data best (Munjal and Ardell, 1975). A problem common to all these methods is that the antiphase boundary energy may change with precipitate radius, composition and/or temperature.

The first principles calculation of the antiphase boundary energy

from the T_c is the most commonly used method of determining the antiphase boundary energy. It is an appealing choice since knowledge of the crystal structure of the ordered phase and the T_c from the phase diagram is all that is required. However, it is hard to get something for nothing, and the assumption that γ is dominated by first nearest neighbor interactions probably means that the calculation is at best somewhat qualitative. While the accuracy is probably better than an order of magnitude, quoting antiphase boundary energies to better than 10% accuracy is clearly unreasonable. The calculation is best used to examine the qualitative effects on the antiphase boundary energy of the T_c, the dominant glide plane and the degree of long-range order.

An additional problem with the theoretical calculation is that while most investigators have assumed that the long range order parameter S is unity, logic and the little available experimental data suggest that this is rarely the case. Since the miscibility gap in which the ordered precipitate is stable has finite width at any temperature below the critical temperature, the precipitate is not expected to be stoichiometric. The long range order parameter must then be less than one. Since γ is proportional to the square of S, even a small deviation from perfect order can cause an additional ten or twenty percent error in the calculated value of the antiphase boundary energy.

The dislocation pair spacing is a commonly used technique for determining the antiphase boundary energy. The contouring of the dislocations means that some type of average spacing must be used. A perhaps more important issue concerns the magnitude of any relaxation that might occur in the thin foil. Nembach, Suzuki, Ichihara and Takeuchi (1985) have shown that qualitatively different results are obtained for thick specimens that resemble bulk material and thin specimens that do not provide sufficient constraint on the dislocations. Other investigators feel that the method is reliable and that any effects of relaxation on the dislocation pair spacing are probably minimal (Ardell, 1986).

The chief source of relaxation is the repulsion between the two dislocations. In particular, the trailing dislocation will relax away from the bowed out first dislocation. The first dislocation is expected to remain bowed even if relaxation is important because the bowout increases the separation of the dislocations. Relaxation is op-

posed by the frictional stress imposed by the matrix and by the precipitates most recently sheared by the second dislocation. It seems unlikely that the second dislocation will shear any precipitates as it moves backward (reintroducing an antiphase boundary), so the magnitude of the relaxation effect should be determined by the relative sizes of the dislocation pair spacing δ and the mean square obstacle spacing l_s. When the obstacles are far apart, the second dislocation may relax backwards for some distance before it prevented from doing so by precipitates. When the obstacles are closely spacing, the backward relaxation is immediately arrested.

The minimum precipitate size for Orowan looping is the other quantity that measures obstacle strength. This method has the drawback that it also requires careful transmission electron microscopy to determine either the minimum looped radius or the maximum sheared precipitae radius. The looping radius can only be related to the other two quantities by a theory of strengthening that includes all operative mechanisms and correctly accounts for the effects of obstacle spacing and size. Therefore, the values for γ and δ are only as good as the strengthening theory used to calculate them. However, this method has the advantage that the strengthening theory can be formulated directly in terms of the looping radius. This technique is in effect a first order perturbation correction to the theory, since the misfit strain is implicitly included in the value of the antiphase boundary energy, although it is not explicitly considered. (Using the dislocation pair spacing would also be a first order perturbation solution, but a much more awkward one.) The improved accuracy of this approach stems from the fact that it accounts for the influence on the strength of effects that are neglected in the theory, at least for the lead dislocation. It has the second advantage that it provides a blind fit to the data; no critical resolved shear stress data are used as input to the theory that is supposed to predict it. On the basis of these arguments, the looping radius would seem to be a highly desirable choice for a measure of precipitate strength.

IV.6 Effect of superdislocations on the critical resolved shear stress.

IV.6.1 Calculation of superdislocation coupling.

In alloys hardened by shearable ordered particles, two or more dislocations may become coupled since the passage of the first dislocation destroys the order of the particle and the passage of some number of subsequent dislocations restores it. Since these dislocations are close together, their effect on the critical resolved shear stress is similar to the uncoupled pileup of dislocations considered in Appendix C. The equations which describe the situation are slightly different since the dislocations are coupled by the antiphase boundary area between them. For the case of a dislocation pair, the force balance is given by

$$\tau_c^1 - \tau_c^{APP} - \tau_c^i = 0 \qquad \text{(IV.51)}$$

$$\tau_c^2 - \tau_c^{APP} + \tau_c^i = 0$$

where τ_c^n is the critical resolved shear stress for glide of the nth dislocation, τ_c^{APP} is the applied resolved shear stress and τ_c^i is the interaction shear stress. The interaction stress can be broken into two terms, one of which describes the dislocation repulsion important above and the second of which describes the effect of the antiphase boundary area between the two dislocations.

Brown and Ham (1971) (and Gleiter and Hornbogen, 1965) specify the values of the shear stresses above for the force balance at the point when the first dislocation breaks through the particle. For volume fractions less than 0.2, using the average obstacle spacings L and particle sizes d along each dislocation and an applied stress τ^{APP} they find

$$d_1\gamma - b\tau^{APP}L_1 - RL_1 = 0 \qquad \text{(IV.52)}$$

$$-d_2\gamma - b\tau^{APP}L_2 + RL_2 = 0$$

where R is the repulsive interaction force per unit length of dislocation. The $d_i\gamma$ and RL_1 terms in equation IV.52 correspond to the τ_c^n and

τ_c^i terms, respectively, in equation IV.51. Eliminating R gives

$$\tau_c^{APP} = (\gamma/2b)(d_1/L_1 - d_2/L_2). \qquad (IV.53)$$

For this equation to be at all useful, we have to make assumptions about the term in parentheses. For instance, letting $d_2/L_2 = 0$ gives the simple pileup case.

Both Brown and Ham and Gleiter and Hornbogen find that if the first dislocation is near looping, the two dislocations will act essentially as simple pileup of two dislocations (i.e. the effect of the antiphase boundary area can be neglected). If the second dislocation is nearly straight, the common case, then the stress on the first dislocation is given by

$$\tau_c^1 = 2\tau_c^{APP} + \gamma f/b$$

where f is the volume fraction of ordered phase. In this case the stress on the first dislocation is greater than for a simple pileup of two dislocations.

Gleiter and Hornbogen (1968) show a plot of decreasing critical resolved shear stress as a function of particle radius due to this effect; however, their illustration exaggerates the magnitude of the effect.

IV.6.2 Experimental Observations

Nembach et al., 1985 show high-voltage electron microscope (HVEM) pictures of superdislocations in a Ni_3Al superalloy. The second dislocation is essentially straight even though the first one is strongly bowed. This observation contradicts suggestions by other workers that the second dislocation is pulled forward by the attraction of the antiphase boundary area between the dislocations. De Hosson, Huis in't Veld, Tamler and Kanert (1984) show HVEM pictures of Al_3Li hardened alloys. They also show an essentially straight second dislocation.

IV.6.3 Strong line approximation

The average line calculations described in IV.6.1 are not really satisfactory for a strong line theory. Fortunately, in some cases the situation is actually simplified by a strong line approximation. If the obstacles are attractive to the second dislocation (e.g. misfit-free ordered precipitates), then in general the stress on the lead dislocation should be greater than $2\tau^{APP}$. Since the critical resolved shear stress is controlled by the strongest line, it should also be controlled by the line on which the applied stress is magnified least. This rationalization justifies the simple solution of taking the stress on the lead dislocation to be precisely double the applied stress (i.e. ignoring the coupling of the dislocations). However, if the obstacles are repulsive to the second dislocation (e.g. precipitates with non-negligible misfit strains), then the second dislocation will take on a local strong line configuration. The stress on the lead dislocation is then some indeterminate amount less than $2\tau^{APP}$. The strength of the joint strong configuration for the two dislocations has not been analyzed statistically.

Another question that remains unsolved is what happens after peak strength when the coupling between dislocations weakens because an increasing number of precipitates are looped rather than sheared. The uncoupling should cause the critical resolved shear stress to drop off after peak strength much more slowly than it would otherwise. However, no theory for this situation currently exists.

V. Theoretical analysis of the precipitate size distribution effect.

It has been recognized for some time that obstacles to dislocation glide in real systems almost always have a range of strengths. It has generally been assumed that the average particle describes the distribution reasonably well. For many purposes, this is in fact the case. However, there have been a few investigations of the effect of this precipitate size distribution on strength that indicate there is an effect. The strong line solution for the critical resolved shear stress described in Section II combined with the analysis of Section IV provides the basic tools for an analysis of the effect of the precipitate size distribution on the aging curve.

The concept of investigating the aging behavior of real alloys with the strong line solution is not new. Melander and coworkers have published a series of papers on the age hardening behavior of various precipitation and dispersion hardened alloys. They use a formalism based on the Hanson and Morris theory that is similar but not identical to the one described here. Melander uses series expansions of the basic formulae (see Altintas, 1978) and a variable line tension (described in Section IV.2). On the basis of these assumptions, computations of the force-distance relation for the dislocation interaction with the precipitates, and one forced match in the strengthening profile, Melander is able to achieve good agreement for the aging curve for oxide-dispersion-hardened copper (1978), underaged and peakaged AlZnMg (Melander and Persson, 1978a and 1978b), and Al-Ag (Jansson and Melander, 1979).

Melander and Persson (1978c) also examine hardening in a γ' hardened nickel alloy. The dislocation-particle interaction is calculated for the superposition of the misfit and ordering-related interactions on the assumption that each dislocation of the pair is decomposed into partials. Edge control of deformation is assumed. The antiphase boundary energy is used as a fitting parameter. Again good agreement is obtained up to peak strength. Melander does not discuss the alloy design implications of his results. This work is reviewed in an article by Melander and Jansson (1979).

This section contains a full derivation using assumptions based on the discussion of Section IV. A discussion of the results comprises

Section VI. The application of the theory to binary aluminum-lithium alloys is discussed in Section VII.

V.1 Assumptions of Model

The random array solution for the critical resolved shear stress for dislocation glide is based on a simple idealization of the general problem. It has been used with reasonable sucess to model a number of experimental situations. The chief assumptions, along with the sections in which they have been discussed, are as follows:

(1) The dislocation is a flexible line of constant line tension T for a given mean square obstacle spacing l_s. (Section II)

(2) The obstacles to dislocation glide are modelled as a random array of immobile point barriers. The properties of the point obstacle are adjusted so that the interaction of the dislocation with the obstacle is mathematically equivalent to its interaction in the glide plane with the physical obstacle. (Section II)

(3) The configuration of the dislocation is described by a unique set of pinning points. The critical resolved shear stress of the array is reached when the dislocation bypasses the weakest point in the strongest configuration. (Section II)

(4) For a random array of identical obstacles the problem may be solved analytically using standard statistical techniques. It is convenient to define a dimensionless critical resolved shear stress

$$\tau^* = \tau l_s b/2T \tag{V.1}$$

where b is the Burgers' vector in the glide plane. The analytic solution is then given by

$$\tau^* = 0.8871(\beta)^{3/2} \tag{V.2}$$

where β is a dimensionless obstacle strength given by

$$\beta = F/2T \tag{V.3}$$

and F is the force to bypass the obstacle. (Section II)

(5) The critical resolved shear stress for a mixture of obstacle types is a quadratic sum

$$\tau^2 = \Sigma\ x_\alpha(\tau_\alpha)^2 \qquad \text{(V.4)}$$

where x_α is the fraction of obstacles of type α and τ_α is the CRSS for an array containing obstacles of type α only. (Sections II and IV.1)

In order to study the effect of the precipitate size distribution on the yield strength of an alloy hardened by coherent, ordered precipitates the following additional assumptions were made:

(6) The precipitates coarsen according to the LSW rate law and at constant volume fraction (in the interior of a grain). (Section IV.4)

(7) The shape of the precipitate size distribution as a function of $r/\bar{r}$ does not evolve during coarsening. (Section IV.4)

(8) Each spherical precipitate may be reduced to a set of point obstacles whose strengths correspond to the effective radii of the precipitate in the glide planes it intersects. Therefore, even if all precipitates are the same size, there will be a distribution of obstacle sizes in the glide plane.

(9) The strength of the obstacles is assumed to be a function of the radius of the sheared ordered precipitate only. This is equivalent to neglecting the misfit of the precipitate. (Section IV.5)

(10) The strength of the obstacle may be related to the maximum obstacle strength, which corresponds to the looping radius. At the looping radius Orowan looping is first preferred over shearing of the precipitate. The Orowan condition puts an upper limit on the strength of the obstacle whatever its physical size. The antiphase boundary energy is not required to compute the obstacle strengths. (Section IV.5)

(11) There is considerable confusion in the literature over the appropriate form of the line tension. Following the approach of Bacon, et al. (1973), we have adopted equation IV.26. The outer and inner cutoff radii are equated with l_s and b respectively. The line tension

for a screw dislocation is then

$$T = [Gb^2/4\pi(1 - \upsilon)]\ln(1_s/b). \qquad (V.5)$$

We have also adopted the upper limit on β of 0.7 suggested by Bacon, et al. (Sections IV.2 and IV.3)

(12) The dislocations move as superdislocation pairs. The effect of the pair is that the actual stress at the obstacle is twice the applied stress. Therefore, the applied shear stress at yielding is half the value it would be if the dislocations moved separately. This factor is not included in the formulae given in this section, but is included in the numerical calculations for Al-Li alloys in Section VI (Section IV.6)

(13) The calculated critical resolved shear stress due to the obstacle distribution represents the increment in the total strength of the alloy due to precipitate hardening only and should properly be denoted $\Delta\tau$. (Section IV.1)

V.2 Critical resolved shear stress for precipitates of uniform size.

V.2.1 Obstacle strength distribution.

Using the formalism described above, the critical resolved shear stress as a function of precipitate radius may be calculated for a random distribution of precipitates coarsening at constant volume fraction. This approach lends itself to the prediction of the shape of an aging curve. Initially, the precipitates are taken to be of uniform size, which is equivalent to shrinking the distribution of precipitate sizes down to a delta function of the same volume fraction. It is both convenient and physically realistic to define a dimensionless precipitate radius

$$r^* = r/b. \qquad (V.6)$$

where r^* is generally rounded to the nearest integer. For notational ease, the integer value is denoted I when it appears as the index of a sum.

Each spherical precipitate of radius r^* may be reduced to a set of point obstacles generated by the intersection of the precipitate with a series of parallel glide planes. The effective radius of the precipitate within the glide plane is assumed to be the radius of the circle defined by the intersection of the precipitate with the glide plane. Since the glide plane lies between two atomic planes, the radius of the precipitate in the glide plane is defined to be the larger of the radii in the two adjacent atomic planes to avoid ambiguity. The intersections of a precipitate of radius r_o^* with the glide planes forms the set of effective radii r_α^* $\{r_o^*, r_1^*, \ldots r_I^*\}$ where

$$r_\alpha^* = [(r_o^*)^2 - \alpha^2]^{1/2}. \tag{V.7}$$

Note that each precipitate contributes two obstacles of each effective radius, one on either side of the central plane (see figure V.1). Each of these effective radii of interaction may be reduced to a point obstacle with strength β_α determined by a force relation that depends on the physical properties of the precipitate as well as on the effective radius. If the precipitates are randomly distributed within a volume, then the obstacle types will be randomly distributed with respect to strength and location within the glide plane. The fraction of obstacles with each strength corresponds to the fraction of obstacles with each effective radius generated by the precipitate. The obstacle strength distribution for this case is shown in figure V.2.

The fraction of obstacles of a given strength is given by the number of obstacles possessing that strength divided by the total number of obstacles, N. Let x_o be the fraction of obstacles with strength β_α. When all the precipitates are the same size, the fractions of all obstacles with radii r_α^* are the same and equal to x_o. The total number of obstacles is given by

$$\sum_\alpha^I x_\alpha = 1 \tag{V.8}$$

where the index α begins at 0. It follows that the fraction of obstacles with strength β_α is given by

$$x_\alpha = 1/I = 1/r^*. \tag{V.9}$$

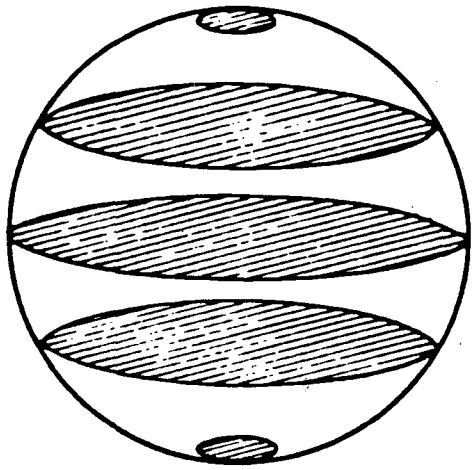

XBL852-5894

Figure V.1 Generation of effective radii of point obstacles from a single physical precipitate intersected by several glide planes.

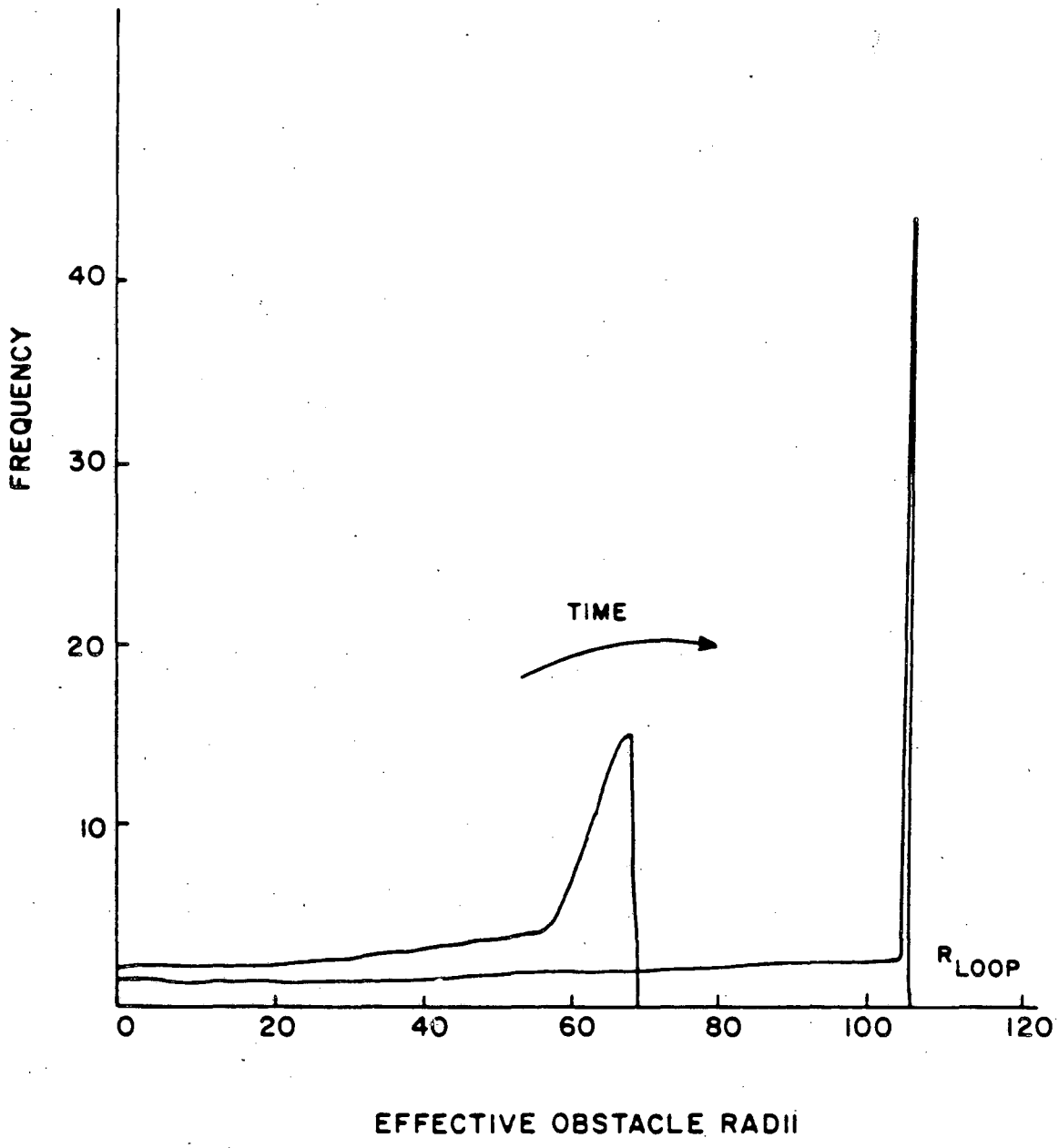

Figure V.2 Distribution of effective obstacle radii for precipitates of uniform size.

The dimensionless critical resolved shear stress for the distribution of obstacles created by precipitates of a single size may now be determined. From equations V.2 and V.4, the critical resolved shear stress for the multiple obstacle type case is

$$(\tau_c^*)^2 = 0.7870 x_o \Sigma_{\alpha=0}^{I} \beta_\alpha^3 \qquad (V.10)$$

where the maximum value of β_α is β_c, the strength at which Orowan looping occurs.

To complete the solution, the equation must be rewritten so that it contains only independent, measurable variables. The variables used to make the problem dimensionless must also be constant with precipitate radius. Any dependence of the variables β, β_c, τ, τ^*, T and l_s on the particle radius must be made explicit.

V.2.2 Mean Square Obstacle Spacing.

If the precipitates are coarsening at constant volume fraction, the value of l_s, the characteristic length, increases with the precipitate radius (or, equivalently, time). The value of l_s is related to the dimensionless obstacle spacing $L^* = n^{1/2}$. Let p represent the number of precipitates in a unit volume at some time t^*, n the corresponding number of obstacles, and let p_0 and n_0 be their initial values. Then the constant volume fraction condition requires

$$p = p_0(r_0/r)^3. \qquad (V.11)$$

The total number of obstacles is given by

$$n = 2pr^* \qquad (V.12)$$

$$= n_0(r_0/r)^2$$

so the dimensionless obstacle spacing is

$$L^* = n^{1/2} = n_o^{1/2}(r_o^*/r^*). \qquad (V.13)$$

The characteristic length l_s is related to the dimensionless spacing by

$$l_s = a^{1/2} = (A/n)^{1/2} = A^{1/2}/L^* \tag{V.14}$$

where A is the area of the glide plane. Therefore the change in the value of l_s as the precipitates coarsen is given by

$$l_{s,t} = l_{s,0}(L_0^*/L_t^*) = l_{s,0}(r^*/r_o^*) \tag{V.15}$$

where $l_{s,t}$ and L_t^* are the characteristic length and dimensionless spacing at time t^* and $l_{s,0}$ and L_0^* are their initial values.

Using relation V.15, the dimensionless critical resolved shear stress may be conveniently redefined so that it is proportional to the actual critical resolved shear stress at all times. Let τ^{o*}, the proportional critical resolved shear stress be defined so that

$$\tau^{o*} = \tau l_{s,0} b/2T \tag{V.16}$$

$$= \tau^*(L_t^*/L_0^*).$$

If the line tension is taken to be constant, all the variables on the righthand side of this equation except τ are constant with time.

The numerical value of $l_{s,0}$, the initial characteristic length, may be determined in terms of experimental parameters: $\emptyset$ the volume fraction of the precipitate, r_o, the initial radius of the precipitate at time t=0, and the Burgers vector for the dislocation in the matrix. From equation V.14, the characteristic length is

$$l_s^2 = A/n = V/bn = 1/bn_v \tag{V.17}$$

where n_v is the number of obstacles per unit volume. The number of precipitates per unit volume, p_v, is related to the volume fraction $\emptyset$ by

$$p_v[(4/3)\pi r^3] = \emptyset \tag{V.18}$$

or, using equation V.12,

$$2n_v(r/b)[(4/3)\pi r^3] = \emptyset. \tag{V.19}$$

From equation V.17, the value of $l_{s,0}$ is given by

$$l_{s,0} = [\{(4/3)\pi r_o^3\}/\{2\emptyset r_o\}]^{1/2} \qquad (V.20)$$

$$= [2\pi/3\emptyset]^{1/2} r_o$$

which is the result quoted by Ardell (1985). The value of r_o is generally taken as proportional to b. For lack of a good argument for a particular value, it is simplest to set r_o equal to b.

This form of l_s makes the dependence of the critical resolved shear stress on the volume fraction of precipitates explicit. The critical resolved shear stress is proportional to the square root of the volume fraction, a standard result.

V.2.3 Obstacle strength.

V.2.3.1 Constant line tension case.

The random array model derived by Hanson and Morris (1975a and 1975b) and many other models of strengthening consider the line tension to be constant. Therefore, it is of interest to determine the variation of the critical resolved shear stress with precipitate radius for constant line tension and then to compare that result to that for variable line tension.

The dimensionless obstacle strength is determined by the force F that the dislocation must exert on the obstacle to bypass it. For ordered precipitates whose strength comes mainly from the antiphase boundary created when they are sheared, the force is linear with the precipitate radius. However, at large precipitate sizes, the precipitate will no longer be sheared, Instead, the dislocation will bypass the precipitate by Orowan looping. The force required for Orowan looping is approximately constant with precipitate size and is related to the minimum precipitate radius r_{loop} at which Orowan looping occurs. When the precipitate is reduced to point obstacles, its strengthening characteristics are retained, and the dimensionless obstacle strength is given by

$$\beta_\alpha = F_\alpha/2T = Br^*_\alpha/2T \qquad r^*_\alpha \leq r^*_{loop} \qquad \text{(V.21a)}$$

$$\beta_c = F_c/2T = Br^*_{loop}/2T \qquad r^*_\alpha > r^*_{loop} \qquad \text{(V.21b)}$$

where r^*_{loop} is the minimum dimensionless radius at which Orowan looping occurs and β_c is the largest value of β observed. The shear strength of the precipitate given in equation V.21a may be rewritten in terms of equation V.21b so that it is expressed in terms of experimentally observable variables

$$\beta_\alpha = \beta_c(r^*_\alpha/r^*_{loop}). \qquad \text{(V.22)}$$

The numerical constant B in equations V.21a and V.21b contains the antiphase boundary energy. The value of β_c has been set at 0.7.

The relationship between β and r^* (equation V.22) makes it possible to rewrite relation V.10 in terms of r^*, viz:

$$(\tau^*_c)^2 = (0.7870/r^*)(\beta_c)^3[\Sigma^I_\alpha (r^*_\alpha/r^*_{loop})^3] \qquad \text{(V.23)}$$

where r^*_α has been redefined to be the <u>effective</u> dimensionless radius and cannot be greater than r^*_{loop}. The proportional critical resolved shear stress is defined as before.

V.2.3.2 Variable line tension.

As discussed in section IV.2, the line tension is not generally constant in physical systems. The model can be reformulated in terms of the line tension of equation IV.26 taken from the results of Bacon et al. (1973) so that

$$T = [Gb^2/4\pi(1 - \upsilon)][\ln (l_s/b)] \qquad \text{(V.24)}$$

for a screw dislocation. In a system coarsening at constant volume, this equation implies that the line tension is an increasing function of time since the value of l_s increases.

The obstacle strength is now given by an analogous pair of equa-

tions to V.21:

$$\beta_\alpha = F_\alpha/2T_I = Br^*_\alpha/2T_I \qquad r^*_\alpha \leq r^*_{loop} \qquad (V.25a)$$

$$\beta_c = F_c/2T_{II} = Br^*_{loop}/2T_{II} \qquad r^*_\alpha > r^*_{loop} \qquad (V.25b)$$

where T_I is the line tension for the configuration of which β_α is a part and T_{II} is the line tension of the configuration for which r^*_{loop} was determined. The shear strength of the precipitate given in equation V.22 may be rewritten in terms of equation V.25 so that it is expressed in terms of experimentally observable variables

$$\beta_\alpha = \beta_c(r^*_\alpha/r^*_{loop})(T_{II}/T_I). \qquad (V.26)$$

Since the line tension T is defined for the entire configuration, the critical resolved shear stress for the distribution of obstacles created by the identical precipitates is

$$(\tau^*_{cT})^2 = (0.7870/r^*)(\beta_c)^3(T_{II}/T_I)^3 \Sigma^I_\alpha\ (r^*_\alpha/r^*_{loop})^3. \qquad (V.27)$$

The ratio of line tensions may be simplified to

$$T_{II}/T_I = \{\ln l_{s,loop}/b\}/\{\ln l_{s,t}/b\}. \qquad (V.28)$$

The variable line tension also affects the answer through the factor of T in the definition of τ^* (equation V.1). Again a new proportional critical resolved shear stress which is constant with time may again be defined

$$\tau_T^{o*} = \tau l_{s,0} b/2T_0 \qquad (V.29)$$

$$= \tau^*_T(L^*_t/L^*_0)\{(\ln l_{s,t}/b)/(\ln l_{s,0}/b)\}$$

where T_0 is the line tension at t = 0. The final equation, in terms of precipitate radius is

$$(\tau^{o*}_{cT})^2 = (0.7870/r^*)(\beta_c)^3(T_{II}/T_I)^3(L^*_t/L^*_0)^2\{(\ln l_{s,t}/b)/(\ln l_{s,0}/b)\}^2$$

$$\cdot \Sigma^I_\alpha\ (r^*_\alpha/r^*_{loop})^3 \qquad (V.30)$$

$$= M(1/r^*)^3\{(\ln l_{s,loop}/b)/(\ln l_{s,0}/b + \ln (r^*/r_o))\}^3 \cdot$$

$$\{1 + [\ln (r^*/r_o)/(\ln l_{s,0}/b)]\}^2 \cdot \Sigma_\alpha^I (r_\alpha^*/r_{loop}^*)^3 .$$

where M includes some of the constant terms. Different precipitate size distributions in the same material generally have different values of $l_{s,0}$. To isolate the effect of coarsening, the critical resolved shear stress may be normalized by dividing out the value $l_{s,o}$. The new normalized critical resolved shear stress is denoted τ_T^{o**}.

V.2.4 Aging curves.

Analyzing equation V.30 for its r-dependence, we find that, neglecting the log terms,

$$\tau_{cT}^{o*} \sim (r^*)^{-3/2}[\ \Sigma_\alpha^I\ (r_\alpha^*)^3]^{1/2}. \qquad (V.31)$$

At very small values of r, the sum is dominated by its largest term and $\tau \sim 1$. If the sum is replaced by r terms which are proportional to r^3, then τ is proportional to $r^{-1/2}$. The actual dependence, which includes the logarithmic terms as well, should be somewhere in between. If we ignore any dislocation uncoupling effects that might occur after looping (possibly a rather poor assumption), the critical resolved shear stress is approximately proportional to 1/r after precipitate looping begins.

The precipitate radius and the aging time are equivalent variables if the precipitate coarsening rate is known. Consequently, the equations can be reformulated in terms of time so that they represent an aging curve.

Coherent, spherical precipitates generally coarsen according to the Lifshitz-Slyozov-Wagner rate law

$$r^3 - r_o^3 = kt \qquad (V.32)$$

where r_o is the initial precipitate radius, r is the radius of the precipitate at time t and k is a rate constant which is a function of the diffusivity and the interfacial surface tension. It is convenient

to write the time in the dimensionless form

$$t^* = kt/r_o^3 \tag{V.33}$$

so that the dimensionless coarsening law is given by

$$(r^*)^3 = (r_o^*)^3(1 + t^*). \tag{V.34}$$

At long times this equation reduces to

$$r^*/r_o^* = (t^*)^{1/3}. \tag{V.35}$$

The critical resolved shear stress may then be rewritten in terms of the time using equation V.34. Rather than substituting in, we can refer to the dimensional analysis of $\tau(r^*)$. The critical resolved shear stress should then increase with time proportional to $(t^*)^{1/6}$. After looping begins, the critical resolved shear stress is proportional to $(t^*)^{-1/2}$.

V.3 Critical resolved shear stress for an arbitrary distribution of precipitate sizes.

In real materials, precipitate sizes are always distributed over some finite range. Consequently, the critical resolved shear stress for an arbitrary distribution of precipitate sizes is the quantity of practical interest. The critical resolved shear stress for multiple precipitate sizes may be obtained by a straightforward extension of the theory for a single precipitate size. The contributions of each precipitate size are summed quadratically in the same way as the contributions of each obstacle type were summed above.

The precipitate size distribution is described by a finite number of elements y_1, y_2 ... y_e ... y_E, where E is the total number of elements in the distribution. Each element is associated with a precipitate radius such that $r_E > r_{E-1}$, etc. Let the fraction of the total number of precipitates included in element e be denoted by f_e. Then the total number of obstacles is given by

$$\sum_1^E x_{0,e} r_e^* = 1 \tag{V.36}$$

where x and r^* have their previous definitions, but now represent the precipitates belonging to element e of the distribution. The fraction of obstacles that would have strength $\beta_{0,e}$ if only obstacles belonging to element e were present is denoted x_0. The fraction of obstacles with radius $x_{0,e}$ is just the fraction of precipitates in element e times x_0. Rewriting equation V.9 for the distribution gives an expression for x_0

$$x_0 = [\Sigma_{e=1}^{E} f_e r_e^*]^{-1}. \tag{V.37}$$

The distribution of obstacle sizes created by a Gaussian distribution of precipitate sizes is shown in figure V.3.

Writing a quadratic sum over the elements of the distribution leads to an expression for the dimensionless critical resolved shear stress over the elements of the distribution analogous to that in equation V.10

$$(\tau^*)^2 = 0.7870 x_0 \Sigma_{e=1}^{E} f_e [\Sigma_{\alpha=0}^{Ie} \beta_{\alpha,e}^3]. \tag{V.38}$$

This equation may be expanded using the expression for x_0 in equation V.37 and the equations for β given in equation V.21 or V.25. As before, r_α^* cannot be greater than r_{loop}^*.

The dimensionless critical resolved shear stress may be related to the proportional critical resolved shear stress as before by requiring the volume fraction of precipitates to be constant. The constant volume fraction condition for a distribution of precipitate sizes is

$$\Sigma_{e=1}^{E} p_{0,e}(r_{0,e})^3 = \Sigma_{e=1}^{E} p_e(r_e)^3 \tag{V.39}$$

where p_e refers to the number of precipitates with radius r_e. Defining P to be the total number of precipitates allows equation V.39 to be rewritten in a more convenient form

$$p_0 \Sigma_{e=1}^{E} f_{0,e}(r_{0,e})^3 = \Sigma_{e=1}^{E} f_e(r_e)^3. \tag{V.40}$$

Using this notation the total number of point obstacles created by these precipitates is given by

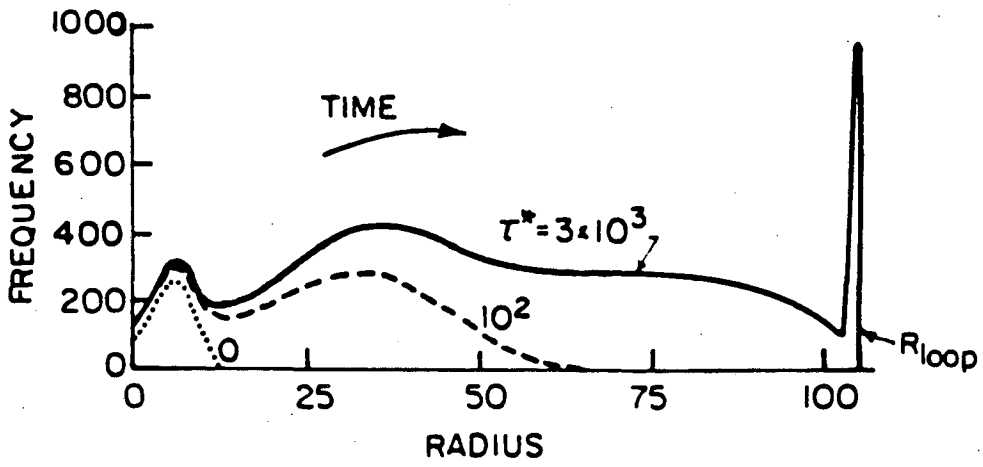

Figure V.3 Distribution of effective obstacle radii for a Gaussian precipitate size distribution as a function of aging time.

$$n = \Sigma_{e=1}^{E} n_e = P\Sigma_{e=1}^{E} f_e r_e^*. \qquad (V.41)$$

Equations V.13, V.15, V.19 and V.41 lead to the dimensionless obstacle spacing and then to the characteristic length $l_{s,t}$, given by

$$(l_{s,t})^2 = (l_{s,0})^2 \frac{\Sigma_{e=1}^{E} f_e r_e^3 \cdot \Sigma_{e=1}^{E} f_e r_{0,e}^*}{\Sigma_{e=1}^{E} f_e (r_{0,e})^3 \cdot \Sigma_{e=1}^{E} f_e r_e^*} \qquad (V.42)$$

The value of the proportional critical resolved shear stress with constant and variable line tension is defined by this ratio in equations V.16 and V.29, respectively.

The equations above for the critical resolved shear stress associated with distribution of precipitate sizes are thus far independent of the coarsening law chosen. However, they cannot be evaluated for a precipitate size distribution unless both the coarsening rate and the evolution of the shape of the distribution are specified.

If self-similar coarsening is assumed, the critical resolved shear stress may be calculated for an arbitrary distribution of precipitate sizes. The value of τ may be calculated using equations V.29, V.30, V.38 and V.42. The equation for τ is complex, but the overall proportionalities of τ to the experimental parameters are the same as those for the uniform precipitate case.

The value of $l_{s,0}$, the initial characteristic length may be determined in a fashion analogous to the way $l_{s,0}$ was determined for the single precipitate case. By analogy to equation V.20, we have

$$(l_{s,0})^2 = \{(4/3)\pi\Sigma_{e=1}^{E} f_e r_{o,e}^3\} / \{\emptyset b\Sigma_{e=1}^{E} 2f_e r_{o,e}^*)\}. \qquad (V.43)$$

The equation for the proportional resolved shear stress may be dimensionalized using this equation.

V.4 Discussion.

This section considers the implications of the model for age-hardening behavior and prediction of microstructures optimized for strength. The discussion focusses on three topics: the effect of precipitate shape, the effect of the dislocation line tension, and finally, the effect of the width of the precipitate size distribution on the strengthening. Results on the latter topic are compared and contrasted with those of other investigators.

V.4.1 Strength of plate-like precipitates.

Plate-like precipitates are usually observed when the misfit strain in the habit plane is relatively high, while spherical precipitates are generally observed when it is low. High-strength alloys are usually hardened by plate-like precipitates. The increase in strength is partially due to the high misfit strain and its localization at the perimeter of the plate, but it can also be shown that increased strengthening should be observed on purely geometric grounds.

Because the plate distributes the precipitated material more efficiently, a higher strength is predicted even if the misfit strain is ignored. Figure V.4 shows a spherical precipitate and a plate-like (disc-shaped) precipitate of equal volume. Since strengthening in athermal glide is determined entirely by the maximum in the force-distance relation for the precipitate-dislocation interaction, the plate strengthens much more efficiently. It provides both more obstacles, because it intersects more glide planes, and stronger obstacles because the width of the plate face is larger than the diameter of the sphere of equivalent volume. The increase in strength could be quantified for a specific plate aspect ratio and habit plane. The misfit strain around the plate could be included in the model by considering the effective size of the plate to be increased.

V.4.2 Advantages of uniform precipitate size

The general form of an aging curve for an order-hardened alloy that obeys Lifshitz-Slyozov-Wagner coarsening is discussed in Section V.2.4. Peak strength occurs because precipitate strength no longer increases with size beyond the looping radius. Since the precipitates

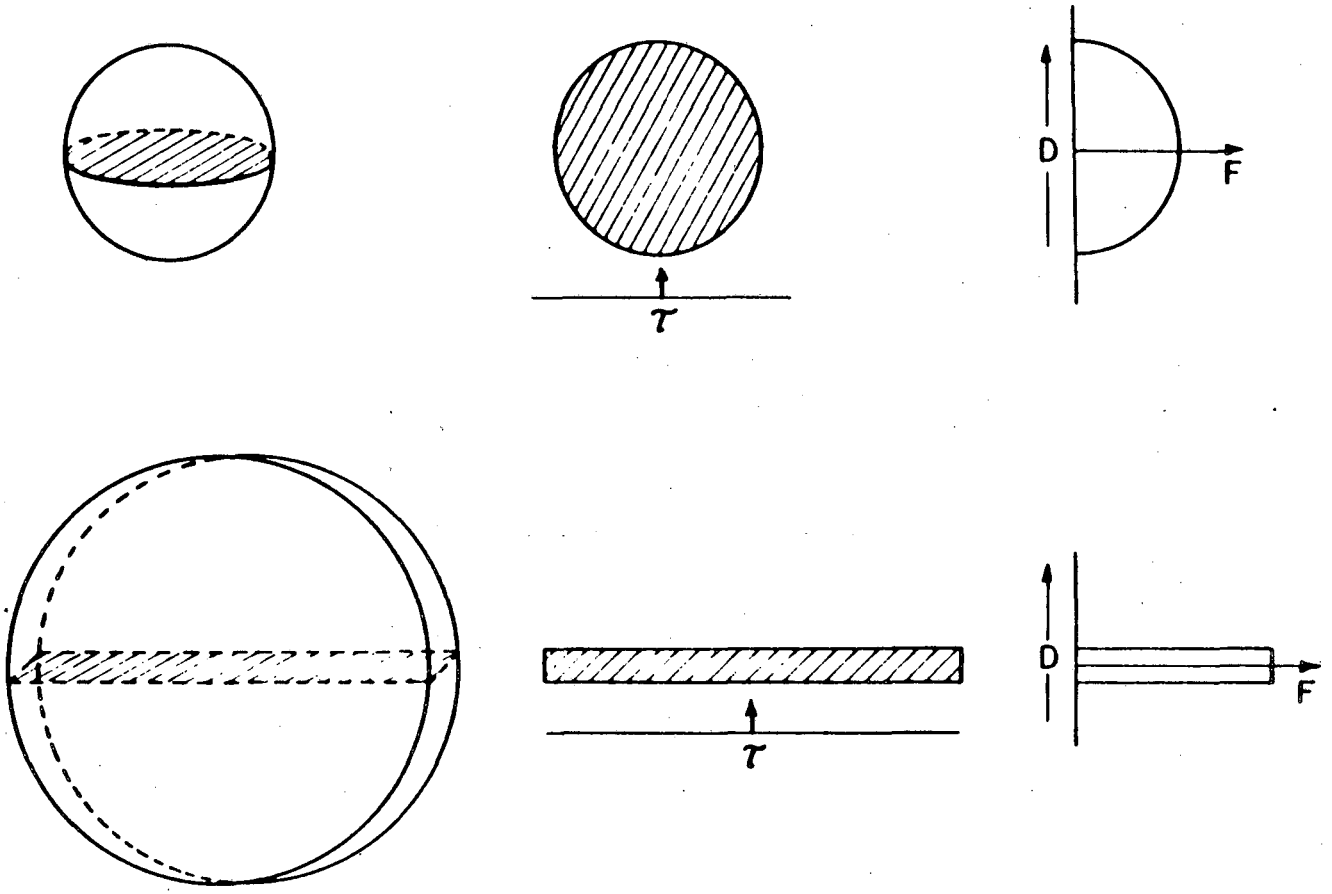

XBL862-7484A

Figure V.4 Comparative strengthening form spherical and plate-like precipitates with equal volume. Hatched areas indicate precipitate cross-section in the glide plane.

are coarsening at constant volume fraction, the largest precipitates are growing at the expense of smaller ones. Consequently, the total number of precipitates is constantly decreasing. When enough of the precipitates have radii greater than the looping radius, the number of precipitates decreases faster than the strength of the remaining precipitates increases. The critical resolved shear stress then begins to decrease.

The value of the critical resolved shear stress depends more strongly on precipitate radius after looping begins than before. Consequently, when a distribution of precipitate sizes exists, this solution predicts that peak strength occurs almost immediately after the largest of the precipitates reaches the looping radius, not when the average-sized precipitate reaches the looping radius. This will be true whether the line tension is assumed to be constant or to vary according to equation V.24. By contrast, the amount of strengthening provided by the precipitates is most closely related to the average precipitate radius or the average obstacle strength. As a result, the maximum achievable strength increases as the precipitate size distribution narrows. As illustrated in figure V.5, when the largest precipitates reach the looping radius, the average precipitate radius of a narrow distribution is greater than the average radius for a broad distribution. The strength of the narrow distribution is correspondingly higher. Figure V.6 shows the same effect quantitatively in aging curves for Gaussian precipitate size distributions of various widths illustrated in figure V.7. The magnitude of this effect for experimentally measured precipitate size distributions in binary aluminum-lithium alloys is considered in Section VI.4.

V.4.3 Effect of line tension assumption.

The variable line tension in the Bacon, et al formulation is given by equation V.26. For a screw dislocation, the line tension is

$$T = [Gb^2/(4\pi)(1 - \upsilon)][\ln (l_{s,t}/b)]. \qquad (V.44)$$

Figure V.8 illustrates the magnitude of the effect of the variation in line tension on the critical resolved shear stress as a function of radius and time for a uniform precipitate size distribution coarsening at constant volume fraction. The strength is decreased by a factor of

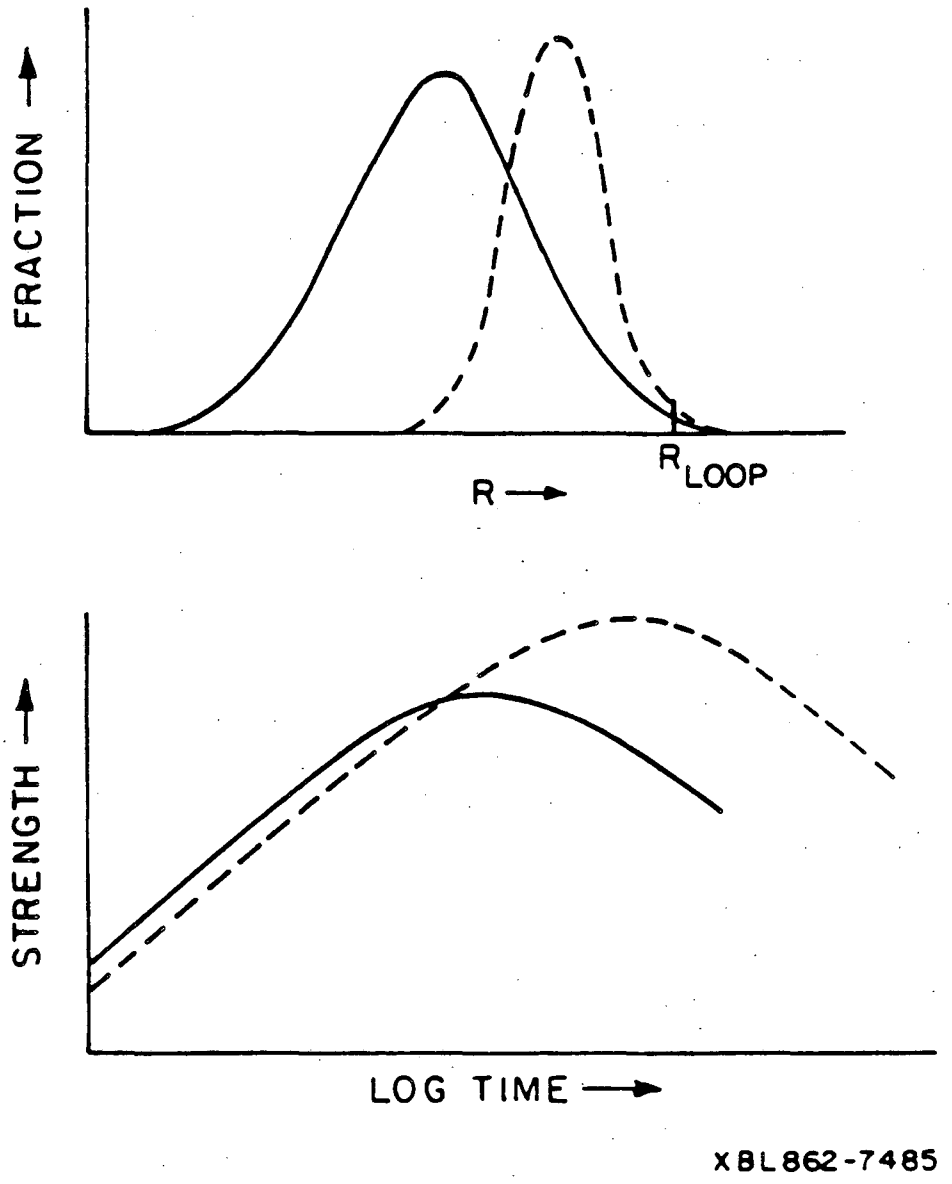

Figure V.5 Schematic illustration of the increase in strength from a narrow precipitate size distribution.

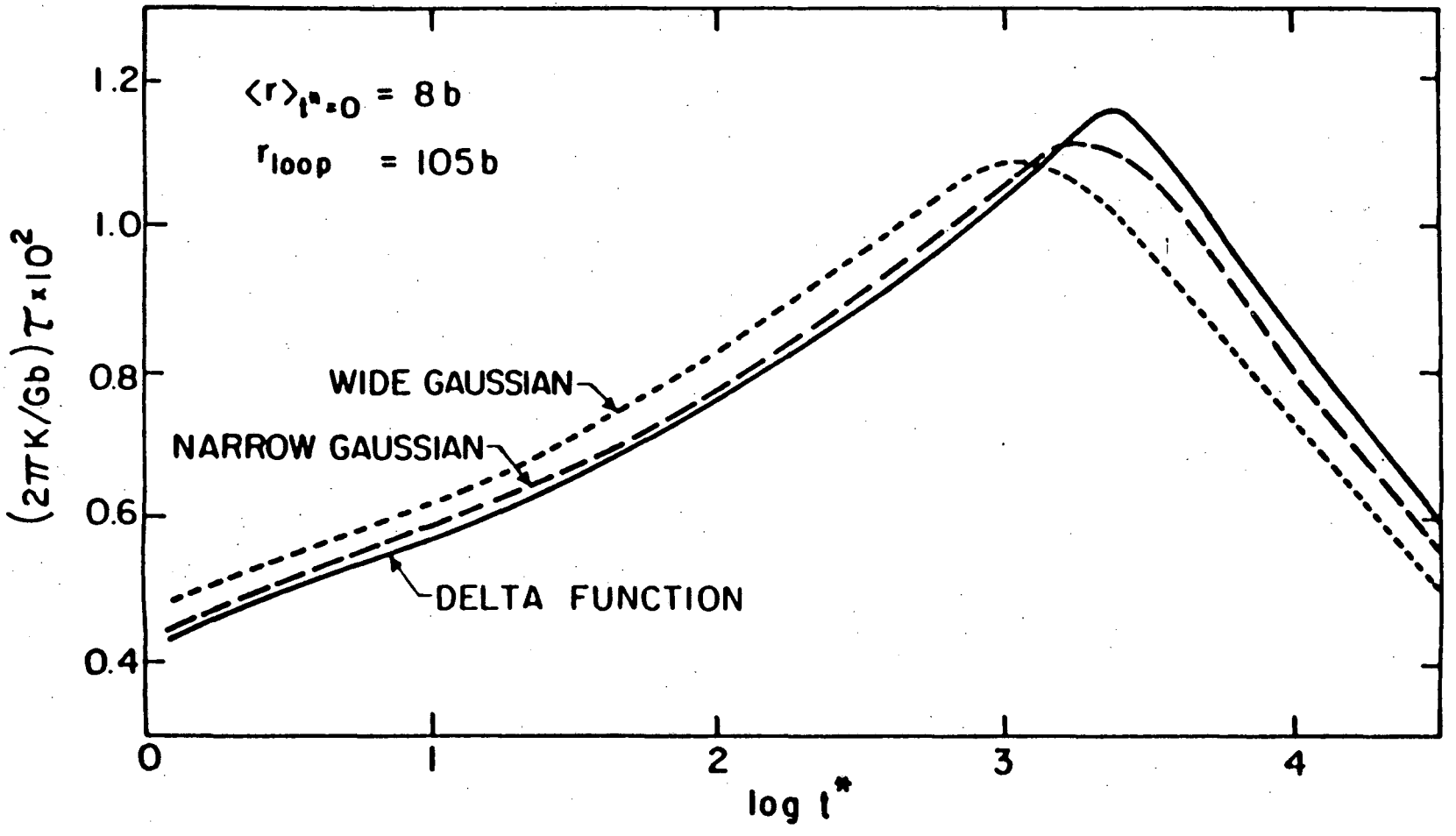

XBL862-7501

Figure V.6 Comparison of strengthening from precipitate size distributions of Figure V.7.

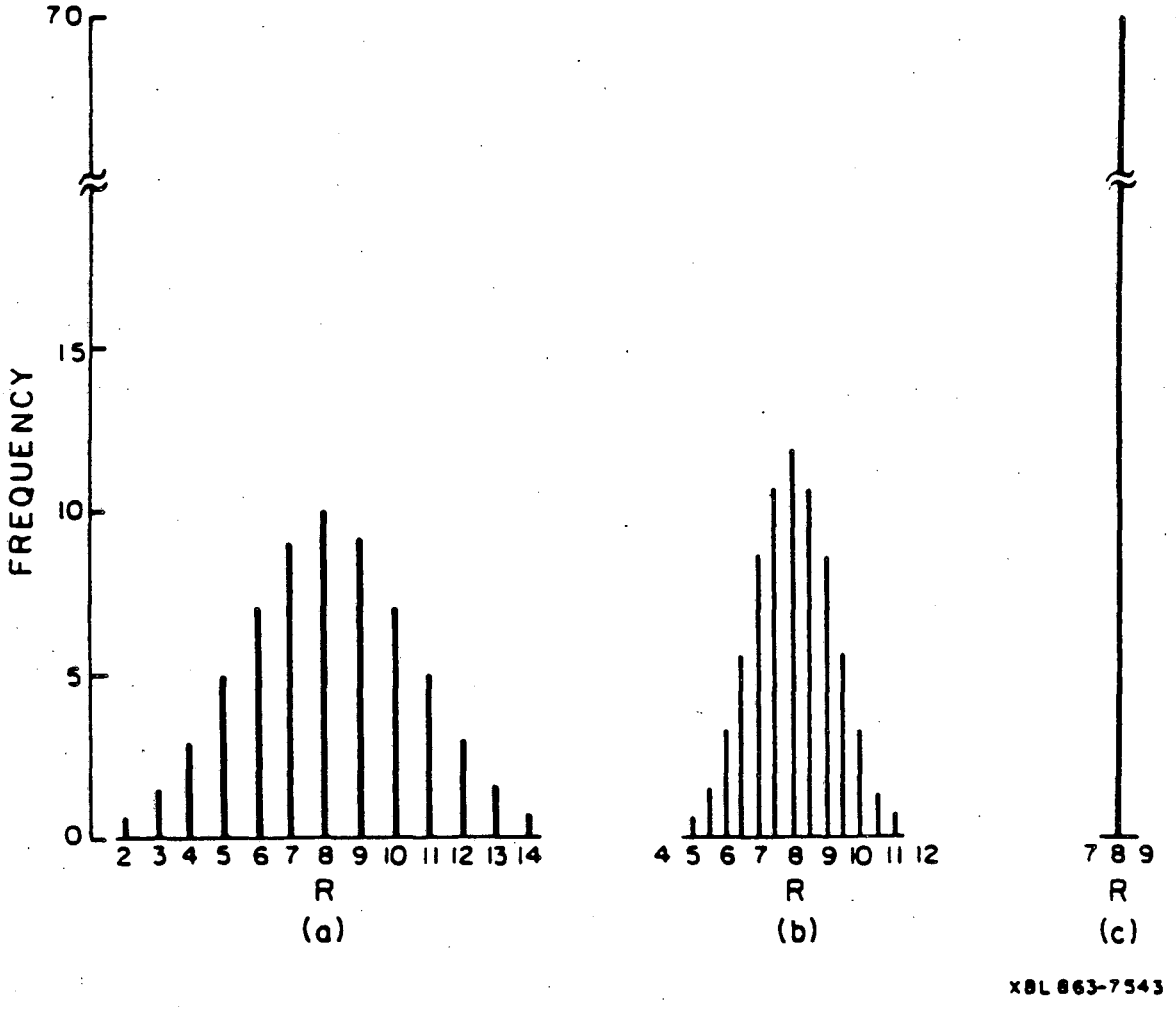

Figure V.7 Histograms of three precipitate size distributions with the same volume fraction used to examine the effect of precipitate size distribution width on strengthening. (a) wide Gaussian, (b) narrow Gaussian, (c) δ-function.

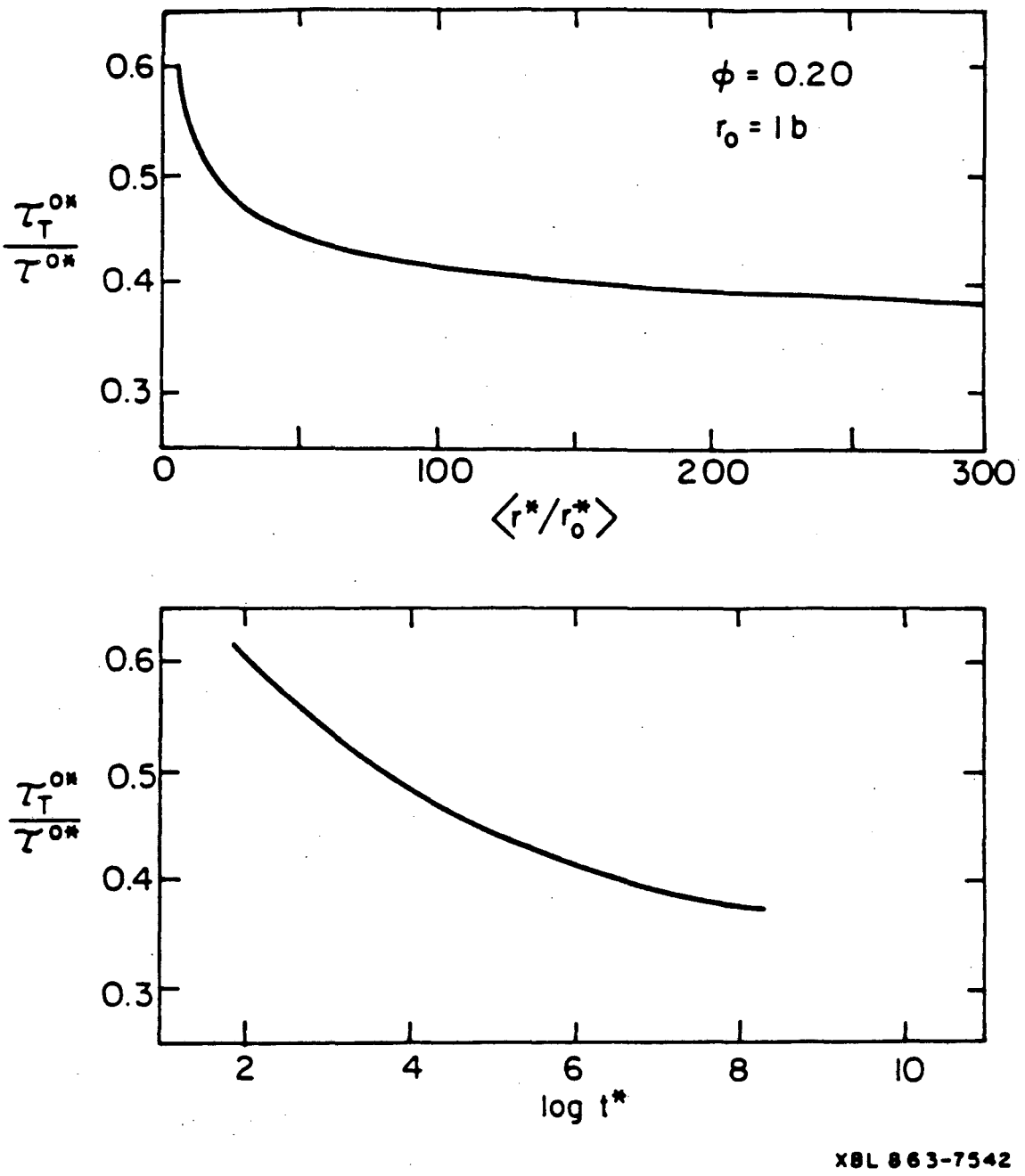

Figure V.8 Effect of variation in dislocation line tension on the critical resolved shear stress as a function of (top) average radius and (bottom) time.

roughly $[\ln (l_{s,t}/b)]^{-1/2}$. The constant line tension is taken as

$$T = Gb^2/2 \qquad (V.45)$$

The constant line tension underestimates the line tension at small radii and overestimates it later on. The effect on the aging curve for a precipitates of uniform size is illustrated in figure V.9. The value of the constant line tension was chosen so that the peak strengths are equal. The choices of the constant line tension and of the inner and outer cutoff radii in the variable line tension are of qualitative importance. However, the shape of the aging curve is not changed dramatically.

V.4.4 Comments on the effect of the width of the precipitate size distribution.

The possible effects of the width of the precipitate size distribution on the critical resolved shear stress have been investigated by computer simulation (Foreman and Makin, 1967; Altintas, 1978), theoretical analysis (Altintas, 1978; Glazer, Edgecumbe and Morris, 1985; Glazer and Morris, 1986) and experimental studies (Munjal and Ardell, 1976). The purpose of this section is to reconcile the results of these authors.

Foreman and Makin considered the effect of distribution width for two types of obstacle distributions in their computer simulations: square breaking angle spectra and square obstacle strength spectra. The square breaking angle spectrum is biased toward strong obstacles. Their results indicate that the wider distribution weakens the array in some regimes and strengthens it in others. Altintas (1978) considered the same cases analytically using the theory of Hanson and Morris (1975a, 1975b). His solutions agree closely with computer simulation results. The results for the square angle distribution from Foreman and Makin and Altintas are reproduced in figure V.10. The excellent agreement between theory and computer simulation suggests that the Hanson and Morris theory and its extensions can be used with confidence to address the effects of distribution width on the critical resolved shear stress.

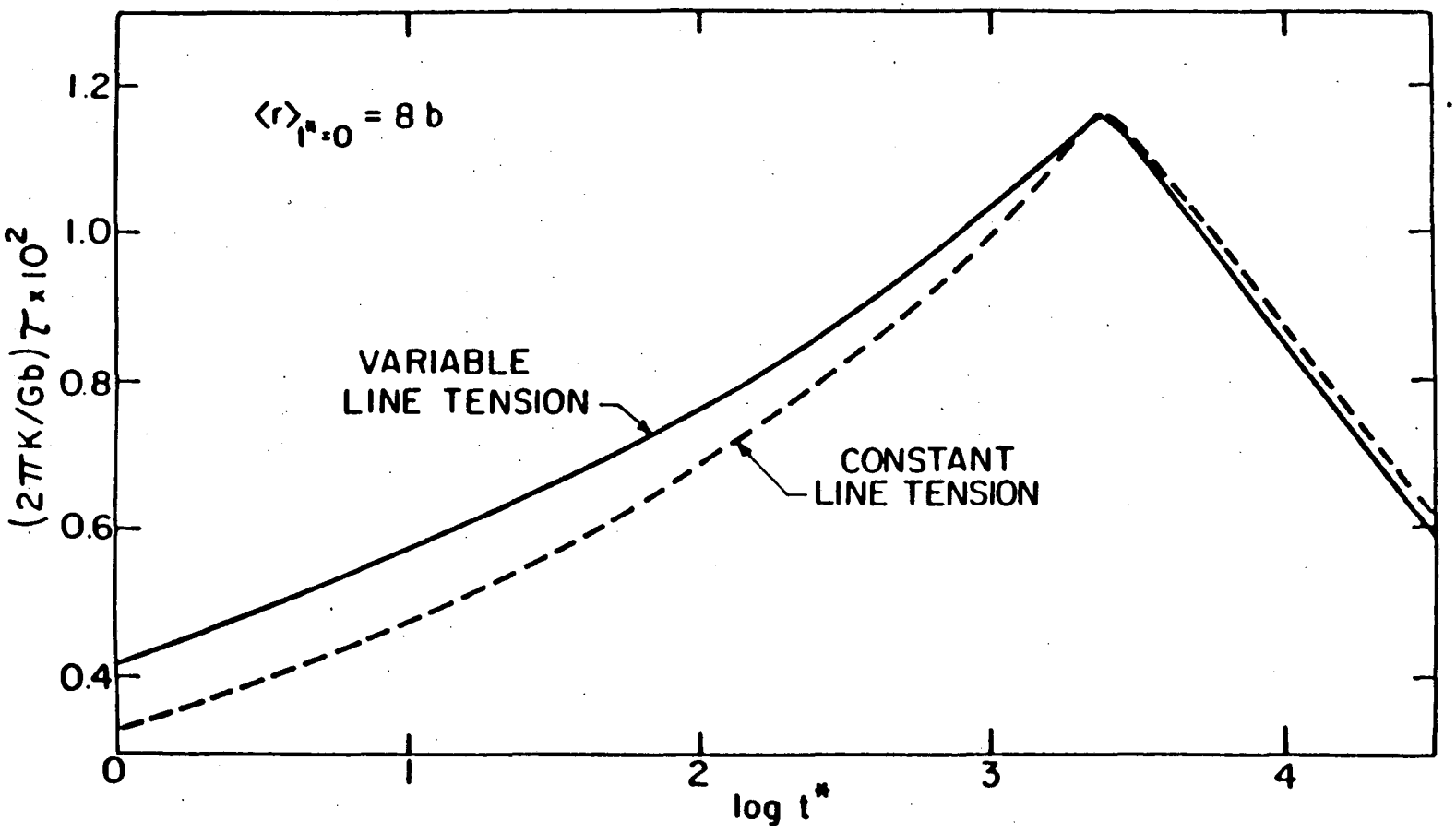

Figure V.9 Comparison of aging curves for precipitates of uniform size under variable and constant line tension assumptions. Agreement at peak strength is fixed.

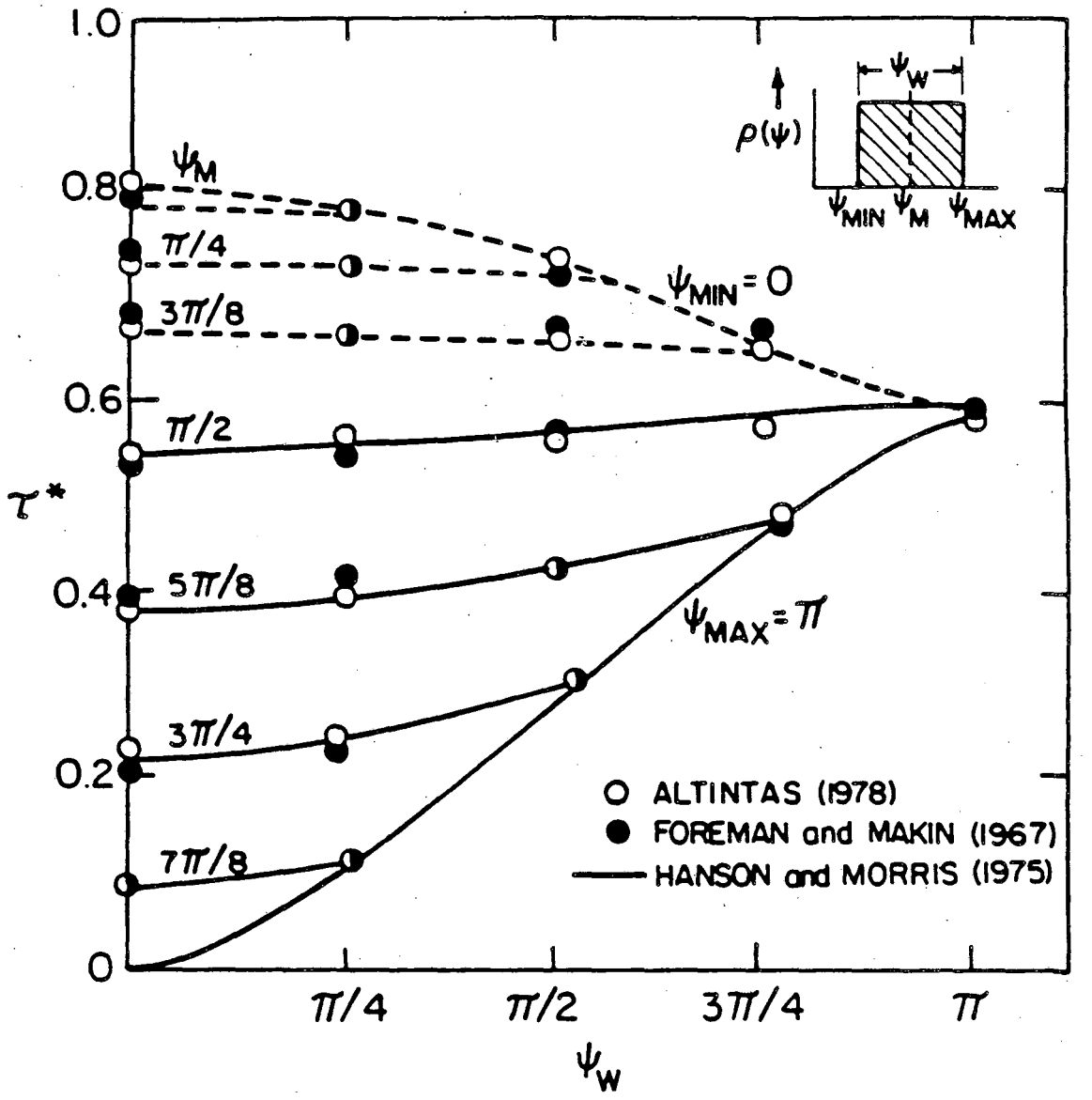

Figure V.10 Comparison of computer simulation results of Foreman and Makin (1967) and Altintas (1978) for variation in strength with the width of a square angle spectrum of obstacle strengths.

Munjal and Ardell (1976) describe the only attempt to measure experimentally the effect of the width of the precipitate size distribution on the critical resolved shear stress. They studied a Ni-Al alloy aged to near peak strength. A 30% increase in the width of the precipitate size distribution was found to result in an 8% decrease in the strengthening increment due to precipitation. Munjal and Ardell compare this result to computer simulation results of Foreman and Makin. Their analysis suggests that Foreman and Makin predict a much smaller effect from the width of the distribution. Since the simulation was performed using point obstacles, Munjal and Ardell suggest that the finite size of the physical obstacles may be responsible for the difference.

Munjal and Ardell make several assumptions to compare their data with Foreman and Makin's results. Foreman and Makin considered square distributions of breaking angles. Although a square distribution of obstacles is unlikely to arise in a real material, Munjal and Ardell argue that the effect of other distributions with the same standard deviation should be similar. Accordingly, they compute a breaking angle histogram for comparison; however, they do so from the distribution of precipitate radii rather than from the distribution of obstacle radii (precipitate radii on glide planes). This choice causes their histograms to be both narrower and strongly biased toward strong obstacles. Both of these errors lessen the size of the distribution width effect predicted by Foreman and Makin. As a consequence, the 8% decrease in strength measured by Munjal and Ardell is not obviously inconsistent with the results of Foreman and Makin.

The results of Munjal and Ardell are consistent with the predictions of the Hanson and Morris theory and the extension to precipitate size distributions given here. Munjal and Ardell compare the critical resolved shear stresses at a fixed average particle radius that corresponds to peak strength for the narrower distribution. Since widening the distribution has the effect of shifting peak strength to smaller average radii, the wider distribution is overaged at this average radius. Consequently, the observed decrease in strength due to the widened distribution is greater than the difference between the respective peak strengths. The change in the critical resolved shear stress is a strong function of the average radius in this regime. If Munjal and Ardell had chosen to fix the average particle radius at the radius

for peak strength of the wider distribution, they might have even concluded that widening the distribution increased the critical resolved shear stress.

VI. Applications of the model to the aluminum-lithium alloy system

VI.1 Importance of the Al-Li system

The properties of binary aluminum-lithium alloys alloys have received a great deal of attention in the last ten years. This research is a consequence of intense industrial interest in commercializing more complex aluminum alloys containing lithium. The driving forces behind the development effort are summarized briefly below.

The dual objectives of minimizing operating costs and maximizing performance of aircraft and aerospace systems provide a powerful incentive to reduce aircraft empty weight. Recent design studies indicate that structural weight is more effectively lowered by reducing the density of structural materials than by improving their mechanical properties (Quist, Narayanan and Wingert, 1981). This conclusion has provided the impetus for the development and application of resin composites. However, the highly anisotropic properties of composites make their application difficult, and it seems likely that at least commercial aircraft will remain primarily aluminum. As a consequence, there is a strong impetus to develop advanced high strength aluminum alloys. This challenge is responsible for a renewed interest in producing low density aluminum alloys to replace current alloys. A promising series of alloys has been developed which contain additions of lithium to reduce their density.

Intensive research and development in the last several years have led to the registration of several aluminum-lithium alloys intended to replace at lower density standard commercial aluminum alloys such as 2024, an Al-Cu-Mg-Si alloy and 7075, an Al-Zn-Mg alloy. One of the new alloys is 2090, designed to have properties similar to those of 7075-T651. In addition to having a significantly lower density, 2090 is superior to 7075 in many respects; in fact, although low toughness has been a problem of aluminum-lithium alloys in the past, the room temperature strength-toughness relationship of 2090 is better that of any other standard aerospace alloy, at least in the longitudinal and transverse directions (Sawtell, Bretz, Petit and Vasudevan, 1984). Its cryogenic properties are also superior to aluminum alloys currently employed for cryogenic tankage, space systems and high-field magnets (Glazer, Verzasconi, Dalder, Yu, Emigh, Ritchie and Morris, 1985).

Aluminum-lithium alloys are expected to be incorporated into commercial aircraft within the next few years.

In the course of the alloy development effort for the high-strength, low density alloys described above, the properties of the binary aluminum-lithium system have received considerable attention. Although the commercial and near-commercial alloys all contain other alloying additions for high strength and toughness, an understanding of the unique properties of the binary system is fundamental to understanding these more complex alloys.

VI.2 Al-Li system as a model system.

The aluminum-lithium system is an excellent model system for the modified strong line solution of the critical resolved shear stress model (Section V). The solution in Section V is designed to predict the aging curve of an alloy strengthened by an ordered precipitate. In the following section, the assumptions of the solution are compared with the actual behavior of the binary aluminum-lithium system. Section VI.3 contains a detailed discussion of the properties of the aluminum-lithium system relevant to each point in this summary.

The assumptions of the solution are:

(1) The binary Al-Li system is hardened by an ordered precipitate Al_3Li, denoted δ'.

The δ' precipitate is the only type of obstacle that contributes significantly to the strength of the alloy.

(2) Each spherical precipitate may be reduced to a set of point obstacles whose strengths correspond to the effective radii of the precipitate in the glide planes it intersects.

The δ' precipitates are spherical and remain so even at very large sizes.

(3) The strength of the obstacles is assumed to be a function of the radius of the sheared ordered precipitate only. This is equiva-

lent to neglecting the misfit of the precipitate.

The misfit of the δ′ precipitate is extremely low, so neglecting its effect is a good assumption.

(4) The precipitates coarsen according to the Lifshitz-Slyozov-Wagner (LSW) rate law.

The precipitates appear to coarsen according to LSW from very small sizes.

(5) The shape of the precipitate size distribution as a function of $r/\bar{r}$ does not change during coarsening.

Precipitate size distributions have been measured and found to coarsen in a self-similar fashion.

(6) The precipitates coarsen at approximately constant volume fraction.

The interfacial energy of the δ′ precipitate in the aluminum matrix is small. Therefore, volume fraction increases during coarsening are small for precipitates of reasonable size and volume fraction.

(7) The line tension for screw dislocations is used.

Line tension considerations suggest that edge dislocations should control deformation because it is more difficult for an edge dislocation to shear an ordered precipitate. However, screw dislocations are observed experimentally to control deformation.

(8) The dislocations move as superdislocation pairs. The effect of this pairing is that the actual stress at the obstacle is twice the applied stress.

Superdislocation pairs are observed and their properties as a function of precipitate distribution have been studied.

(9) The strength of an obstacle may be related to the maximum obstacle strength. An obstacle of maximum strength corresponds to a precipitate of radius greater than or equal to the looping radius, the size at which Orowan looping is first preferred over shearing of the precipitate.

The looping radius has been determined by transmission electron microscopy.

(10) The calculated critical resolved shear stress due to the obstacle distribution represents the increment in the total strength of the alloy due to precipitate hardening only and should properly be denoted $\Delta\tau$.

Several investigators have tried to address the contribution of the matrix to the strength and to examine the effect of solid solution hardening and variations in grain size.

VI.3 Properties of the aluminum-lithium alloy system.

Each of the items in the previous section will now be discussed in more detail. The discussion will again be limited to binary or near-binary aluminum-lithium alloys.

VI.3.1 The precipitate.

The strengthening precipitate in the binary Al-Li system is Al_3Li (δ'), which has the face-centered cubic based $L1_2$ ordered crystal structure (Silcock, 1960; Noble and Thompson, 1971). Precise values for the solubility of lithium in aluminum are difficult to determine because of the difficulty in detecting lithium with most analytical techniques. However, considerable progress has been made. The data on the Al-rich portion of the phase diagram including the region in which the δ' precipitate is observed have been summarized by Williams (1981). A binary phase diagram for the Al-rich portion of the phase diagram is included as figure VI.1 (Sanders and Starke, 1983). A more complete phase diagram for the Al-Li system is given by McAllister (1982).

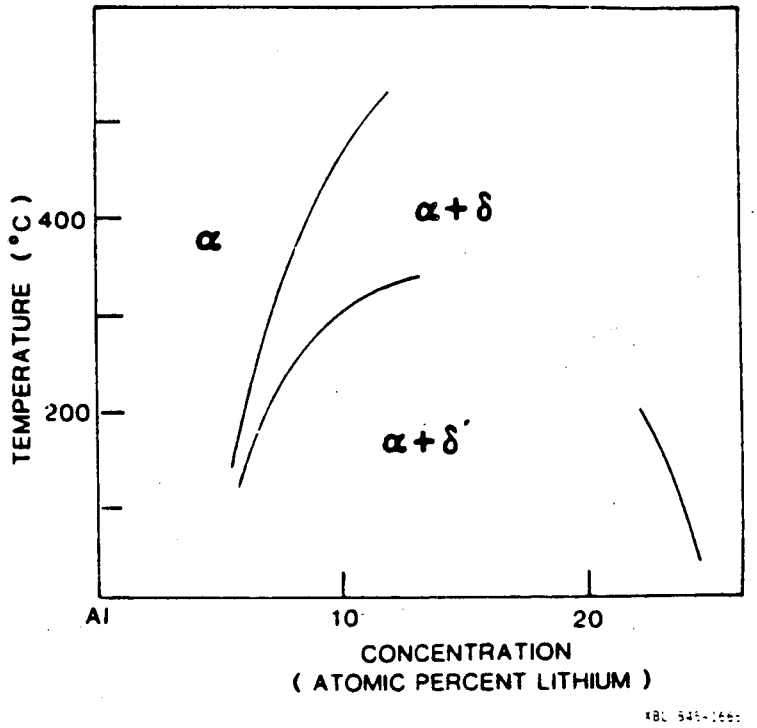

Figure VI.1 Aluminum-rich portion of the binary aluminum-lithium phase diagram (after Sanders and Starke, 1983) illustrating the region in which the δ' precipitate is observed.

As suggested in the solution of Section V, the Burgers vector is the natural unit of length for precipitate dimensions. The Burgers vector **b** of the {111} planes in aluminum is the length $(a_o/2)\langle 110\rangle$, which has magnitude b = 0.29 nm.

VI.3.2 Precipitate shape.

Precipitates of δ′ are almost always very close to spherical in shape (Kulwicki and Sanders, 1983) although other shapes (Baumann and Williams, 1985a) and discontinuously precipitated material (Williams and Edington, 1976; Makin and Ralph, 1984) are sometimes observed. Gu et al. (1985b) have measured the aspect ratio of nearly spherical δ′ precipitates. At small sizes some ellipsoidal precipitates are observed (possibly products of precipitate coalescence), but at longer aging times, the precipitates are increasingly spherical. Unlike the analogous $L1_2$ precipitate γ′ found in superalloys, which becomes cuboidal at large sizes, the δ′ precipitates are neither observed nor expected to change shape as they coarsen (Glazer, et al, 1985; Muller, Bubeck and Gerold, 1985). The precipitate shape is in excellent correspondence with the spherical precipitate assumption used to generate the obstacle strength distribution in Section V.

VI.3.3 Degree of order strengthening.

The lattice mismatch between the δ′ precipitate and the matrix is extremely small. Estimates range from -0.0018 to -0.0008 (Noble and Thompson, 1971;Williams and Edington, 1975; Sainfort and Guyot, 1985; Tamura, Mori and Nakamura, 1970; Baumann and Williams, 1983). The actual value is probably at the lower end of this range. Because the mismatch is so small, it is reasonable to make the simplifying assumption that coherency strengthening can be entirely neglected in favor of order hardening.

VI.3.4 Precipitate coarsening behavior.

The coarsening behavior of δ′ is discussed in numerous papers (Noble and Thompson, 1971; Williams and Edington, 1974; Kulwicki and Sanders, 1983; Baumann and Williams, 1984; Jensrud and Ryum, 1984). The δ′ precipitates coarsen according to Lifshitz-Slyozov-Wagner kinetics. The LSW rate constant is required if the solution for the criti-

cal resolved shear stress is to be interconvertible between precipitate radius and aging time. It has been determined for a variety of lithium contents and temperatures by the above-mentioned investigators.

It is not clear at this time if the δ′ precipitates form by nucleation and growth, from GP zone precursors or because the solid solution is unstable with respect to decomposition followed by ordering. Plots of precipitate coarsening behavior as a function of time suggest an initial radius very near zero. There have been two attempts to determine a critical radius for homogeneous nucleation. Baumann and Williams (1984) measured a critical radius of 2 nm (~ 7b) at 473 K for an alloy containing 7.9 a/o Li in a reversion experiment. Livet and Bloch (1985) determined the critical radius by small angle x-ray scattering to be 0.6 nm (~2b) at 423 K for an alloy containing 7.5 a/o Li. However, there is some evidence for a precursor to the δ′ precipitate (Ceresara, Giarda and Sanchez, 1977; Nozato and Nakai, 1977).

VI.3.5 Precipitate size distributions.

Precipitate size distributions of various shapes can be created by appropriate thermal treatments. This point is illustrated by the sample distributions for binary aluminum-lithium alloys shown in figure IV.10 (Gu et al., 1985a; Baumann, 1984; see also Jensrud and Ryum, 1983). At least some of these are almost certainly non-equilibrium distributions; their coarsening behavior is not known.

The element Zr is often added to aluminum alloys because it forms the compound Al_3Zr, which inhibits recrystallization. The δ′ phase may precipitate on the Al_3Zr particles forming composite spheroids (Makin and Ralph, 1984; Gayle and Vandersande, 1985). The δ′ on these particles coarsens at the same rate as the isolated δ′. If these particles are not distinguished from δ′ particles that do not have an Al_3Zr core, the δ′ precipitate size distribution will be improperly biased toward large particles (Gu et al., 1985a). The strengthening behavior of these composite particles is not understood.

Gu et al. (1985b, 1986) have done an extensive study of the behavior of the precipitate size distribution in binary aluminum-lithium alloys. The precipitate size distribution coarsened self-similarly

over the range of compositions examined. They found that it was possible to specify the precipitate size distribution as a function of lithium content by the two parameters of a Weibull distribution. These distributions were essentially independent of aging temperature and time. The distributions had a symmetrical shape better approximated by a normal curve than by the skewed curves suggested by most of the theories discussed in section IV.4; however, Gu et al. could not find evidence for the encounters assumed by the Davies et al. model, which does predict a normal curve.

VI.3.6 Volume fraction effects during coarsening.

As discussed in Section IV.4, the equilibrium solubility in the matrix decreases as the precipitates coarsen due to the decreasing importance of the surface energy of the precipitate. As a consequence, the precipitate volume fraction increases during coarsening. In this section, the magnitude of the effect in the aluminum-lithium system is estimated.

Numerous investigators have attempted to measure the interfacial surface energy between the δ′ precipitate and the matrix. Some measured values and techniques by which they were determined are given in Table 2. Most of the measurements of the surface energy are made by determining the diffusivity, D, and the LSW coarsening constant K (denoted D,K in the table). These parameters are related by the equation

$$K = 8\gamma_{\alpha\beta}X_o V_m^2 D/9RT \qquad \text{(VII.1)}$$

where V_m is the molar volume. Both D and K are strong functions of temperature; $\gamma_{\alpha\beta}$ varies much less. The interfacial surface energy almost certainly varies with temperature since the solubility of lithium in the matrix changes; however, the range of measured values far exceeds the expected variation.

Kulwicki and Sanders (1983) note that in other systems containing coherent precipitates, the interfacial energy is always less than 250 mJ/m^2. For precipitates with misfits less than 1% (cf δ′ ~ 0.2%), the interfacial surface energy is generally less than 20 mJ/m^2. On this basis, the lower values in Table 2 seem more reliable. The D,K method

Table 2. Measurements of Al-Al_3Li surface energy.

Investigator	Alloy	Method*	Surface Energy (mJ/m^2)
Tamura, Mori and Nakamura (1970)	?	?	180
Noble and Thompson (1971)	4 a/o	D,K	240
Williams and Edington (1975)	n/a	misfit vs other $L1_2$ mat'ls	25
Jensrud and Ryum (1984)	3 w/o	D,K	50
Baumann and Williams (1984)	8 a/o	critical radius	14
Livet and Bloch (1985)	7.5 a/o	D,K	14
Sainfort and Guyot (1985)	2-3 w/o	D,K	<30

* D,K refers to calculations based on the relationship between the diffusivity D and the Lifshitz-Slyozov-Wagner coarsening constant K.

is suspect since both of these parameters vary strongly with temperature and precipitate volume fraction. The value of 14 mJ/m^2 obtained by Baumann and Williams (1984) is used here to calculate the change in equilibrium precipitate volume fraction during coarsening

The effect on the equilibrium volume fraction is illustrated for binary aluminum-lithium alloys in figure IV.11. The effect is large only for extremely small precipitates or very small volume fractions (and even then only a few percent for this alloy system). Most investigations seem to agree with this finding (e.g. Baumann and Williams, 1985b); however, Miura, Matsui, Furukawa and Nemoto (1985) found that the volume fraction increased substantially throughout the aging process and did not stabilize until after peak strength was reached for an Al-3w/o Li alloy.

VI.3.7 Dislocation line tension.

Line tension considerations suggest that edge dislocations should control yielding at least until Orowan looping begins at or near peak strength. However, Miura, et al. (1985) observed long straight screw dislocations in the underaged material, indicating that screw dislocations may actually control the yield strength. Cross-slip of screw dislocations is known to be an important factor controlling the variation of yield strength with temperature in $L1_2$ ordered alloys. The applicability of this theory to alloys hardened by relatively small volume fractions of $L1_2$ precipitates is still in question, but it is possible that cross-slip prevents the screw dislocations from gliding out. However, Miura, et al. did not observe any slip on {010} planes even in favorably oriented single crystals.

The numerical value of the line tension may be calculated as function of l_s if the shear modulus is known. A good estimate is 3/8 the value of the elastic modulus, which is easily measured in uniaxial tension. A representative value for the shear modulus is 30 GPa. There is a subtlety here that Ardell (1985) points out. The relevant shear modulus is the shear modulus in the glide plane. In anisotropic crystals, the modulus will be different along each plane. Since aluminum is very close to isotropic, the error in ignoring this correction is small (from 25.9 to 24.9 GPa (Ardell, 1985)). The shear modulus of

aluminum-lithium has been measured by a number of investigators (Miura et al. (1985) suggests 30.2 GPa; Jensrud (1985) suggests 27.6 or 28.6 GPa for the matrix and 30.6 for the precipitate; Muller et al (1985) found 26-28.5 for an Al-Al_3Li mixture containing 0-4 a/o Li at room temperature).

VI.3.8 Superdislocations.

Deformation in aluminum-lithium alloys occurs by the motion of dislocations along {111} planes, the close-packed planes in the face-centered cubic structure. In underaged and peak-aged alloys, in which δ' precipitates are sheared, dislocations occur in pairs since the Burgers' vector of the δ' precipitate is twice that of the matrix.

As mentioned earlier, the Burgers vector of the {111} planes in the aluminum matrix is the length $(a_o/2)\langle 110\rangle$, which is approximately 0.29 nm.

As expected, the dislocations are not coupled in the overaged condition when Orowan looping is dominant (Sainfort and Guyot, 1985; Miura, et al., 1985). The uncoupling is reflected in a rapid increase in the dislocation pair spacing as a function of aging time when the precipitates are large (Tamura, Mori and Nakamura, 1972).

VI.3.9 Obstacle strength.

The preferred method for quantifying the obstacle strength is experimental measurement of the looping radius (see Section IV.5). The needed experimental data is available for the aluminum-lithium system and is discussed in Section VI.3.9.1. The obstacle strength may also be calculated; the computation is included as Section VI.3.9.2.

VI.3.9.1 Direct measurements of the looping radius.

The minimum size at which the Orowan condition is observed puts an upper limit on the strength of the obstacle, whatever its physical size. Miura, et al. (1985) have determined that dislocation loops do not stand away from δ' precipitates by a measurable distance. This

means that measuring the minimum dislocation loop size is equivalent to measuring the minimum size of looped precipitates. Only upper and lower limits on the looping radius can be determined from photographic observations, since only precipitate sizes clearly visible in the micrographs can be considered. In addition it is not always possible to ascertain if the observed loop lies on a glide plane that is also a precipitate diameter. Transmission electron micrographs from de Hosson, et al. (1984) suggest an upper limit on the looping radius in a 2.2 w/o Li alloy of approximately 25 nm for a mean square particle spacing of about 0.9 μm. Sainfort and Guyot (1985) measured a looping radius of 18 nm for an Al-3w/o Li with a volume fraction of 25 percent. Miura, et al. (1985) measured a looping radius of approximately 30 nm in a similar alloy. Furukawa, et al. (1985) quote 25 nm.

VI.3.9.2 Calculations of the antiphase boundary energy.

Calculations of the sort described in Section IV.5 that quantify the strength of the particle may be performed for the aluminum-lithium system.

VI.3.9.2.1 Calculations of γ for Al_3Li.

Two investigators have calculated the antiphase boundary energy for the δ' precipitate to date; unfortunately, neither calculation is done correctly.

Recall from Section IV.5.1 that the energy of an antiphase boundary of type $a_o/2\langle 110\rangle$ in the $L1_2$ crystal structure may be calculated from the formula

$$\gamma = 2.42\ hk_BT_c/N^{1/2}a^2 \qquad \text{(IV.40)}$$

where $h \geq k$, a is the lattice parameter of the disordered phase, T_c is the critical order-disorder temperature (determined from the phase diagram), k_B is Boltzmann's constant, and $N = h^2+k^2+l^2$.

The first calculation is done by Furukawa, et al (1985). There apparently is a misprint in the paper and "a" should be "a^2." In addition, the formula is missing the multiplicative factor 1/0.82. Their calculation is done using a critical ordering temperature of 548

K, which is lower than the peak temperature at which δ′ is observed. The second calculation is done by Jensrud (1985) ostensibly using the same theory for the calculation. However, the formula he quotes is completely wrong, causing him to get an unreasonably high value for the antiphase boundary energy and distorting his other calculations.

A lower limit on the antiphase boundary energy can be estimated by using the peak temperature at which the δ′ phase is experimentally observed. The values in the literature range from 573 K (Noble and Thompson, 1971) to 613 K (Williams and Edington 1975). From these temperatures, a lower limit on the antiphase boundary energy is approximately 70 mJ/m^2. The actual antiphase boundary energy is expected to be greater.

VI.3.9.2.2 Superdislocation spacings.

A number of investigators have attempted to determine the antiphase boundary energy from dislocation pair spacings (Sainfort and Guyot, 1985; Tamura et al, 1972; de Hosson et al, 1984; Huang and Ardell, 1986). The values of the antiphase boundary energy measured in this way range from 130 to 195 mJ/m^2.

VI.3.9.2.3 Calculation from minimum looped particle size for Al-Li.

No calculations of this sort exist in the literature. However, sufficient data exist for one case in de Hosson et al. (1984). For r_{loop} = 25-30 nm and $L = l_{s_{max}} = 0.9 \times 10^3$ nm, the antiphase boundary energy from the equation IV.42 is 110-135 mJ/m^2. A looping radius of 25 nm is in the middle of the range of the reported values. The choice fortuitously leads to exactly the antiphase boundary energy calculated by de Hosson et al. from superdislocation pair spacings. Assuming a looping radius of 20 nm for the same mean square precipitate spacing leads to an antiphase boundary energy of about 170 mJ/m^2. All of these values are in reasonable agreement with values determined from superdislocation pair spacings.

VI.3.10 Total strength.

Several investigators have attempted to determine the relative contributions of all the hardening mechanisms that impart strength to

binary aluminum-lithium alloys (Miura et al., 1985; Jensrud and Ryum, 1985). While it is generally agreed that order hardening dominates the strength; the superpositiion techniques used to determine the influence of other factors are questionable.

Jensrud and Ryum (1984) measured the variation in the critical resolved shear stress with grain size. The alloys obey a Hall-Petch relationship in all aging conditions. The Hall-Petch coefficient k is approximately 0.1 MPa$\sqrt{m}$ in the as-quenched material, about 0.82 in underaged material and 0.90 in overaged material. These results contradict results of Hansen and Bronsted (1985) that k_{HP} decreases during aging.

VI.4 Predictions of the critical resolved shear stress in Al-Li alloys.

Using the solution for the critical resolved shear stress in Section V and numerical values from Section VI.3, the critical resolved shear stress can be determined. Calculated 'aging curves' for the experimentally obtained precipitate size distributions measured by Gu et al. (1985a) and Baumann (1984) (shown in figure IV.10) are given in figure VI.2. The results of Section V for uniform precipitate size are shown for comparison. These calculations assume a looping radius of 30 nm for l_s = 0.9 μm and an initial radius of 1b. The distributions were normalized to a volume fraction of 0.2. As can be seen from the figures, the more sharply peaked the distribution, the more effectively it strengthens. The theoretical increment in $\Delta\tau_c$ is large enough to have alloy design implications. It should be noted that the effect of grain size is assumed to be constant along the aging curve and is therefore included in the matrix strength (see Section IV.1.4.3).

Direct comparison of the theoretical and experimental strengthening increment from the coarsening of δ′ is possible for the precipitate size distribution shown in figure VI.3 from Gu et al. (1985b) for Al-2.78Li-0.3Mn aged at 200°C. Theoretical aging curves were calculated for a looping radius of 25 nm, which is an intermediate choice from the currently available data. The experimental and theoretical aging curves are shown in figure VI.4. (It should be noted that this plot differs from the one in Glazer, et al. (1985) and Glazer and Morris (1986) both in the choice of looping radius and in the proper

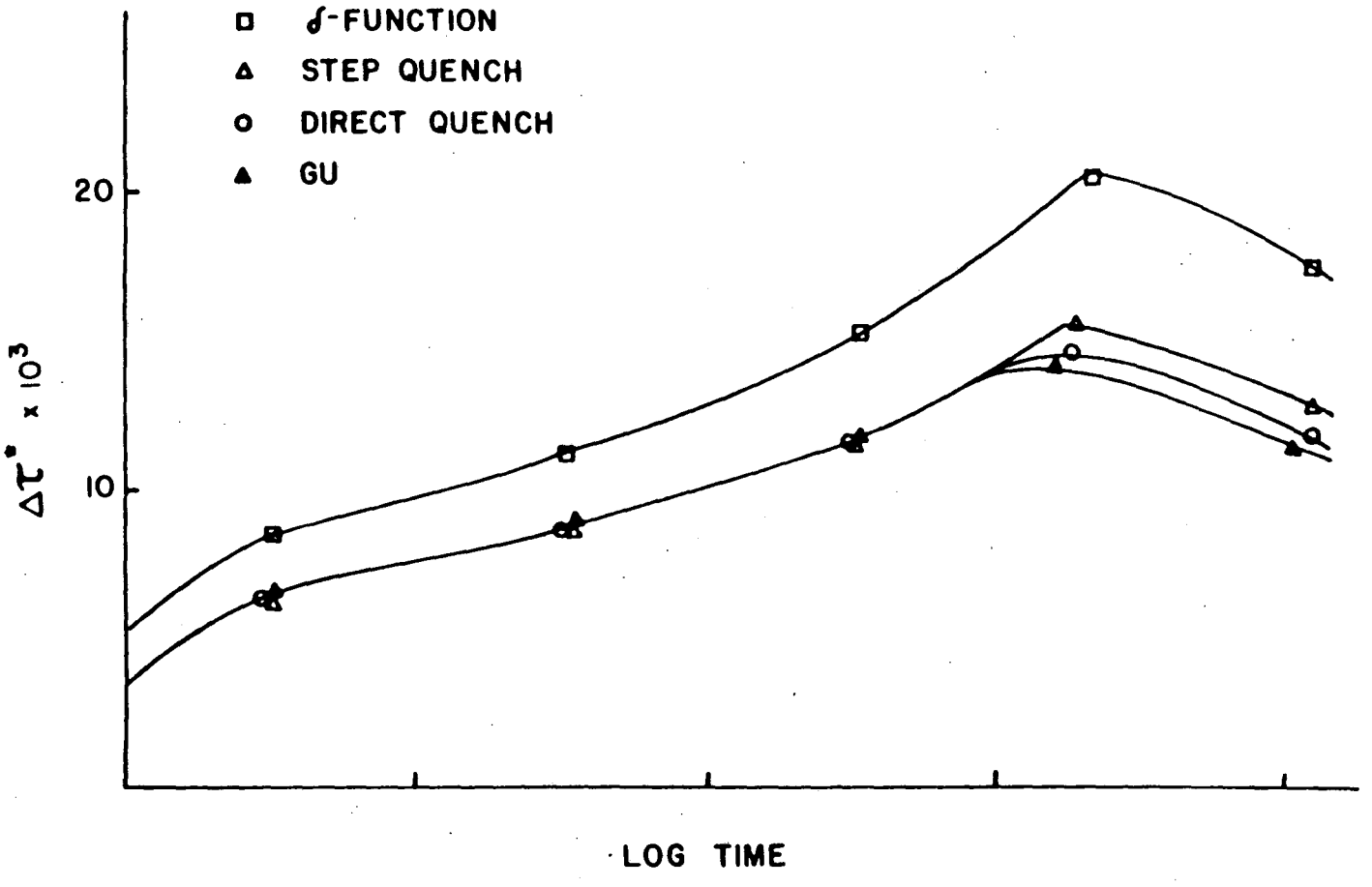

XBL 856-2858

Figure VI.2 Comparison of strengthening for precipitate size distributions in Figure IV.10.

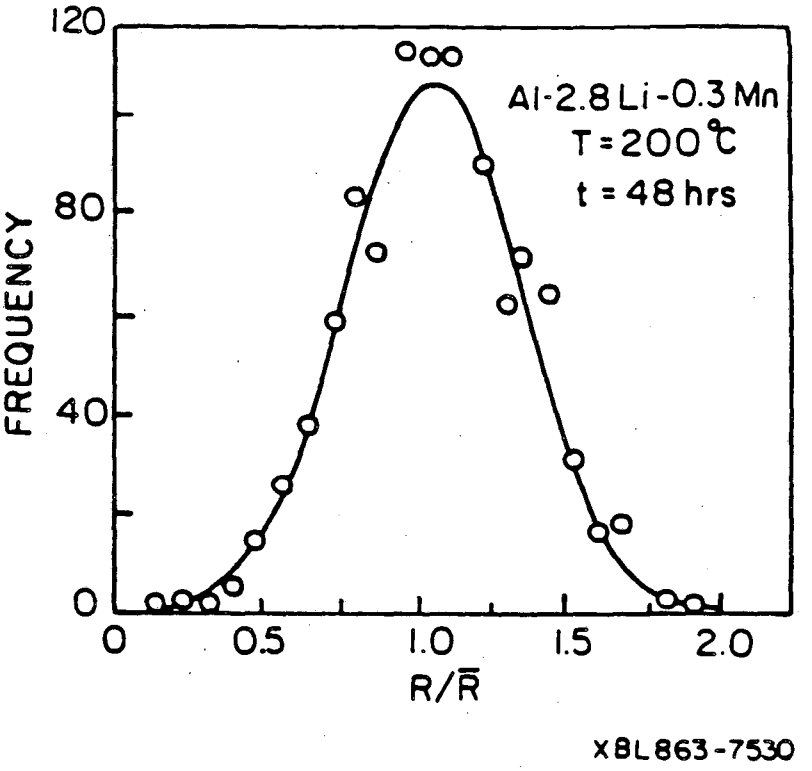

Figure VI.3 Precipitate size distribution from Gu et al, 1985b.

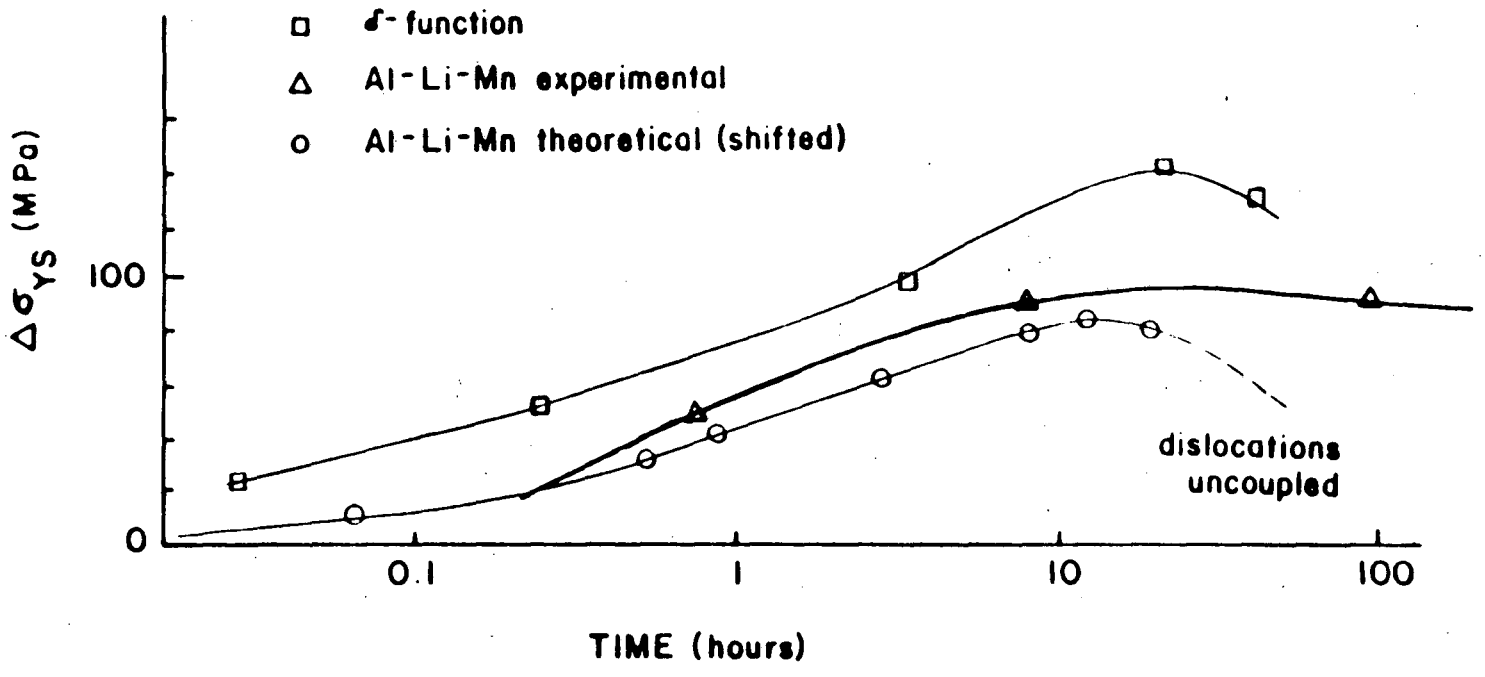

XBL 856-2840

Figure VI.4 Comparison of experimentally measured and predicted aging curves for the precipitate size distribution in Figure VI.3. The theoretical distribution is shifted to slightly shorter aging times to account for atom clustering during quenching.

incorporation of the fact that much of the lithium remains in solution.) The theoretical coarsening rate has been fixed using the experimentally determined LSW rate constant. Since the quenched alloy undoubtedly contains some atom clusters, the theoretical aging curve has been shifted to slightly shorter times to obtain the best fit. The strength increment for both yield strength curves is the increase over the lowest measured strength. To convert theoretical critical resolved shear stress values to yield strengths, a Taylor factor of 3 has been assumed. The figure shows that the theoretical and experimental aging curves are in excellent agreement up to peak strength. Beyond peak strength, the model is no longer valid since it does not account for the uncoupling of paired dislocations after Orowan looping begins. This uncoupling would cause the strength to drop off more gradually after the peak.

VII. Conclusion.

This paper outlines the development of a model of the age-hardening behavior of alloys strengthened by coherent, ordered precipitates. The model is then used to consider the effect of the precipitate size distribution on the critical resolved shear stress and finally, to obtain quantitative predictions for strengthening in binary aluminum-lithium alloys hardened by δ′ precipitates.

The problem considered here is a special case of the general problem of modeling the strengthening of a crystalline material by inhomogeneities that interact with gliding dislocations. A model of precipitate hardening must also account for the observed rise and fall in strength as the precipitates coarsen. The random array model has been most useful in modeling this behavior. This model has four basic premises:

(1) The material is modelled in terms of a dislocation glide plane, a hypothetical plane between two atomic planes.
(2) The obstacles to dislocation glide are idealized as point obstacles which interact similarly with the dislocation.
(3) The obstacles are randomly distributed in the glide plane.
(4) The dislocation is treated as a flexible, extensible string with a definite line tension.

The random array model was first proposed in the late 1950's. There have been many attempts to solve it mathematically since then. This paper has focussed on one of the more accurate solutions to the model for relatively strong obstacles, the Hanson and Morris strong line model. The distinguishing feature of this model is its focus on the interaction of the dislocation configuration with the array rather than on the interaction of isolated dislocation segments with particular obstacles. This view makes it possible to equate the critical resolved shear stress with the stress required to bypass the strongest line in the array, a powerful concept. The Hanson and Morris solution also led to a quadratic summing rule to describe the effects of obstacles of various strengths.

The Hanson and Morris solution contains the elements of the age-hardening problem; however, there are a large number of problems that must be addressed to make it apply quantitatively or, in some cases, qualitatively, to real systems. These include the variability of the line tension with dislocation character, the relative energies associated with particle shear and looping, the actual strengths of the

obstacles, and the effect of superdislocations on order hardening, to name a few. Not all of these problems have been solved satisfactorily, but it is possible to account for their effects at least partially. It is probable that at least their qualitative consequences can be properly included.

Probably the single most important problem that remains is the proper incorporation of the results of Bacon et al. on the effects of dislocation self-interactions on particle shear and looping. The initial steps here do not fully consider the effects of dislocation self-interactions on the effective line tension and, therefore, on the consequences of self-interactions for quantitative determinations of particle strength. The impact of these results on summing rules for combinations of obstacles that include some very strong obstacles is also as yet unknown.

The solution for the critical resolved shear stress derived in Section V is a modified version of the Hanson and Morris solution for a random array of point obstacles. This solution leads to predictions of aging behavior that are in reasonably good quantitative agreement with measured behavior in binary aluminum-lithium alloys hardened by δ' precipitates. These results are a vindication, to some extent, of the assumptions incorporated in the model. They suggest that the solution may be used with confidence to do theoretical "experiments" that lead to predictions of more optimized microstructures. The precipitate shape and precipitate size distribution are two microstructural features whose consequences can be explored using this solution. In both cases, it can be concluded that strengthening is most efficient for a particular microstructure (e.g. plate-like precipitates and uniform precipitate size distribution). Undoubtedly, there are other important microstructural characteristics whose consequences can be considered in a similar fashion.

REFERENCES

Altintas, S., 1978, PhD thesis, University of California, Berkeley.

Altintas, S., Hanson, K. and Morris, J.W. Jr., 1976, J. Eng. Mat. Tech., Vol. 98, p. 86.

Altintas, S. and Morris, J.W., Jr., 1986a, Acta Metall., Vol. 34, p. 801.

Altintas, S. and Morris, J.W., Jr., 1986b, Acta Metall., Vol. 34, p. 809.

Ardell, A.J., 1972, Acta Metall., Vol. 20, p. 61.

Ardell, A.J., 1985, Met. Trans. A, Vol. 16A, p.2131.

Ardell, A.J., 1986, private communication.

Ardell, A.J., Chellman, D.J. and V. Munjal, 1976, in "Strength of Metals and Alloys," Proceedings of the 4th International Conference on theStrength of Metals and Alloys,Vol. 1, p. 209.

Ardell, A.J., Munjal, V., and Chellman, D.J., 1976, Met. Trans. A, Vol. 7, p. 1263.

Bacon, D.J., Kocks, U.F. and Scattergood, R.O., 1973, Phil. Mag., Vol. 28, p. 1241.

Baumann, S.F., 1984, unpublished work.

Baumann, S.F. and Williams, D.B., 1983, "Proceedings of the 1st International Conference on Aluminum-Lithium Alloys," T.H. Sanders and E.A. Starke, Jr., eds., AIME, Warrendale, PA, p. 17.

Baumann, S.F. and Williams, D.B., 1984, Scr. Met., Vol. 18, p. 611.

Baumann, S.F. and Williams, D.B., 1985a, Met. Trans. A, Vol. 16A, p. 1203.

Baumann, S.F. and Williams, D.B., 1985b, Acta Metall., Vol. 33, p. 1069.

Brailsford, A.D. and Wynblatt, P., 1979, Acta Metall., Vol. 27, p. 489.

Brown, L.M. and Ham, R.K., 1971, in "Strengthening Methods in Crystals," A. Kelly and R.B. Nicholson, eds., John Wiley and Sons, New York, p. 9.

Buttner, N. and Nembach, E., 1983, in "Deformation of Multi-Phase and Particle Containing Materials," Proceedings of the 4th Risø Int'l. Symposium on Metallurgy and Materials Science, J.B. Bilde-Sorensen, N. Hansen, A. Horsewell, T. Leffers and H. Lilholt, eds., Risø Nat'l Laboratory, Roskilde, Denmark, p. 189.

Ceresara, S., Giarda, A. and Sanchez, A., 1977, Phil. Mag., Vol. 35, p. 97.

Chaturvedi, M.C., Lloyd, D.J. and Chung, D.W., 1976, Met. Sci., Vol. 10, p. 373.

Copley, S.M. and Kear, B.H., 1967, Trans. AIME, Vol. 239, p. 984.

Cottrell, A.H., 1953, "Dislocations and Plastic Flow in Crystals," Oxford Press.

Cottrell, A.H., 1964, "The Mechanical Properties of Matter," Wiley and Sons, New York.

Davies, C.K.L., Nash, P. and Stevens, R.N., 1980, Acta Metall., Vol. 28, p. 179.

De Wit, G. and J.S. Koehler, 1959, Phys. Rev., Vol. 116, p. 1113.

De Hosson, J.Th. M., Huis in't Veld, A., Tamler, H. and Kanert, O., 1984, Acta Metall., Vol. 32, p. 1205.

Ebeling, R. and Ashby, M.F., 1966, Phil. Mag., Vol. 13, p.805.

Flinn, P.A., 1960, Trans. AIME, Vol. 218, p. 145.

Fleischer, R.L., 1964, in "The Strengthening of Metals," D. Peckner, ed., Reinhold Publ. Corp., New York, p. 93.

Fleischer, R.L. and Hibbard, W.R., 1963, in "The Relation between the Structure and Mechanical Properties of Metals," H.M. Stationery Office, London, p. 262.

Foreman, A.J.E. and Makin, M.J., 1966, Phil. Mag., Vol. 14, p. 911.

Foreman, A.J.E. and Makin, M.J., 1967, Can. J. Phys., Vol. 45, p. 511.

Friedel, J., 1956, "Les Dislocations," Gauthier-Villars, Paris.

Friedel, J., 1964, "Dislocations," Addison-Wesley, Reading, MA.

Furukawa, M., Miura, Y. and Nemoto, M., 1985, Trans. JIM, Vol. 26, p. 230.

Gayle, F.W. and Vandersande, J.B., 1985, in "Proceedings of the 43rd Annual Meeting of the Electron Microscopy Society of America," San Francisco Press, San Francisco, p. 26.

Gil Sevillano, J., van Houtte, P. and Aernoudt, E., 1981, Prog. Mat. Sci., Vol. 25, p. 69.

Glazer, J., Edgecumbe, T.S. and Morris, J.W., Jr., 1985, in "Proceedings of the 3rd International Conference on Aluminum-Lithium Alloys,"Oxford, England, in press.

Glazer, J. and Morris, J.W. Jr., 1986, in "Aluminum Alloys: Physical and Mechanical Properties," E.A. Starke, Jr., ed., Engineering Materials Advisory Service, Ltd., in press.

Glazer, J., Verzasconi, S.L., Dalder, E.N.C., Yu, W., Emigh, R.A., Ritchie, R.O. and Morris, J.W., Jr., 1985, Adv. Cryo. Eng., in press.

Gleiter, H. and Hornbogen, E., 1965, Phys. Stat. Solidi, Vol. 12, p. 235.

Gleiter, H. and Hornbogen, E., 1968, Mat. Sci. Eng., Vol. 2, p. 285.

Grohlich, M., Haasen, P. and Frommeyer, G., 1982, Scr. Met., Vol. 16, p. 367.

Gu, B.P., Liedl, G.L., Sanders, T.H., Jr. and Welpmann, K., 1985a, Mat. Sci. Eng., Vol. 76, p. 147.

Gu, B.P., Liedl, G.L., Kulwicki, J.H. and Sanders, T.H., Jr., 1985b, Mat. Sci. Eng., Vol. 76, p. 217.

Gu, B.P., Liedl, G.L., Mahalingham, K. and Sanders, T.H., Jr., 1986, Mat. Sci. Eng., in press.

Haasen, P. and Labusch, R., 1979, in "Strength of Metals and Alloys," Proceedings of the 5th International Conference on theStrength of Metals and Alloys, P. Haasen, V. Gerold and G. Kostorz, eds., Pergamon Press, Oxford, England, p. 639.

Hall, E.O., 1951, Proc. Phys. Soc., Vol. B64, p. 747.

Hansen, N., 1985, Met. Trans. A, Vol. 16A, p. 2167.

Hansen, N. and Bronsted, P., 1980, Res Mech., Vol. 1, p. 197.

Hanson, K.L., 1975, PhD thesis, University of California, Berkeley.

Hanson, K. and Morris, J.W., Jr., 1975a, J. Appl. Phys., Vol. 46, p. 983.

Hanson, K. and Morris, J.W., Jr., 1975b, J. Appl. Phys., Vol. 46, p. 2378.

Hanson, K. and Morris, J.W., Jr., 1978, J. Appl. Phys., Vol. 49, p. 3266.

Hanson, K., Altintas, S. and Morris, J.W., Jr., 1976, in "Proceedings of Conference on Computer Simulation for Materials Applications," NBS, Gaithersburg, MD, p. 917.

Huang, J. and Ardell, A.J., "Aluminium Technology '86," Book 3, Session 3, conference preprint, Institute of Metals, 1986.

Humphreys, F.J., 1985, in "Dislocations and Properties of Real Materials," Proceedings of conference to celebrate the 50th anniversary of the concept of dislocation in crystals, The Institute of Metals, London, p. 175.

Jansson, B. and Melander, A., 1979, Z. Metall., Vol. 70, p. 811.

Jensrud, O., 1985, in "Proceedings of the 3rd International Conference on Aluminum-Lithium Alloys," Oxford, England, in press.

Jensrud, O. and Ryum, N., 1984, Mat. Sci. Eng., Vol. 64, p. 229.

Kelly, A. and Nicholson, R.B., 1963, Prog. Mat. Sci., Vol. 10, p. 149.

Kocks, U.F., 1966, Phil. Mag., Vol. 13, p. 541.

Kocks, U.F., 1967, Can. J. Phys., Vol. 45, p. 737.

Kocks, U.F., Argon, A.S. and Ashby, M.F., 1975, Prog. Mat. Sci., Vol. 19, p. 1.

Kocks, U.F., Labusch, R. and Schwarz, R.B., 1976, in "Strength of Metals and Alloys," Proceedings of the 4th International Conference on theStrength of Metals and Alloys,Vol. 1, p. 275.

Koppenaal, T.J. and Kuhlmann-Wilsdorf, D., 1964, Appl. Phys. Lett., Vol. 4, p. 59.

Kulwicki, J.H and Sanders, T.H., Jr., 1983, in "Proceedings of the 2nd International Conference on Aluminum-Lithium Alloys," T.H. Sanders, Jr. and E.A. Starke, Jr., eds., AIME, Warrendale, PA, p. 31.

Labusch, R., 1970, Phys. Stat. Sol., Vol. 41, p. 659.

Labusch, R., 1972, Acta Metall., Vol. 20, p. 917,

Labusch, R., 1977, J. Appl. Phys., Vol. 48, p. 4550.

Lee, E.J. and Ardell, A.J., 1979, in "Strength of Metals and Alloys," Proceedings of the 5th International Conference on the Strength of Metals and Alloys, P. Haasen, V. Gerold and G. Kostorz, eds., Pergamon Press, Oxford, England, p. 633.

Li, J.C.M., 1963, Trans. AIME, Vol. 227, p. 239.

Lifshitz, I.M. and Slyozov, V.V., 1961, J. Phys. Chem. Solids, Vol. 19, p. 35.

Livet, F. and Bloch, D., 1985, Scr. Met., Vol. 10, p. 1151.

McAllister, A.J., 1982, Bull. Alloy Phase Diag., Vol. 3, p. 177.

Mahin, K.W., Hanson, K. and Morris, J.W. Jr., 1980, Acta Metall., Vol. 28, p. 443.

Makin, P.L. and Ralph, B., 1984, J. Mat. Sci., Vol. 19, p. 3835.

Marcinkowski, M., 1963,in "Electron Microscopy and Strength of Crystals," eds. G. Thomas and J, Washburn, Interscience, New York, p. 333.

Melander, A., 1977, Phys. Stat. Sol. (a), Vol. 43, p. 223.

Melander, A., 1978, Scand. J. Metall., Vol. 7, p. 109.

Melander, A., and Jansson, B., 1979, in "Strength of Metals and Alloys," Proceedings of the 5th International Conference onthe Strength of Metals and Alloys, P. Haasen, V. Gerold and G. Kostorz, eds., Pergamon Press, Oxford, England, p. 627.

Melander, A. and Persson, P.Å., 1978a, Acta Metall., Vol. 26, p. 267.

Melander, A. and Persson, P.Å., 1978b, Scand. J. Metall., Vol. 7, p. 181.

Melander, A. and Persson, P.Å., 1978c, Met. Sci., Vol. 13, p. 391.

Miura, Y., Matsui, A., Furukawa, M. and Nemoto, M., 1985, in "Proceedings of the 3rd International Conference on Aluminum-Lithium Alloys," Oxford, England, in press.

Morris, J.W. Jr. and Klahn, D.H., 1973, J. Appl. Phys., Vol. 44, p. 4882.

Morris, J.W. Jr. and Klahn, D.H., 1974, J. Appl. Phys., Vol. 45, p. 2027.

Morris, J.W. Jr. and Syn, C.K., 1974, J. Appl. Phys., Vol. 45, p. 961.

Mott, N.F. and Nabarro, F.R.N., 1940, Proc. Phys. Soc., Vol. 52, p. 86.

Mott, N.F. and Nabarro, F.R.N., 1948, Phys. Soc., Vol. 1, p. 1.

Muller, W., Bubeck, E. and Gerold, V., 1985, in "Proceedings of the 3rd International Conference on Aluminum-Lithium Alloys, "Oxford, England, in press.

Munjal, V. and Ardell, A.J., 1975, Acta Metall., Vol. 23, p. 513.

Munjal, V. and Ardell, A.J., 1976, Acta Metall., Vol. 24, p. 827.

Muto, T. and Takagi, Y., 1955, Solid State Physics, Vol. 1, p. 193.

Nabarro, F.R.N., 1972, J. Less Common Met., Vol. 28, p. 257.

Nabarro, F.R.N., 1977, Phil. Mag., Vol. 35, p. 613.

Nabarro, F.R.N., 1985, in "Dislocations and Properties of Real Materials," Proceedings of conference to celebrate the 50th anniversary of the concept of dislocation in crystals, The Institute of Metals, London, p. 175.

Nembach, E., 1981, Z. Metall., Vol. 72, p. 401.

Nembach, E. and Martin, M., 1980, Acta Metall., Vol. 28, p. 1069.

Nembach, E. and Neite, G., 1985, Prog. Mat. Sci., Vol. 29, p. 177.

Nembach, E., Suzuki, K., Ichihara, M. and Takeuchi, S., 1985, Phil. Mag., Vol. 51, p. 607.

Noble, B. and Thompson, G.E., 1971, Met. Sci., Vol. 5, p. 114.

Nozato, R. and Nakai, G., 1977, Trans. JIM, Vol. 18, p. 679.

Petch, N.J., 1953, J. Iron Steel Inst., Vol. 174, p. 25.

Porter, D.A. and Easterling, K.E., 1981, "Phase Transformations in Metals and Alloys," Van Nostrand Reinhold, Berkshire, England.

Quist, W.H., Narayanan, G.H. and Wingert, A.L., 1981, in "Proceedings of the 1st International Conference on Aluminum-Lithium Alloys," T.H. Sanders and E.A. Starke, Jr., eds., AIME, Warrendale, PA, p. 313.

Raynor, D. and Silcock, J.M., 1970, Met. Sci., Vol. 4, p. 121.

Reppich, B., Schepp, P., and Wehner, G., 1982, Acta Metall., Vol. 30, p. 95.

Russell, K.C. and Brown, L.M., 1972, Acta Metall., Vol. 20, p. 969.

Sainfort, P. and Guyot, P., 1985, in "Proceedings of the 3rd International Conference on Aluminum-Lithium Alloys, "Oxford, England, in press.

Sanders, T.H. Jr. and Starke, E.A. Jr., 1983, "Proceedings of the 1st International Conference on Aluminum-Lithium Alloys," T.H. Sanders and E.A. Starke, Jr., eds., AIME, Warrendale, PA, p. 1.

Sawtell, R.R., Bretz, P.B., Petit, J.I. and Vasudevan, A.K., 1984, in "Proceedings of 1984 SAE/Aerospace Congress and Exposition," Long Beach, CA, in press.

Scattergood, R.O. and Bacon, D.J., 1975, Phil. Mag., Vol. 31, p. 179.

Schwarz, R.B. and Labusch, R., 1978, J. Appl. Phys., Vol. 49, p. 5174.

Silcock, J.M., 1960, J. Inst. Met., Vol. 88, p. 357.

Syn, C.K., 1973, PhD thesis, University of California, Berkeley.

Tamura, M., Mori, T., and Nakamura, T., 1970, J. Jap. Inst. Met., Vol. 34, p. 919.

Thompson, A. and Brooks, J.A., 1982, Acta Metall., Vol. 30, p. 2197.

Voorhees, P.W. and Glicksman, M.E., 1984, Acta Metall., Vol. 32, p. 2001.

Voorhees, P.W. and Glicksman, M.E., 1984, Acta Metall., Vol. 32, p. 2013.

Wagner, C., 1961, Z. Electrochem, Vol. 65, p. 581.

Williams, D.B., 1981, in "Proceedings of the 1st International Conference on Aluminum-Lithium Alloys," T.H. Sanders, Jr. and E.A. Starke, Jr., eds., AIME, Warrendale, PA, p. 89.

Williams, D.B. and Edington, J.W., 1974, Phil. Mag., Vol. 30, p. 1174.

Williams, D.B. and Edington, J.W., 1975, Met. Sci., Vol. 9, p. 529.

Williams, D.B. and Edington, J.W., 1976, Acta Metall., Vol. 24, p. 323.

Appendix A. Derivation of Friedel relation.

The Friedel relation may be simply derived using geometrical arguments for the case in which all obstacles are randomly distributed and have the same strength. The line tension of the dislocation is assumed to be constant. The argument depends on two assumptions; the dislocation must bow-out in a circular shape with a large radius (so that the angles involved are small) and a steady state unzipping condition must hold.

A.1 Circular bow-out of the dislocation

The first of these assumptions makes it possible to write a force balance for an infinitesimal length of the dislocation such as that shown in figure A.1. The force on the dislocation, given by

$$\tau b(\delta l_f) = F \tag{A.1}$$

is balanced by a restoring force due to the line tension of the dislocation of

$$2T\sin(\delta\Psi/2) = T(\delta\Psi) \tag{A.2}$$

where the equality holds if the angle Ψ is small. Equating A.1 and A.2 gives a relation between τ and the bow-out radius

$$\tau = T/bR. \tag{A.3}$$

The value of R may be found in terms of the effective obstacle spacing l_f (as distinct from the mean square obstacle spacing l_s). The proof depends on the rarely stated assumption that the obstacles along the dislocation line are collinear. For figure A.2, recalling that β is defined to be $\sin(\Psi/2)$, the relationship is

$$R\sin(\Psi/2) = l_f/2$$

$$R = l_f/2\beta \tag{A.4}$$

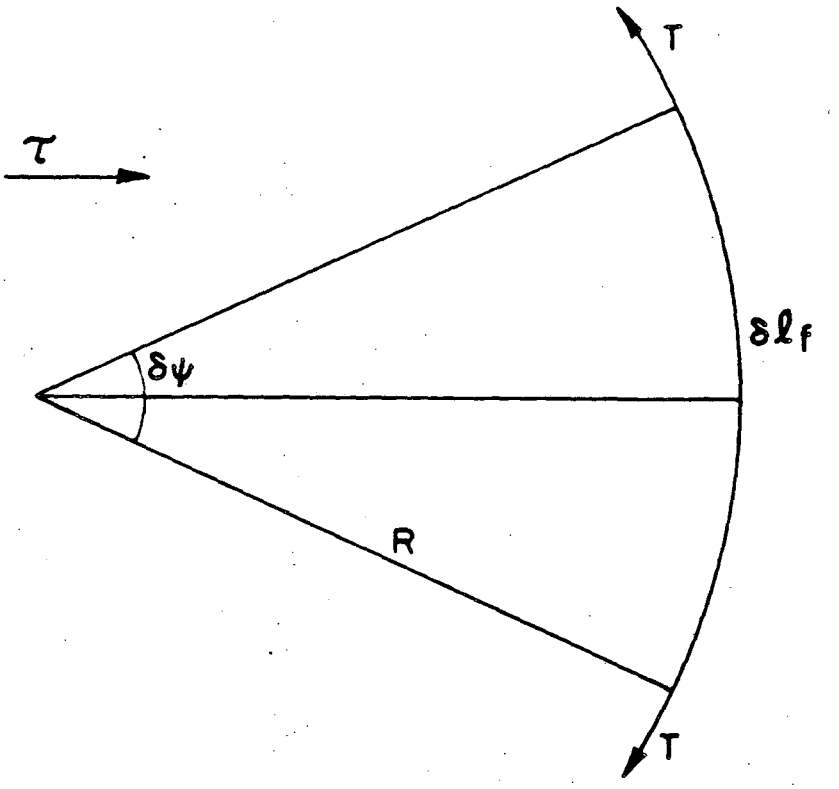

Figure A.1 Geometry illustrating the force balance between the bow-out of the dislocation of constant line tension under an applied stress τ and the restraining force imposed by the dislocation line tension.

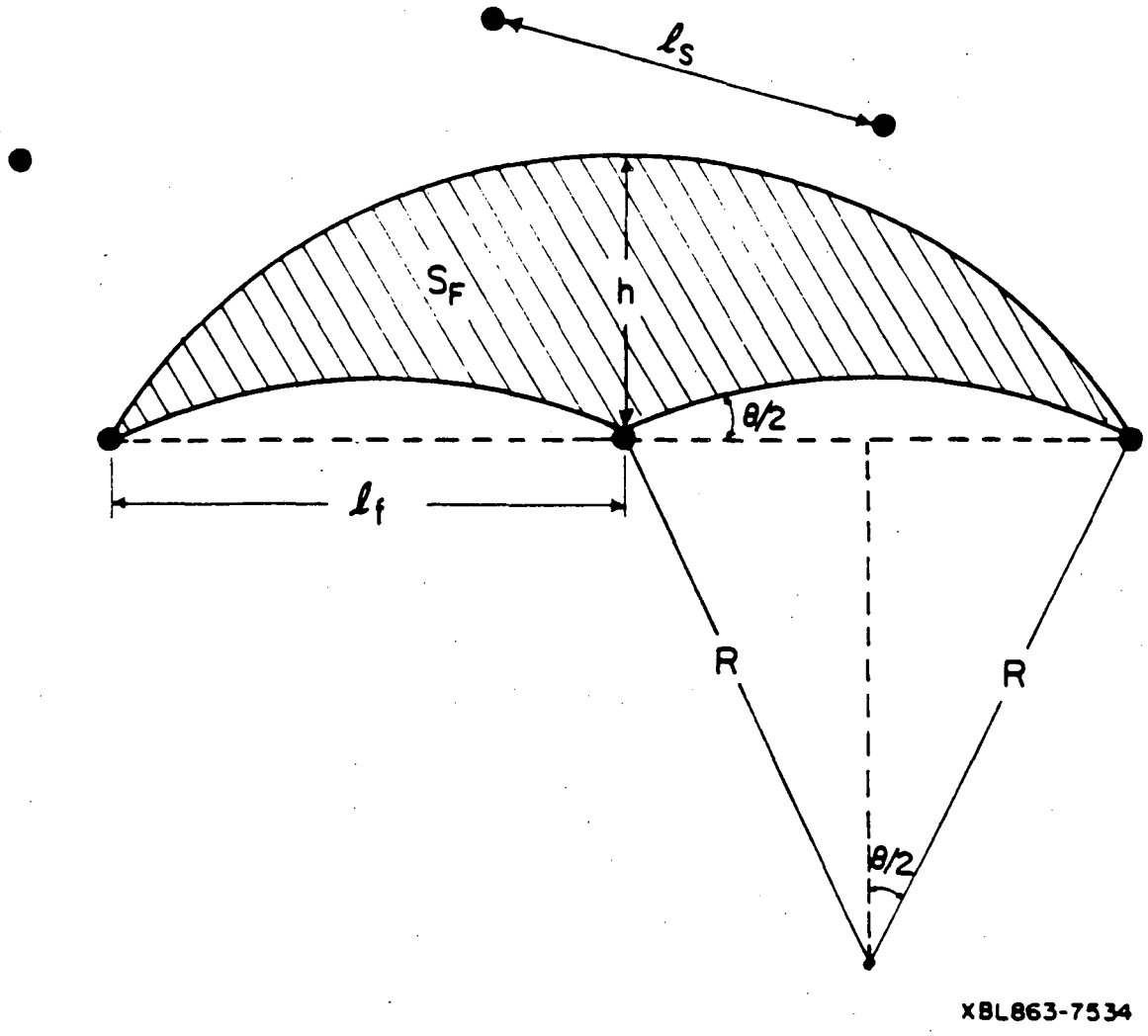

Figure A.2 Dislocation-obstacle geometry from which the Friedel relation is derived.

Substituting A.4 into A.3 we get the relation

$$\tau = 2T\beta/bl_f \tag{A.5}$$

A.2 The Friedel relation

The problem now is to find the effective obstacle spacing, l, in terms of the mean square obstacle spacing l_s, a known parameter of the array. The proof is based on the steady state unzipping condition for the geometry of figure A.2. As shown in the figure, the steady state unzipping condition requires that when the dislocation bypasses an obstacle and bows outward it will be pinned by exactly one new obstacle. The mathematical expression of this condition is

$$S_f n_s = 1 \tag{A.6}$$

where S_f is the area the dislocation sweeps out as it moves forward and n_s is the number of obstacles per unit area. Since $l_s = n_s^{-1/2}$,

$$S_f = l_s^2 = l_f h \tag{A.7}$$

when the bow-out radius is large. The height h can be eliminated from the equation by relating it to l_f and R since

$$\begin{aligned} l_f^2 + (R-h)^2 &= R^2 \\ l_f^2 &= 2Rh \end{aligned} \tag{A.8}$$

where the second equality is true because h is small compared to R. Eliminating h from equations A.7 and A.8 and substituting for r using equation A.4 gives the desired relation between l and l_s,

$$l^2 = l_s^2/\beta \tag{A.9}$$

Substituting into A.5 gives

$$\tau = 2T\beta^{3/2}/bl_s \tag{A.10}$$

Defining $\tau^* = \tau l_s b/2T$ gives

$$\tau^* = \beta^{3/2} \tag{A.11}$$

which is the Friedel relation.

Appendix B. Derivation of eqns 1 and 2 of Haasen and Labusch (1979).

For the purpose of calculating the critical resolved shear stress, Nabarro (1972, 1977, 1985) distinguishes between localized and diffuse obstacles on the basis of the size of the parameter κ (which he and Labusch call β). It pertinent to give this parameter a physical significance before continuing.

B.1 Rationale for the Labusch κ.

Labusch chooses κ as a convenient parameter in his statistical solution for solid solution hardening. He then concludes that the value of κ describes regimes of behavior in which obstacles behave in a localized or a diffuse manner. He does not attempt to provide a physical rationalization for his choice of parameter. According to the scheme for differentiating localized and diffuse obstacles in Section I, solute atoms may act as either type of obstacle depending on their concentration. Consequently, it makes sense that there should be a parameter like κ that defines points along the continuum between localized and diffuse obstacles. It can be shown that the Schwarz and Labusch η is directly proportional to Labusch's κ. Nabarro illustrates the relationship between κ and the obstacle concentration and spacing as part of a series of review papers on solid solution hardening (1972, 1977, 1985).

The value of κ may be used to arbitrarily define the regimes in which localized and diffuse obstacle statistics apply. Nabarro's papers (1972, 1975, 1985) are inconsistent about whether the point of division is at $\kappa = 1$ or $\kappa = 1/2$. The reasons for the confusion are highlighted in the following discussion.

The parameter κ is defined in terms of the characteristics of the dislocation and the obstacles it encounters:

$$\kappa = F/4Tcw^2 \qquad (B.1)$$

where $2w$ is the range of interaction of the obstacle and c is the concentration of solute atoms per unit area.

To rationalize this choice for the diffuseness parameter, Nabarro begins by defining an effective obstacle spacing

$$L = 1/2cw. \qquad (B.2)$$

The reasoning behind equation B.2 is worthy of comment since there is some confusion in the literature on this point. The geometry of the situation is shown in figure B.1 (after Kocks, Argon and Ashby, 1975). At zero stress the dislocation lies in a pipe of width 2w, the range of interaction. The concentration of obstacles per unit area is given by c, so the number of obstacles per unit length in a pipe of width 2w is 2wc. It follows that the average spacing between obstacles along the the dislocation line is L = 1/2cw. In some papers the diameter of the range of interaction of the obstacles is given as w' rather than 2w, which leads to a spacing of L = 1/cw'.

There is an additional inconsistency in the derivation that relates to whether the dislocation must be bowed through the radius or the diameter of the obstacle's range of interaction to bypass it. Since the solute atom restrains the motion of the dislocation either as it approaches or as it leaves, but not both, it seems reasonable to consider the halfwidth of the interaction range (as in Nabarro, 1972).

With these comments in mind, the derivation of the critical points of κ is most easily accomplished using the derivation of Nabarro 1977 or 1985. The geometry is shown in Figure B.2. If the dislocation bypasses the obstacle it must be turned through an angle $\theta/2$ given by

$$\sin(\theta/2) = w/L = 2cw^2. \qquad (B.3)$$

The restoring force opposing the forward motion of the dislocation is given by

$$\sin(\theta/2) = F/2T. \qquad (B.4)$$

If the restoring force is greater than the forward force then the dislocation is stable and the perturbation theory used by Labusch for diffuse obstacles is justified. The inequality that defines the diffuse obstacle regime is

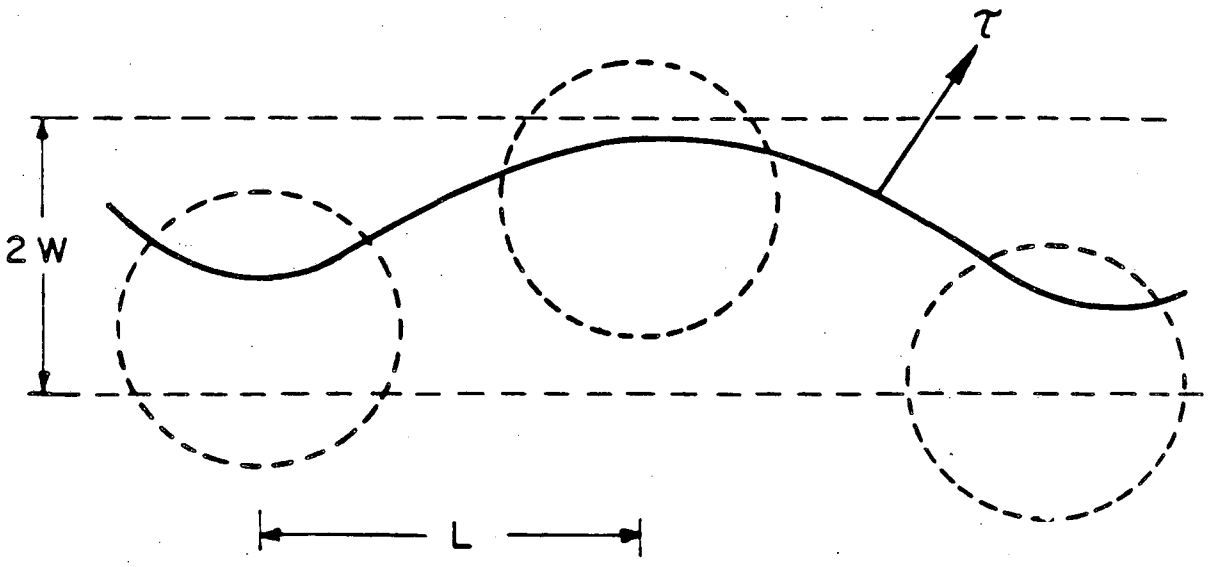

XBL862-7505

Figure B.1 Defining geometry for the effective obstacle spacing L = 1/2cw for diffuse obstacles (after Kocks, Argon and Ashby, 1975).

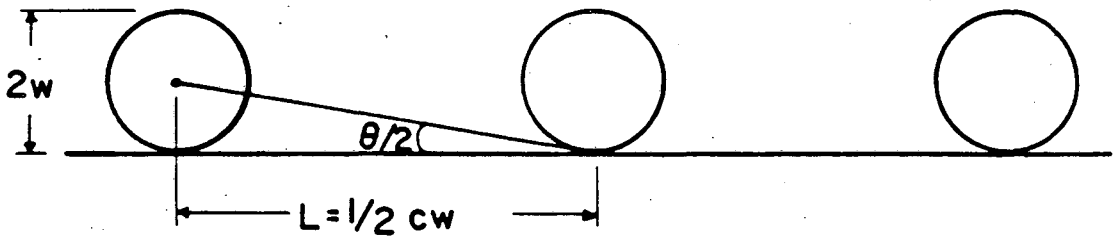

XBL 863-7535

Figure B.2 Geometry for derivation of the critical points of κ, the diffuseness parameter defined by Labusch.

$$F/2T > 2cw^2$$

or
$$\kappa = F/4Tcw^2 > 1 \qquad (B.5)$$

for obstacles of effective diameter 2w.

In comparing this result to the parameter η used by Schwarz and Labusch, another discrepancy appears. The equivalence between volume fraction and areal fraction is generally invoked (Nabarro, 1972; Schwarz and Labusch, 1978; Kocks, Ashby and Argon, 1975). However, the glide plane of the dislocation lies between two planes of atoms (Syn, 1973; Nabarro, 1985). The dislocation sees the atoms in both planes, so the effective concentration per unit area is

$$c = 2v/b^2 \qquad (B.6)$$

and not half of that. It follows that the value of l_s^2 is given by

$$l_s^2 = 1/c = b^2/2v. \qquad (B.7)$$

Schwarz and Labusch's definition is off by a factor of two, but if we use it and define y_o, the range of interaction, to be 2w, then we have (for a $\kappa = 1$ criterion) that the critical value of η is $\sqrt{2}$ rather than 1. If we define l_s correctly and use $y_o = w$, we get $\eta = 1$ as the criterion corresponding to the $\kappa = 1/2$ criterion in the paper they reference by Nabarro (1972). The correct value, using the $\kappa = 1$ criterion, is again $\eta = \sqrt{2}$. The relationship between the two variables is therefore

$$\eta^2 = 2/\kappa. \qquad (B.8)$$

B.2 Critical resolved shear stress equations.

Nabarro (1977) considers 3 distinct cases ($\kappa=1$, $\kappa<<1$, $\kappa>>1$). In each case he starts from the common relation

$$\tau bL = F \qquad (B.9)$$

where F is the maximum force exerted by the dislocation on the obstacle

and defines an appropriate value of L for the case in question. The effective spacings that Nabarro defines all represent average line solutions. It is important to note that while Schwarz and Labusch use a parameter like κ in their solution, they use an average obstacle spacing only for dimensional purposes. Their solution is still a strong line solution.

Case 1. For an almost straight dislocation, Nabarro takes

$$L = L_o = 1/2cw. \tag{B.10}$$

Substituting in equation B.9 gives

$$\tau_o = 2Fcw/b. \tag{B.11}$$

Case 2. For the Mott model ($\kappa << 1$, diffuse obstacles) he finds

$$L = L_M = (T/2Fc^2w)^{1/3} = L_o/\kappa^{1/3} \tag{B.12}$$

where $\kappa = F/4Tcw^2$ which gives the result

$$\tau_M = (2F^4c^2w/T)^{1/3}(1/b) = \kappa^{1/3}\tau_o. \tag{B.13}$$

Letting $c = v/r^2$ where v is the volume fraction of solute is what Haasen and Labusch calls c and letting E_1, the line energy be equal to T the line tension and the range of interaction w be equal to the precipitate radius r, we have

$$\tau_M = (2F^4v^2w/Tr)^{1/3}(1/rb)$$

$$\tau_M = (2F^4v^2/T)^{1/3}(1/rb)$$

$$\tau_M = CF^{4/3}v^{2/3}/(2\pi T)^{1/3}rb \tag{B.14}$$

which is Haasen and Labusch's equation 2.

Case 3. For the Friedel model (also called the Fleischer regime), ($\kappa >> 1$, discrete obstacles) Nabarro has

$$L = L_F = (2T/cF)^{1/2} = \sqrt{2}L_M/\kappa^{1/6} = \sqrt{2}L_o/\kappa^{1/2} \tag{B.15}$$

so that

$$\tau_F = (F^3 c/2T)^{1/2}(1/b). \qquad \text{(B.16)}$$

Making the same substitutions as before,

$$\tau_F = CF^{3/2}{}_v{}^{1/2}/(2\pi T)^{1/2}(1/rb) \qquad \text{(B.17)}$$

which is Haasen and Labusch's equation 1.

Appendix C. Force from a dislocation pileup.

Dislocations may be found in close proximity in a crystal for various reasons. They always maintain a separation δ fixed by the repulsion between them. This repulsion is caused by the stress fields associated with the dislocations which decay as 1/r. The repulsive force between the dislocations can be simply calculated for simple cases for which the dislocation stress field is known, such as pure edge or pure screw dislocations that have the same Burgers vector.

The force on the lead dislocation in a pileup of dislocations may be calculated as follows. Let the critical resolved shear stress for glide of the nth dislocation be τ_c^n, the interaction shear stress be τ_i and the applied resolved shear stress be τ_c^{APP}. Then the force balance for the nth dislocation is

$$\tau_c^n - \tau_c^{APP} - \tau_i = 0. \tag{C.1}$$

Solving n equations of this form simultaneously gives the equation

$$n\tau_c^{APP} = \tau_c^1 + \tau_c^2 + \ldots + \tau_c^n. \tag{C.2}$$

When τ_c^n is zero for all dislocations except the first (i.e. only the first dislocation in the pileup is being restrained by a physical obstacle), then the resolved shear stress on the lead dislocation is given by

$$\tau_c^1 = n\tau_c^{APP}. \tag{C.3}$$

Friedel (1964, pp. 260-261) obtains the same result by using a trivial work argument. If the lead dislocation moves forward by an amount dx, then the other dislocations in the pileup also can move forward by dx and maintain the same spacing. The total work produced by the shear stress must then be

$$W = (ndx)(\tau_c^{APP})bL = (\tau_c^1 bL)dx \tag{C.4}$$

so the force on the lead dislocation is again given by equation C.3.

Note that the dislocations are not coupled in any way. The increased stress at the head of the pileup is often used to explain the increase in yield strength with decreasing grain size; as the grain size decreases the maximum pileup length and the force on the lead dislocation on any given slip line decreases. This model of grain boundary strengthening is discussed at more length in the section on summing of strengthening mechanisms.

LAWRENCE BERKELEY LABORATORY
TECHNICAL INFORMATION DEPARTMENT
UNIVERSITY OF CALIFORNIA
BERKELEY, CALIFORNIA 94720